DEVELOPMENT OF NOVEL FOOD-DERIVED ANTIFREEZE PROTEINS AND PEPTIDES: INVESTIGATING STRUCTURE-FUNCTION RELATIONSHIPS IN ICE RECRYSTALLIZATION INHIBITION

A Dissertation Presented for the

Doctor of Philosophy

Degree

The University of Tennessee, Knoxville

Yuan Yuan

May 2025

Copyright © 2025 by Yuan Yuan.

All rights reserved.

DEDICATION

Dedicated to my beloved parents, for their unwavering love and support. It was you who taught me how to love and be loved. Without your constant encouragement, I could not have completed this work in the spring of my life.

ACKNOWLEDGEMENTS

I would first like to express my sincere gratitude to my advisors, Dr. Tong Wang and Dr. Vermont Dia, for offering me this Ph.D. position. With their constant support, patience, and insightful feedback, they helped me grow both as a scholar and as a person. This experience has forever shaped how I see and engage with science.

I would also like to thank my committee members, Dr. Smith and Dr. Zhong, for their insightful advice, constructive critiques, and for encouraging me to aim higher. Their expertise helped shape my research and challenged me to become a better scholar.

I extend my heartfelt appreciation to all my lab mates—Madison Fomich, Caleb Metzcar, Francisco Leyva Gutierrez, Joshua Saad, Celeste Chadwick, Ripley Vaughan, Avery Ollis—as well as my friends, and the staff in the Department of Food Science at the University of Tennessee. Sharing both the challenges and the triumphs with such wonderful people has made this journey even more meaningful.

ABSTRACT

The formation and growth of ice crystals during frozen storage negatively affect the quality of frozen foods, necessitating the development of novel, safe, and effective ice recrystallization inhibition (IRI) agents. Protein hydrolysates are promising alternatives due to abundant raw materials and safety for consumption. The first chapter explored succinylation of zein and gelatin hydrolysates, showing that modified peptides significantly improved IRI activity by reducing ice crystal size by approximately 40%, linked to enhanced amphiphilicity. The second chapter investigated wheat glutenin hydrolysates prepared by Alcalase and trypsin. Trypsin-derived hydrolysates displayed higher IRI activity, especially under low ionic strength and in $CaCl_2$ solutions, with increased α-helix content correlating to improved antifreeze function. The third chapter identified two wheat flour-derived water-soluble proteins, including WDAI-3, with strong IRI activity. Molecular dynamics simulations confirmed that WDAI-3's antifreeze behavior was linked to structural rigidity and protein-water interactions. The fourth chapter demonstrated that gelatin hydrolysates' IRI activity was enhanced by xanthan gum (XG), even at low concentrations (0.1%), with stabilization above 0.4%. Molecular weight, mixing time, and secondary structure (rich in β-sheets and α-helices) further influenced the IRI activity of XG-gelatin complexes. The final chapter employed molecular dynamics simulations to examine peptides with varied chain lengths and secondary structures derived from trypsin hydrolysis, revealing a strong correlation between structural features and antifreeze efficiency. Overall, this dissertation provides foundational insights into designing and understanding antifreeze peptides for food

preservation and other biomaterial applications.

TABLE OF CONTENTS

Chapter One Introduction 1

Background and motivation 1

Antifreeze proteins and peptides as cryoprotectants 1

Ice recrystallization process and application 2

Mechanisms of antifreeze proteins and peptides 3

The influence of chain length 4

The influence of structural conformation 4

The influence of charge 5

The influence of surface amphiphilicity 6

Evaluation and factors affecting antifreeze activity 7

Evaluation methods 7

Effect of salt on IRI activity 8

Effect of other components on food systems 9

Research Gap and Hypothesis 10

Research Objectives 11

Appendix 21

Chapter Two Succinylation of Zein and Gelatin Hydrolysates Improved Their Ice Recrystallization Inhibition Activity 22

Abstract 23

Introduction 23

Materials and methods 26

Materials 26
Preparation of zein and gelatin hydrolysates by Alcalase 27
Quantifying the degree of hydrolysis (DH) by the o-pthaldialdehyde (OPA) method 27
Determining average molecular weight of gelatin and zein hydrolysates by size exclusion chromatography 28
Measuring the surface hydrophobicity of the hydrolysate samples 29
Modification of hydrolysates by succinylation reaction 29
Determining secondary structure by Fourier-transform infrared spectroscopy (FTIR) 30
Analyzing IRI activity of hydrolysates by splat assay 30
Statistical analysis 31
Results and Discussion 31
Degree of hydrolysis (DH) and average molecular weight (M_w) of peptides 31
Modification of zein and gelatin hydrolysates by succinylation reactions 32
Physicochemical characteristics of the modified hydrolysates 34
The effect of concentrations of succinylated hydrolysates on IRI activity 36
Effect of pH on the IRI activity of SA and OSA modified zein hydrolysates 37
Conclusion 38
Appendix 46
Chapter Three The Ice Recrystallization Inhibition Activity of Wheat Glutenin Hydrolysates and Effect of Salt on Their Activity 52

Abstract 53
Introduction 55
Materials and methods 58
Materials 58
Glutenin hydrolysates preparation 58
Amino acid composition and protein content determination 59
Phenol-sulfuric acid method for total carbohydrates assay 60
Size exclusion chromatography for average molecular weight determination 60
O-pthaldialdehyde (OPA) method for determining relative degree of hydrolysis ... 61
Splat assay for IRI activity 61
Fourier transform infrared (FTIR) for secondary structure analysis of hydrolysates 62
Statistical analysis 62
Results and discussion 63
Effect of enzyme type and hydrolysis time on peptides' size and IRI activity 63
Effect of amino acid profile on IRI activity 64
Effect of salt concentration in dispersing media on IRI activity 65
Effect of different cations on the IRI activity of wheat glutenin hydrolysates 67
Effect of dispersing medium on IRI activity of peptides 68
The importance of dispersing medium on IRI activity of glutenin hydrolysates 70
Conclusion 71
Appendix 80

Chapter Four Identification of Antifreeze Albumin Protein From Wheat Flour and Insights From Molecular Dynamics Simulation 89
Abstract 90
Introduction 91
Materials and methods 94
Materials. 94
Extraction of albumin from wheat flour. 94
Removal of protein or polysaccharides from crude albumin to identify the IRI activity 94
Fractionation of wheat albumin using gel filtration chromatography. 95
Determination of molecular weight of albumin extract and their fractions. 96
Determination of protein content by total amino acid composition analysis 96
Determination of total polysaccharide. 97
SDS-PAGE for characterization of albumin extract and their fractions. 97
Periodic acid-schiff (PAS) stain for glycoprotein. 98
Splat assay for IRI activity determination. 98
Protein identification by LC/MS methods. 99
Molecular dynamic simulation analysis 100
Statistical analysis. 102
Results and Discussion 102
Identification of compound with IRI activity from crude wheat albumin extract. . 102
Isolation of IRI active wheat albumin fraction by gel filtration chromatography. . 103

LC/MS analysis of the potent species in wheat albumin fractions. 105
MD simulation analysis of alpha-amylase inhibitor protein-water-ice interactions under freezing-like conditions. 106
Conclusion 110
Appendix 118
Chapter Five Ice Recrystallization Activity of Gelatin Hydrolysates Is Affected By The Presence of Xanthan Gum 128
Abstract 129
Introduction 130
Methods and materials 133
Preparation of protein hydrolysates 133
Measurement of the molecular weight of gelatin hydrolysates by HPLC 133
Preparation of XG-protein hydrolysates mixture or complex 134
Measurement of IRI activity by splat assay 134
Measurement of the surface amphiphilicity by the pendant drop method 134
Measurement of microstructure of complex by confocal laser scanning microscopy (CLSM) 135
Measurement of secondary structure of complex by circular dichroism (CD) 136
Statistical analysis 136
Results and discussion 136
The impact of XG on the IRI activity of gelatin hydrolysates 136

The impact of the molecular weight (MW) of hydrolysates on IRI activity of complex 138
The impact of stirring time on the IRI activity of complex 138
Confocal laser scanning microscopy (CLSM) observation of the complex 139
Surface amphiphilicity of the complex 140
Conformational changes of complex by mixing 142
Conclusion 142
Appendix 149
Chapter Six Exploring the Role of Secondary Structure on The Antifreeze Activity of Plant Food Derived Peptides: a Molecular Dynamics Study 158
Abstract 159
Introduction 160
Methods 162
Experimental design 162
Protein selection 162
Peptides preparation and modeling 163
MD simulation 163
Statistical analysis 164
Results and Discussion 164
Peptides and their secondary structure 164
Ice percentage changes of these peptides during freezing conditions 165

The relationship between conformation flexibility and antifreeze activity of peptides 167

The relationship between protein-water interaction and their antifreeze activity... 168

Conclusion 170

Appendix 178

Chapter Seven Conclusion and Future Work 188

Summary and key findings 188

Future work 189

Vita 191

LIST OF TABLES

Table 2.1. Degree of hydrolysis (DH) and average molecular weight (M_w) of protein hydrolysates generated by Alcalase treatment at different times. 46

Table 2.2. Secondary structure profiles of different hydrolysates as determined by FTIR. 47

Table 3.1 Yield and property of hydrolysates of wheat glutenin made by two proteases. 80

Table 3.2 The amino acid composition of the isolated glutenin fraction and its hydrolysates 81

Table 4.1. Impact of enzymatic hydrolysis on protein and polysaccharides content and IRI activity of crude wheat albumin isolated from wheat flour. 118

Table 4.2. The average molecular weight, protein and polysaccharides composition, and IRI activity of crude wheat albumin extract and their corresponding fractions separated by gel filtration chromatography. 119

Table 5.1 The molecular weight profiles of gelatin hydrolysates. 149

Table 5.2 Statistical analysis results of linear regression models at different xanthan gum concentrations 150

Table 5.3 The secondary structure profile of XG-gelatin hydrolysates complex 151

Table 6.1 Generated functioned proteins and their molecular characteristics and secondary structure compositions of peptides. 178

Table 6.2 Peptide–water short-range interaction energies over the final 10 ns of stable simulation, including LJ-SR (short-range Lennard-Jones) and Coul-SR (short-range Coulombic energy. 179

LIST OF FIGURES

Figure 1.1 Mechanism of action of antifreeze molecules. A) ice shaping, B) Thermal hysteresis, and C) ice recrystallization inhibition. 21

Figure 2.1. The degree of modification of zein hydrolysate (3 h) modified by SA (ZH + SA), and gelatin hydrolysates (0.25 h) modified by OSA (GH + OSA) during 35 h reaction at room temperature. 48

Figure 2.2. (A-B) Effect of hydrolysis time and succinylation modification on average Feret's diameter of ice crystal as affected by 40 mg/mL zein (A) and gelatin (B) and their succinylated forms. Different lowercase letters represent significantly different means of unmodified hydrolysates and capital letters represent significantly different means of succinylated samples ($p < 0.05$). (C) Microscopic images of PEG, ZH (3 h), ZH + SA, GH (0.25 h), and GH + OSA solution at 40 mg/mL concentration after annealing for 30 min at -8 ℃ under 20x/0.40 lens (scale = 50 μm). (D) The surface hydrophobicity of hydrolysates and their corresponding modified samples. The data were shown as the ratio of hydrolysates or modified hydrolysates to their corresponding protein. 49

Figure 2.3. The FTIR spectra of amide I band (1700-1600 cm-1) of ZH (A), ZH + SA (B), GH (C) and GH + OSA (D) in 1xPBS buffer at 40 mg/mL concentration and at room temperature. 50

Figure 2.4. (A-B) Average Feret's diameter of ice crystals affected by succinylated ZH (3 h) and gelatin (0.25 h) hydrolysates by SA (A) and OSA (B) analyzed by splat assay in 1xPBS at different concentrations after 60 min at -8 °C annealing. (C-E) Average

Feret's diameter of ZH and ZH + SA ice crystals measured by splat assay in 1xPBS (pH = 7.3) (C), 180 mm HCl (pH = 1.20) (D), and 180 mM NaOH (pH = 12.46) (E) solutions at 40 mg/mL (w/v) for 60 min. (F-H) Microscope images of ZH + SA in 1xPBS (pH = 7.3) (F), 180 mm HCl (pH = 1.20) (G), and 180 mM NaOH (pH = 12.46) (H) solution (c = 40 mg/mL) after annealing for 60 minutes at -8℃ under 20x/0.40 lens (scale = 50 μm). 51

Figure 3.1 Enzymatic hydrolysis and PBS concentration affected the IRI activity of wheat glutenin. A) IRI activity of Alcalase hydrolysates, B) IRI activity of trypsin hydrolysates, and C) representative ice images as affected by PBS concentration. . 82

Figure 3.2 Ionic strength and cation type affected the IRI activity of wheat glutenin hydrolysates (A: Alc 5m; B: Alc 30m; C: Try 1h; D: Try 2h, E: representative ice 83

Figure 3.3 The FTIR spectra of amide I band (1700-1600 cm-1) of glutenin hydrolysates in different dispersing media at 40 mg/mL concentration and at room temperature. 84

Figure 3.4 The effect of dispersing media on secondary structure of glutenin hydrolysates 85

Figure 3.5 Pearson's correlation coefficients for the secondary structure and IRI activity of glutenin hydrolysates in different dispersing media. 86

Figure 3.6 Discriminant analysis of glutenin hydrolysates in various dispersing media (blue: 1 x PBS, black: 0.1 x PBS, green: 10 mM NaCl, red: 10 mM CaCl2, and navy blue: 30 mM NaCl): a PCA-based classification model using scores plot and loading plots with 95% confidence ellipses. 87

Figure 3.7 Score plots (A), and 200 permutation tests (B) for the PLS-DA model of glutenin hydrolysates in different dispersing media. 88
Figure 4.1 Fractionation of filtered crude wheat albumin extract by gel filtration chromatography 120
Figure 4.2. SDS-PAGE (left figure) and PAS glycoprotein analysis (right figure) of albumin and different fractions with controls. P: positive control for glycoprotein detection, N: negative control for glycoprotein detection, C: crude albumin extract from wheat, F followed by a number refers to a gel filtration chromatography fraction, filter: albumin after 0.22 µm filtration using PVDF membrane..... 121
Figure 4.3. The structural models of trypsin inhibitors from soybean (A) and wheat alpha-amylase inhibitors proteins (B-C). Yellow: α-helix, Blue: β-sheet, Green: loops and undefined structures 122
Figure 4.4. Time evolution of the percentage of ice molecules during the simulation. The error bars represent the standard deviation calculated from 3 independent simulation runs..... 123
Figure 4.5. Corresponding representative snapshots of simulation systems during 100 ns at 265.15 K. Yellow: ions of sodium chloride. 124
Figure 4.6. Time evolution of water and water interactions among three proteins during simulation. (A) the proximal radial distribution function between the water oxygen atoms and the protein non hydrogen atoms of the three different proteins, (B) tetrahedral order parameters of oxygen atom of water molecules, (C) autocorrelation of hydrogen bond between water and water, (D) mean squared displacement of

oxygen atom of water molecules. The shaded areas around each curve represent the standard deviation (SD) values 125
Figure 4.7. Time evolution of conformational changes among three proteins during simulation. (A) radius of gyration, (B) normalized hydrogen bond between protein and protein based on total possible hydrogen bond, (C) root mean square deviation of protein, (D) mean squared displacement of protein. The shaded areas around each curve represent the standard deviation (SD) values. Note that MSD calculations were performed over the timeframe 50ns to 100ns. 126
Figure 4.8 Time evolution of normalized hydrogen bond between water and protein during simulation. 127
Figure 5.1 The average ice crystal size (ICS) relative to the same concentration of negative control sample (PEG) under the different percentages of xanthan gum. The red curve represents the quadratic fitting model, while the shaded area indicates the 95% confidence interval of ICS predictions. 152
Figure 5.2 The relationship between the molecular weight and ICS of gelatin hydrolysates at different xanthan gum concentrations..... 153
Figure 5.3 Effect of physical mixing on the IRI activity of XG-hydrolysate mixtures at different XG concentrations: (A) 0.1 %, (B) 0.2 %, (C) 0.3 %, and (D) 0.4 %..... 154
Figure 5.4 Confocal laser scanning microscopy images of the polysaccharides stained with rhodamine B (red) and, proteins stained with fluorescein 5-isothiocyanate (green) for gelatin hydrolysates-xanthan gum mixtures. The white circle means the formation of small aggregations. 155

Figure 5.5 Critical micelle concentration of complexes formed with gelatin hydrolysates produced by trypsin at different hydrolysis durations (1h, 3h, and 6h) and two XG concentrations (0.3 and 0.4%). A-C corresponds to 0.3 % XG: (A) 1 hour hydrolysis, (B) 3 hours hydrolysis, (C) 6 hours hydrolysis. D-F corresponds to 0.4 % XG: (D) 1 hour hydrolysis, (E) 3 hours hydrolysis, (F) 6 hours hydrolysis. 156

Figure 5.6 Circular dichroism spectra of complexes with different hydrolysis times (1h, 3h, and 6h) and two XG concentrations (0.3 and 0.4%). (A–C) Correspond to 0.3 % XG: (A) 1 hour hydrolysis, (B) 3-hour hydrolysis, (C) 6-hour hydrolysis. (D–F) Correspond to 0.4 % XG: (D) 1 hour hydrolysis, (E) 3-hour hydrolysis, (F) 6-hour hydrolysis. 157

Figure 6.1. Molecular dynamics workflow for antifreeze peptide discovery. 180

Figure 6.2. The structural models of peptides with different secondary structures and chain lengths. The number before each structure type indicates the peptide length in amino acid residues. 181

Figure 6.3 Time evolution of the percentage of ice molecules during the simulation. A: short chain length group, B: intermediate chain length group, C: long chain length group. Shaded areas represent the standard deviation based on three independent simulation replicates. 182

Figure 6.4. The relationship between peptide secondary structure and average ice content. A) Ice content as a function of helical and coil structure, B) Ice content as a function of sheet and coil structure. 183

Figure 6.5. Time evolution of radius of gyration (A-C) and normalized hydrogen bond between peptide and peptide (D-F) during 100 ns simulations, categorized by peptide chain length (A and D for short, B and E for intermediate, and C and F for long). 184
Figure 6.6. Time evolution of root mean square deviation (A-C) and root mean square fluctuation (D-F) of peptides during 100 ns simulations, categorized by peptide chain length (A and D for short, B and E for intermediate, and C and F for long). 185
Figure 6.7. Time evolution of mean square displacement (A-C) and normalized peptide-water hydrogen bonds (D-F) for peptides during 100 ns simulations, categorized by chain length (A and D for short, B and E for intermediate, and C and F for long). 186
Figure 6.8. Correlation between average peptide structural flexibility (RMSD) and hydration bonds between peptides and water molecules during the final 10 ns of simulation..... 187

CHAPTER ONE INTRODUCTION

Background and motivation

Freezing is an essential preservation method for fresh foods, extending shelf life by inhibiting microbial growth. However, ice nucleation and subsequent crystal growth can cause mechanical damage, leading to undesirable texture and flavor changes. These effects are exacerbated by ice recrystallization, a process driven by Ostwald ripening, where larger ice crystals grow at the expense of smaller ones. This phenomenon significantly diminishes product quality, contributing to an estimated $5.89 billion in frozen food wasted annually (Conrad, 2020). Thus, controlling ice crystal formation is crucial for maintaining frozen food stability.

Various cryoprotectants have been employed to mitigate ice damage. Traditional cryoprotectants, such as sucrose and sorbitol, effectively regulate ice crystal size but require high concentrations, potentially affecting taste, sugar content, and caloric load of food products. This limitation has spurred interest in alternative cryoprotectants, particularly proteins and peptides, which can inhibit ice growth with minimal impact on food composition (Eskandari, Leow, Rahman, & Oslan, 2020).

Antifreeze proteins and peptides as cryoprotectants

Antifreeze proteins (AFPs), first discovered in Antarctic fish in the 1960s, have been identified in various organisms, including fish, insects, and plants. These proteins lower the freezing point of solutions and inhibit ice recrystallization, preventing ice crystal formation or inhibiting further growth without the drawbacks associated with sugar-based cryoprotectants. Notable examples include gelatin hydrolysates (Chen, Li, Yang, Wu, &

Wang, 2020), silver carp hydrolysates, which mitigate protein denaturation in frozen surimi (Luo et al., 2023), and *Tenebrio Molitor* beetle beetle-derived proteins, which reduce freezing points by up to 7.9 °C at a concentration of 1 mg/mL (Gruneberg, Graham, Eves, Agrawal, Oleschuk, & Davies, 2021).

Despite their effectiveness, the industrial application of AFPs remains limited due to high production costs, allergenicity concerns, and regulatory restrictions on animal-derived proteins. As an alternative, plant-derived proteins and peptides have gained attention. For instance, soybean hydrolysates have been shown to reduce ice crystal size by 29-57 % (Fomich, Día, Premadasa, Doughty, Krishnan, & Wang, 2023), showing their potential in frozen food systems. Additionally, chemical synthesis and structural modifications can enhance antifreeze activity. For example, Judge, Georgiou, Bissoyi, Ahmad, Heise, and Gibson (2023) synthesized polyproline peptides with strong ice-binding capacity, demonstrating that engineered peptides could mimic natural AFPs while overcoming cost and availability challenges.

Ice recrystallization process and application

The mechanisms of AFPs generally include thermal hysteresis (TH), dynamic ice shaping (DIS), and ice recrystallization inhibition (IRI) (**Figure 1.1**) (all tables and figures can be found in the chapter appendix). Among these, IRI is the most relevant to antifreeze activity (Gruneberg et al., 2021).

TH activity refers to lowering the freezing point without significantly affecting the melting point by binding to ice surfaces. If the TH activity is high, the nucleated ice crystals will not be stable or remain small when the temperature is below zero degree

Celsius. When the temperature falls below the TH gap, the ice crystal begins to grow. In general, AFPs from fish usually exhibited TH nearly 2 ℃, while that from insects will above 5 ℃ (Wu, Yao, Zhang, & Li, 2021).

Dynamic ice shaping (DIS) refers to the ability of AFPs to modify the morphology of ice crystals (Li, Luckett, & Wu, 2022). Both TH and DIS ability reflect the polymer have ice-binding activity. Both TH and DIS indicate direct ice-binding activity, meaning that the AFPs physically interact with ice surfaces. However, not all materials with strong IRI activity exhibit TH or DIS, suggesting that different cryoprotective materials may operate through distinct mechanisms, some of which may not involve direct ice binding.

IRI is primarily governed by Ostwald ripening, a process where smaller ice crystals melt and subsequently reform into larger ones due to their lower surface energy. Additionally, the accretion process contributes to increased ice volume in the system. During accretion, adjacent ice crystals merge by freezing the liquid water between them, further promoting crystal growth and altering ice structure. Accretion dominates when ice crystals are small and close together, whereas Ostwald ripening dominates when crystals are larger and more dispersed (Midya & Bandyopadhyay, 2024). Unlike AFPs from animals, plant-derived AFPs generally exhibit modest TH activity but demonstrate strong IRI activities (Olijve et al., 2016).

Mechanisms of antifreeze proteins and peptides

The mechanism of each class of cryoprotective compound may be different (Biggs, Stubbs, Graham, Fayter, Hasan, & Gibson, 2019), and some of them still hard to explain.

However, several key molecular characteristics have been identified among these IRI active polymers.

The influence of chain length

Molecular weight (MW) appears to be a significant factor influencing the antifreeze activity of peptides and proteins. Gelatin hydrolysates with the MW ranging from 700-1400 Da have been shown to significantly inhibit ice crystal growth more effectively than other peptides (Wang, Agyare, & Damodaran, 2009), hydrolysates from tilapia scales, with sizes below 2000 Da, have demonstrated cryoprotectant activity in preserving *S. thermophilus* (Chen et al., 2020). Research by Fu et al. (2019) also demonstrated that hydrolysates produced by alkaline protease from *Scomberomorus niphonius*, showed substantial antifreeze ability when their molecular weight is from 1426 to 1810 Da, exhibited substantial antifreeze activity. This consistency across different sources suggests an optimal size range for antifreeze activity of antifreeze peptides.

The influence of structural conformation

In addition to MW, the structural conformation of AFPs and antifreeze glycoproteins (AFGPs) are strongly associated with their cryoprotective properties. Type I and IV AFPs and AFGPs, known for their high IRI activity, usually possess rigid structures such as α-helix and polyproline II helix, respectively (Mochizuki & Molinero, 2018; Nishimiya et al., 2006; Sicheri & Yang, 1996). This structural rigidity has also been exploited in the synthetic design of triplex metallohelices, which exhibit potent IRI activity, further highlighting the importance of helical structures in effective ice interaction (Mitchell, Clarkson, Fox, Vipond, Scott, & Gibson, 2017).

Our previous study on proteins extracted from black soldier fly larvae found that albumin proteins rich in β-sheets demonstrated better IRI activity (Fomich, Yuan, Krishnan, Dia, & Wang, 2025). Additionally, α-helical peptides are associated not only with IRI activity but also with enhanced TH activity, another key property indicative of antifreeze activity (Rojas, Aróstica, Carvajal-Rondanelli, Albericio, Guzmán, & Cárdenas, 2022). Similarly, insect-derived AFPs with a rigid β-helical structure have been linked to higher TH activity (Liou, Tocilj, Davies, & Jia, 2000). These findings suggest that both rigid structures conformations (α-helical and β-sheet) may contribute significantly to cryoprotective activity.

Furthermore, naturally antifreeze peptides from sources such as shrimp (Zhu, Zheng, & Dai, 2022), silver carp (Wang et al., 2021), *Taki Fugu obscurus* skin (Yang et al., 2022), and Antarctic yeast protein (Shah et al., 2012) are all characterized by an α-helix structure, reinforcing the hypothesis that structural stability is a key determinant of antifreeze functionality. This is further supported by studies demonstrating a strong correlation between α-helices and enhanced antifreeze activity (Zhang, Liu, Li, Gutowski, Yin, & Wang, 2018).

The influence of charge

Beyond structural conformation, the electrostatic properties of peptides also contribute to their effectiveness in inhibiting ice crystal growth. For example, hydrolysates exhibit more potent activity in alkaline environments, where they maintain a negative charge, compared to their performance in acidic or neutral conditions (Yuan, Fomich, Dia, & Wang, 2023). Similarly, effective antifreeze peptides extracted from gelatin and silver

carp hydrolysates are characterized by the presence of alkaline amino acid residues, which contribute to their functionality (Luo et al., 2023). Interestingly, even among peptides from the same material, such as fish gelatin, cationic peptides have exhibited superior IRI activity compared to others (Damodaran & Wang, 2017).

The influence of surface amphiphilicity

The mechanism of ice binding involves multiple molecular interactions, and previous studies suggested that hydrogen bonding seems to serve as the main driving force (Damodaran, 2007; Damodaran et al., 2017). For example, peptides from gelatin, rich in hydroxyl groups, can bind to the prism face of ice by hydrogen bonding (Damodaran et al., 2017) and inhibit ice recrystallization and growth. Wu et al. (2021) found that some cryoprotectants, such as dimethyl sulfoxide and graphene oxide, lower the freezing point or stick to the surface of ice crystals through hydrogen bonds. Meanwhile, polyvinyl alcohol (PVA) prevents ice growth through adjacent hydroxyl groups (Wu et al., 2021). In addition, hydrophobic interactions represent another crucial aspect of IRI. Type I and III AFPs bind ice via methyl group (Hudait, Qiu, Odendahl, & Molinero, 2019).When a hydrophobic dimethylfulvene residue was incorporated on the glycan-opposing face, which was hydrophilic, the IRI activity of glycopolymers was significantly increased (Graham, Fayter, Houston, Evans, & Gibson, 2018). Similarly, the IRI activity of the alkylated galactose derivatives increased when the addition of hydrophobic moieties (alkyl chains) went from seven to nine carbon atoms (Trant, Biggs, Capicciotti, & Ben, 2013). Furthermore, Hudait et al. (2019) used molecular simulations to show that methyl

groups slow the movement of water at the ice-binding surface and stabilize the clathrate-like water in the anchored clathrate motif that binds these proteins to ice.

However, the effectiveness of antifreeze peptides depends on a delicate balance between hydrophobic and hydrophilic properties. Excessive hydrophobicity can lead to aggregation and reduced solubility, ultimately diminishing IRI activity (Biggs et al., 2019; Graham et al., 2018). For example, PVA, AFPs, and AFGPs are known to be amphipathic (Biggs et al., 2019; Mitchell et al., 2017; Mitchell & Gibson, 2015). Mochizuki et al. (2018) also detected the conformation structure of AFGPs and found that they can bind to the ice by hydrophobic methyl group, while hydrophilic side is important to stabilize the unique structure. Based on this, several polymers were developed, including self-assembled triplex metallohelices (Mitchell et al., 2017) and Polyfluorene (Graham et al., 2018), to mimic the amphiphilic structure of AFGPs and demonstrate strong IRI activity. Also, it was found that some other IRI active materials had amphiphilic structures on their faces (Mitchell et al., 2015).

Evaluation and factors affecting antifreeze activity

Evaluation methods

The IRI effect of antifreeze polymers is commonly determined by a splat assay or sandwich assay. The standard splat assay is a commonly used method for detecting IRI activity (Delesky & Srubar, 2022). Typically, this assay is conducted in the presence of >2 mM NaCl or 1 x phosphate-buffered saline (PBS), which contains NaCl, KCl, Na_2HPO_4, and KH_2PO_4, to prevent false positives results (Voets, 2017). The temperature

is also crucial, with -6 to -8 °C often used, with lower temperatures potentially not allowing for recrystallization and yielding false positives (Midya et al., 2024).

The sandwich assay represents an alternative methodology that differs primarily in its sample preparation and analysis procedure. In this approach, test materials are dissolved in solutions containing varying concentrations of sucrose or other sweeteners. The experiment involves a droplet of the sample solution between a glass slide and cover slip, followed by rapid freezing to -40°C using liquid nitrogen, dry ice, or a controlled cooling stage. Subsequent analysis involves maintaining the samples at specific subzero temperatures (typically -6°C or -8°C) for durations ranging from 30 min to several days and then analyzing the ice crystal size.

For TH activity assessment, differential scanning calorimetry (DSC) serves as the primary analytical tool. This technique operates by measuring the thermodynamic parameters of crystallization, specifically quantifying changes in exothermic and endothermic enthalpies throughout the crystallization process. Through this analysis, researchers can accurately determine the initial crystallization temperature and evaluate the compound's freezing point depression capabilities.

Effect of salt on IRI activity

The current understanding of how salt concentration influences the IRI activity of antifreeze polymers remains underexplored and is characterized by conflicting findings, as highlighted below. Delesky (2020) found that the addition of 151 mM salts of $CaCl_2$, $MgCl_2$, $CuCl_2$, or $AlCl_3$ reduced the IRI activity of poly(2-hydroxypropylmethacrylamide) and eliminated the IRI activity of polythreonine. In

contrast, Hayakari and Hagiwara (2012) found that the interaction of winter flounder antifreeze proteins and the ice surface was strengthened by the addition of 147 mM NaCl. Leiter, Rau, Winger, Muhle-Goll, Luy, and Gaukel (2016) also found that the addition of 30 mM NaCl improved the activity of AFP III under a 49 % sucrose solution condition. However, they did not explain the reason, and the sucrose concentration may be too high to accurately describe the effect of salt. This suggests a complex relationship between salt concentration and IRI activity.

Moreover, the type of salts in the dispersing media can also influence the IRI effects of peptides. For example, Suris-Valls and Voets (2019) compared the ice crystal size of antifreeze glycoprotein (AFGP)1-5 and type III AFP in sodium nitrate, sodium chloride, sodium borate, sodium phosphate, and sodium citrate buffers and discovered that the citrate buffer consistently led to higher IRI activity for both proteins. In addition, certain Ca^{2+} ions have an additional impact on the antifreeze activity of proteins. For example, type II AFP exhibits Ca^{2+} dependent activity (Arai, Nishimiya, Ohyama, Kondo, & Tsuda, 2019).

Effect of other components on food systems

In real food systems, the interaction between antifreeze proteins/peptides and other components, particularly polysaccharides, significantly influences IRI activity. In our previous study, we found that the water-soluble fractions from black soldier fly larvae (comprising approximately 50% polysaccharides and 50% proteins exhibited the highest IRI activity (Fomich et al., 2025). Some polysaccharides themselves are recognized as cryoprotectants for frozen foods, such as κ-carrageenan (Leiter, Emmer, & Gaukel,

2018). Additionally, polysaccharides have been shown to influence the activity of AFPs. For example, the presence of corn starch (Monalisa, Shibata, & Hagiwara, 2021) and wheat flour (Monalisa, Shibata, & Hagiwara, 2023) can reduce ice crystal size in systems containing AFP III. This synergistic effect may be attributed to the hydration properties of starch, which may weaken water-AFP III interactions while simultaneously enhancing protein binding to ice crystal surfaces (Monalisa et al., 2023). Moreover, gum-based polysaccharides, including κ-carrageenan, also show cryoprotective synergy when combined with AFP I and antifreeze glycoproteins (AFGPs) (Gaukel, Leiter, & Spieß, 2014). However, other studies have showed antagonistic effects: in a system with whey protein isolate (WPI) and carrageenan, adding 5% WPI resulted in larger ice crystals than using carrageenan alone (Chun, Kim, & Min, 2012). These contrasting behaviors highlights the complexity of protein-polysaccharide interactions.

Research Gap and Hypothesis

While AFPs and protein hydrolysates have shown promise as cryoprotectants, their widespread industrial application still faces several challenges. First, the high cost and limited availability of current AFP sources necessitate the exploration of more accessible alternatives. Second, the structure-function relationships underlying ice crystallization process and how it can be inhibited by these polymers are complex and remain poorly understood, which restricts further design and identification of new peptides with enhanced IRI activity. Third, The IRI activity of antifreeze proteins and peptides may be influenced by salt concentrations, polysaccharides, and other food components when applied in real food systems.

To address these gaps, this project aims to develop novel antifreeze peptides and proteins derived from readily available and cost-effective food sources. Specifically, we focused on common food proteins such as zein, gelatin, and wheat proteins, which are abundant, economical, and widely accepted in food applications. Through chemical modification, enzymatic hydrolysis, purification and extraction, we identified and created peptides and proteins with enhanced IRI activity and elucidated their activity by structure-function relationships and interaction with water/ice. Furthermore, the influence of environmental factors, such as salt concentration and the presence of other components like polysaccharides, was systematically evaluated to optimize their performance in complex food systems. We further used molecular dynamics simulation to provide mechanistic explanation on the antifreeze activity. These comprehensive studies will ultimately contribute to improving the quality and stability of frozen foods.

Research Objectives

This project aims to develop novel anti-freeze peptides and proteins from widely available food proteins and investigate the relationship between their structure (e.g., conformation, surface amphiphilicity) and IRI activity.

Specific Objectives:

(1) To increase the IRI activity of zein and gelatin hydrolysate through modulating their surface amphiphilicity by succinylation modification.

(2) To study the effect of salt in dispersing media on IRI-active hydrolysates from wheat glutenin.

(3) To characterize IRI-active proteins from wheat flour and investigate their interactions with water and ice using molecular dynamics simulations.

(4) To investigate the effect of polysaccharides on the IRI activity of protein hydrolysates

(5) To examine how peptide secondary structure influences IRI activity through molecular dynamics simulations.

REFERENCES

Arai, T., Nishimiya, Y., Ohyama, Y., Kondo, H., & Tsuda, S. (2019). Calcium-binding generates the semi-clathrate waters on a type II antifreeze protein to adsorb onto an ice crystal surface. *Biomolecules, 9*(5). https://doi.org/10.3390/biom9050162.

Biggs, C., Stubbs, C., Graham, B., Fayter, A. E. R., Hasan, M., & Gibson, M. I. (2019). Mimicking the ice recrystallization activity of biological antifreezes. when is a new polymer "active"? *Macromol Biosci, 19*(7), e1900082. https://doi.org/10.1002/mabi.201900082.

Chen, X., Li, L., Yang, F., Wu, J., & Wang, S. (2020). Effects of gelatin-based antifreeze peptides on cell viability and oxidant stress of Streptococcus thermophilus during cold stage. *Food and Chemical Toxicology, 136*, 111056. https://doi.org/https://doi.org/10.1016/j.fct.2019.111056.

Chun, J.-Y., Kim, J.-M., & Min, S.-G. (2012). Effect of whey protein isolate on ice recrystallization characteristics in whey protein isolate/κ-carrageenan matrix. *Food Science of Animal Resources, 32*(5), 627-634.

Conrad, Z. (2020). Daily cost of consumer food wasted, inedible, and consumed in the United States, 2001–2016. *Nutrition Journal, 19*(1), 35. https://doi.org/10.1186/s12937-020-00552-w.

Damodaran, S. (2007). Inhibition of ice crystal growth in Ice cream mix by gelatin hydrolysate. *J. Agric. Food Chem.*(55), 10918–10923.

Damodaran, S., & Wang, S. (2017). Ice crystal growth inhibition by peptides from fish gelatin hydrolysate. *Food Hydrocolloids, 70*, 46-56. https://doi.org/10.1016/j.foodhyd.2017.03.029.

Delesky, E. A. (2020). Ice recrystallization inhibition of ice-binding proteins and bioinspired synthetic mimics in non-physiological environments. University of Colorado at Boulder.

Delesky, E. A., & Srubar, W. V., 3rd. (2022). Ice-binding proteins and bioinspired synthetic mimics in non-physiological environments. *iScience, 25*(5), 104286. https://doi.org/10.1016/j.isci.2022.104286.

Eskandari, A., Leow, T. C., Rahman, M. B. A., & Oslan, S. N. (2020). Antifreeze Proteins and Their Practical Utilization in Industry, Medicine, and Agriculture. *Biomolecules, 10*(12), 1649. https://www.mdpi.com/2218-273X/10/12/1649.

Fomich, M., Día, V. P., Premadasa, U. I., Doughty, B., Krishnan, H. B., & Wang, T. (2023). Ice recrystallization inhibition activity of soy protein hydrolysates. *Journal of Agricultural and Food Chemistry, 71*(30), 11587-11598.

Fomich, M., Yuan, Y., Krishnan, H., Dia, V., & Wang, T. (2025). Isolation and characterization of ice recrystallization inhibitory molecules from black soldier fly larvae. *Journal of Insects as Food and Feed, 1*(aop), 1-21.

Fu, W., Wang, P., Chen, Y., Lin, J., Zheng, B., Zeng, H., & Zhang, Y. (2019). Preparation, primary structure and antifreeze activity of antifreeze peptides from Scomberomorus niphonius skin. *LWT, 101*, 670-677. https://doi.org/https://doi.org/10.1016/j.lwt.2018.11.067.

Gaukel, V., Leiter, A., & Spieß, W. E. L. (2014). Synergism of different fish antifreeze proteins and hydrocolloids on recrystallization inhibition of ice in sucrose solutions. *Journal of Food Engineering, 141*, 44-50. https://doi.org/10.1016/j.jfoodeng.2014.05.016.

Graham, B., Fayter, A. E. R., Houston, J. E., Evans, R. C., & Gibson, M. I. (2018). Facially amphipathic glycopolymers inhibit ice recrystallization. *J Am Chem Soc, 140*(17), 5682-5685. https://doi.org/10.1021/jacs.8b02066.

Gruneberg, A. K., Graham, L. A., Eves, R., Agrawal, P., Oleschuk, R. D., & Davies, P. L. (2021). Ice recrystallization inhibition activity varies with ice-binding protein type and does not correlate with thermal hysteresis. *Cryobiology, 99*, 28-39. https://doi.org/10.1016/j.cryobiol.2021.01.017.

Hayakari, K., & Hagiwara, Y. (2012). Effects of ions on winter flounder antifreeze protein and water molecules near an ice/water interface. *Molecular Simulation, 38*(1), 26-37.

Hudait, A., Qiu, Y., Odendahl, N., & Molinero, V. (2019). Hydrogen-bonding and hydrophobic groups contribute equally to the binding of hyperactive antifreeze and ice-nucleating proteins to ice. *J Am Chem Soc, 141*(19), 7887-7898. https://doi.org/10.1021/jacs.9b02248.

Judge, N., Georgiou, P. G., Bissoyi, A., Ahmad, A., Heise, A., & Gibson, M. I. (2023). High Molecular Weight Polyproline as a Potential Biosourced Ice Growth Inhibitor: Synthesis, Ice Recrystallization Inhibition, and Specific Ice Face

Binding. *Biomacromolecules, 24*(6), 2459-2468. https://doi.org/10.1021/acs.biomac.2c01487.

Leiter, A., Emmer, P., & Gaukel, V. (2018). Influence of gelation on ice recrystallization inhibition activity of κ-carrageenan in sucrose solution. *Food Hydrocolloids, 76*, 194-203. https://doi.org/10.1016/j.foodhyd.2016.11.028.

Leiter, A., Rau, S., Winger, S., Muhle-Goll, C., Luy, B., & Gaukel, V. (2016). Influence of heating temperature, pressure and pH on recrystallization inhibition activity of antifreeze protein type III. *Journal of Food Engineering, 187*, 53-61. https://doi.org/10.1016/j.jfoodeng.2016.04.019.

Li, M., Luckett, C. R., & Wu, T. (2022). Potent Time-Dependent Ice Recrystallization Inhibition Activity of Cellulose Nanocrystals in Sucrose Solutions. *Biomacromolecules, 23*(2), 497-504. https://doi.org/10.1021/acs.biomac.1c01201.

Liou, Y.-C., Tocilj, A., Davies, P. L., & Jia, Z. (2000). Mimicry of ice structure by surface hydroxyls and water of a β-helix antifreeze protein. *Nature, 406*(6793), 322-324.

Luo, W., Yuan, C., Wu, J., Liu, Y., Wang, F., Li, X., & Wang, S. (2023). Inhibition mechanism of membrane-separated silver carp hydrolysates on ice crystal growth obtained through experiments and molecular dynamics simulation. *Food Chem, 414*, 135695. https://doi.org/10.1016/j.foodchem.2023.135695.

Midya, U. S., & Bandyopadhyay, S. (2024). Ice Recrystallization Unveils the Binding Mechanism Operating at a Diffused Interface. *J Phys Chem B, 128*(5), 1170-1178. https://doi.org/10.1021/acs.jpcb.3c05934.

Mitchell, D. E., Clarkson, G., Fox, D. J., Vipond, R. A., Scott, P., & Gibson, M. I. (2017). Antifreeze protein mimetic metallohelices with potent ice recrystallization inhibition activity. *J Am Chem Soc, 139*(29), 9835-9838. https://doi.org/10.1021/jacs.7b05822.

Mitchell, D. E., & Gibson, M. I. (2015). Latent ice recrystallization inhibition activity in nonantifreeze proteins: Ca2+-activated plant lectins and cation-activated antimicrobial peptides. *Biomacromolecules, 16*(10), 3411-3416. https://doi.org/10.1021/acs.biomac.5b01118.

Mochizuki, K., & Molinero, V. (2018). Antifreeze glycoproteins bind reversibly to ice via hydrophobic groups. *J Am Chem Soc, 140*(14), 4803-4811. https://doi.org/10.1021/jacs.7b13630.

Monalisa, K., Shibata, M., & Hagiwara, T. (2021). Ice Recrystallization Behavior of Corn Starch/Sucrose Solutions: Effects of Addition of Corn Starch and Antifreeze Protein III. *Food Biophysics, 16*(2), 229-236. https://doi.org/10.1007/s11483-020-09664-6.

Monalisa, K., Shibata, M., & Hagiwara, T. (2023). Ice recrystallization inhibition behavior by wheat flour and its synergy effect with antifreeze protein III. *Food Hydrocolloids, 143*. https://doi.org/10.1016/j.foodhyd.2023.108882.

Nishimiya, Y., Kondo, H., Yasui, M., Sugimoto, H., Noro, N., Sato, R., . . . Tsuda, S. (2006). Crystallization and preliminary X-ray crystallographic analysis of Ca2+-independent and Ca2+-dependent species of the type II antifreeze protein. *Acta*

Crystallographica Section F: Structural Biology and Crystallization Communications, 62(6), 538-541.

Olijve, L. L., Meister, K., DeVries, A. L., Duman, J. G., Guo, S., Bakker, H. J., & Voets, I. K. (2016). Blocking rapid ice crystal growth through nonbasal plane adsorption of antifreeze proteins. *Proc Natl Acad Sci U S A, 113*(14), 3740-3745. https://doi.org/10.1073/pnas.1524109113.

Rojas, R., Aróstica, M., Carvajal-Rondanelli, P., Albericio, F., Guzmán, F., & Cárdenas, C. (2022). Relationship between type II polyproline helix secondary structure and thermal hysteresis activity of short homopeptides. *Electronic Journal of Biotechnology, 59*, 62-73. https://doi.org/10.1016/j.ejbt.2022.08.003.

Shah, S. H., Kar, R. K., Asmawi, A. A., Rahman, M. B., Murad, A. M., Mahadi, N. M., . . . Bhunia, A. (2012). Solution structures, dynamics, and ice growth inhibitory activity of peptide fragments derived from an antarctic yeast protein. *PLoS One, 7*(11), e49788. https://doi.org/10.1371/journal.pone.0049788.

Sicheri, F., & Yang, D. (1996). Structure determination of a lone α-helical antifreeze protein from winter flounder. *Acta Crystallographica Section D: Biological Crystallography, 52*(3), 486-498.

Suris-Valls, R., & Voets, I. K. (2019). The impact of salts on the ice recrystallization inhibition activity of antifreeze (glyco)proteins. *Biomolecules, 9*(8). https://doi.org/10.3390/biom9080347.

Trant, J. F., Biggs, R. A., Capicciotti, C. J., & Ben, R. N. (2013). Developing highly active small molecule ice recrystallization inhibitors based upon C-linked

antifreeze glycoprotein analogues. *RSC Advances, 3*(48). https://doi.org/10.1039/c3ra43835j.

Voets, I. K. (2017). From ice-binding proteins to bio-inspired antifreeze materials. *Soft Matter, 13*(28), 4808-4823. https://doi.org/10.1039/c6sm02867e.

Wang, F., Cui, M., Liu, H., Li, X., Yu, J., Huang, Y., & Liu, Y. (2021). Characterization and identification of a fraction from silver carp (Hypophthalmichthys molitrix) muscle hydrolysates with cryoprotective effects on yeast. *LWT, 137*. https://doi.org/10.1016/j.lwt.2020.110388.

Wang, S., Agyare, K., & Damodaran, S. (2009). Optimisation of hydrolysis conditions and fractionation of peptide cryoprotectants from gelatin hydrolysate. *Food Chemistry, 115*(2), 620-630. https://doi.org/10.1016/j.foodchem.2008.12.079.

Wu, X., Yao, F., Zhang, H., & Li, J. (2021). Antifreeze proteins and their biomimetics for cell cryopreservation: Mechanism, function and application-A review. *Int J Biol Macromol, 192*, 1276-1291. https://doi.org/10.1016/j.ijbiomac.2021.09.211.

Yang, F., Jiang, W., Chen, X., Chen, X., Wu, J., Huang, J., . . . Wang, S. (2022). Identification of novel antifreeze peptides from takifugu obscurus skin and molecular mechanism in inhibiting ice crystal growth. *J Agric Food Chem, 70*(44), 14148-14156. https://doi.org/10.1021/acs.jafc.2c04393.

Yuan, Y., Fomich, M., Dia, V. P., & Wang, T. (2023). Succinylation of zein and gelatin hydrolysates improved their ice recrystallization inhibition activity. *Food Chem, 424*, 136431. https://doi.org/10.1016/j.foodchem.2023.136431.

Zhang, Y., Liu, K., Li, K., Gutowski, V., Yin, Y., & Wang, J. (2018). Fabrication of anti-icing surfaces by short alpha-helical peptides. *ACS Appl Mater Interfaces, 10*(2), 1957-1962. https://doi.org/10.1021/acsami.7b13130.

Zhu, K., Zheng, Z., & Dai, Z. (2022). Identification of antifreeze peptides in shrimp byproducts autolysate using peptidomics and bioinformatics. *Food Chem, 383*, 132568. https://doi.org/10.1016/j.foodchem.2022.132568.

APPENDIX

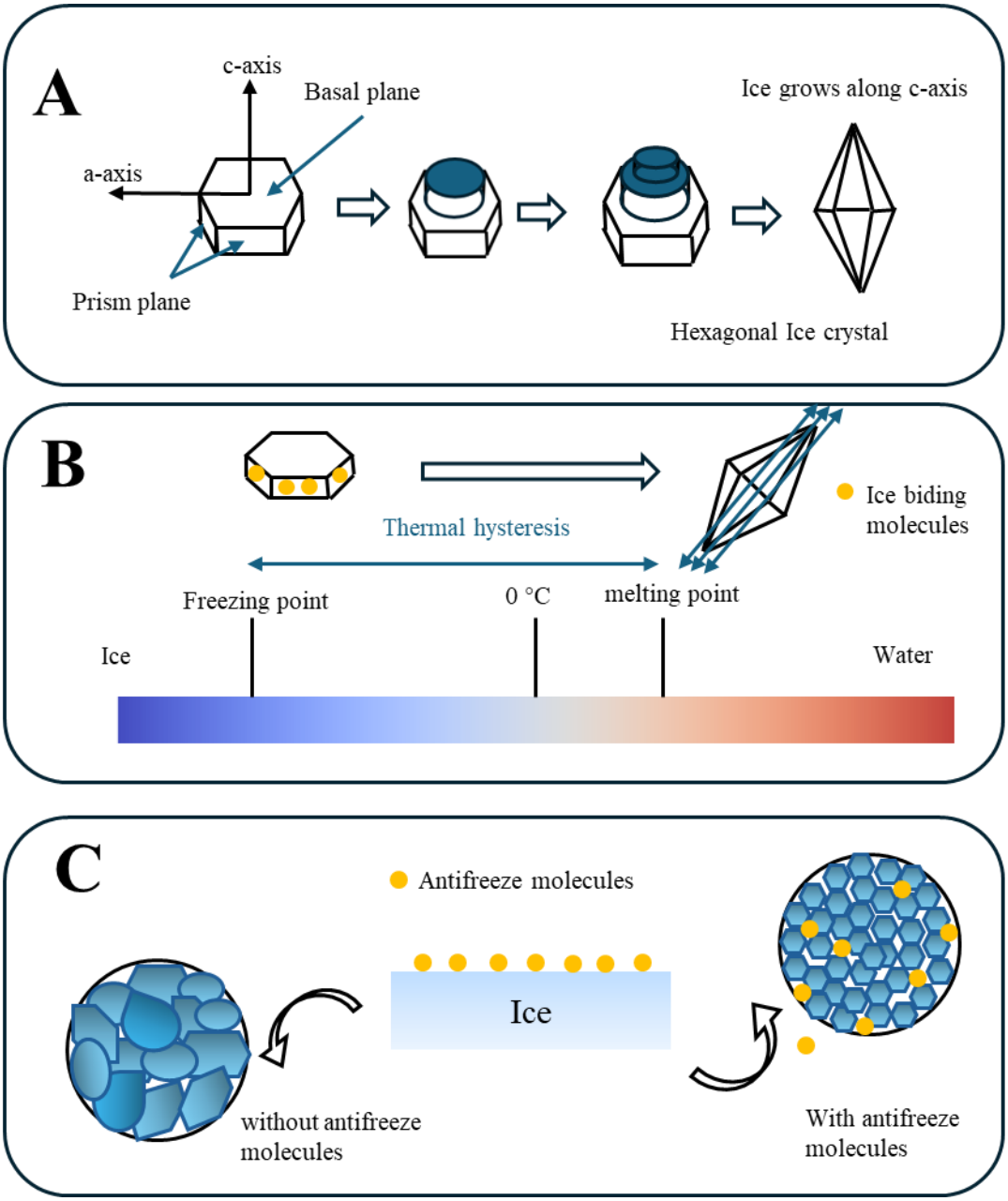

Figure 1.1. Mechanism of action of antifreeze molecules. A) ice shaping, B) Thermal hysteresis, and C) ice recrystallization inhibition.

CHAPTER TWO

SUCCINYLATION OF ZEIN AND GELATIN HYDROLYSATES IMPROVED THEIR ICE RECRYSTALLIZATION INHIBITION ACTIVITY

A version of this chapter was originally published by Yuan Yuan, Madison Fomich, Vermont P. Dia, and Tong Wang.

Vera:

Yuan, Y., Fomich, M., Dia, V. P., & Wang, T. (2023). Succinylation of zein and gelatin hydrolysates improved their ice recrystallization inhibition activity. Food Chemistry, 424, 136431.

Abstract

The goal of this research was to enhance the ice recrystallization inhibition (IRI) activity of zein and gelatin hydrolysates (ZH and GH, respectively) by succinylation modification. ZH was prepared by Alcalase treatment for 3 h and then modified by succinic anhydride (SA); whereas GH was made by Alcalase hydrolysis for 0.25 h and succinylated by n-octylsuccinic anhydride (OSA). After 0.5 h of annealing at -8 °C at 40 mg/mL, modified hydrolysates decreased the average Feret's diameter of ice crystal from 50.2 μm (polyethylene glycol, negative control) to 28.8 μm (SA modified ZH) and 29.5 μm (OSA modified GH) in comparison to the unmodified hydrolysates, which had the crystal size of 47.2 μm (ZH) and 45.4 μm (GH). Also, the two succinylated samples had altered surface hydrophobicity, which potentially contributed to their enhanced IRI activity. Our results indicate that succinylation of food-derived protein hydrolysates can improve their IRI activity.

Introduction

Ice crystal growth during cold storage is a quality issue in frozen foods, and finding effective agents to prevent ice from continuing to grow is an active research topic.

Antifreeze proteins (AFPs) are excellent candidates for inhibiting ice crystal growth and are produced in nature by fish, arthropods, winter plants, bacteria, and fungi that have evolved to survive in sub-freezing temperatures. AFPs help reduce cell damage during cryopreservation ((Damodaran, 2007; Harding, Anderberg, & Haymet, 2003). Although the mechanisms of AFPs generally include thermal hysteresis (TH) and ice binding activity, with the latter being considered to be more relevant (Gruneberg, Graham, Eves, Agrawal, Oleschuk, & Davies, 2021), the mechanism of each class of cryoprotective compound may be different (Biggs, Stubbs, Graham, Fayter, Hasan, & Gibson, 2019). Previous studies suggested that hydrogen bonding is the main driving force of ice binding (Damodaran, 2007; Damodaran & Wang, 2017). For example, peptides from gelatin, rich in hydroxyl groups, can bind to the prism face of ice by hydrogen bonding (Damodaran et al., 2017) and inhibit ice recrystallization and growth. Meanwhile, polyvinyl alcohol (PVA) prevents ice growth through adjacent hydroxyl groups (Wu, Yao, Zhang, & Li, 2021). In addition, hydrophobicity is an important characteristic of antifreeze activity (Hudait, Qiu, Odendahl, & Molinero, 2019). Mutants' substitution experiments indicate that hydrophobic methyl groups of type I and III AFPs contribute to the ice growth inhibition (Haymet, Ward, & Harding, 1999; Hudait et al., 2019). Furthermore, the addition of long hydrophobic groups (alkyl chains) significantly increased galactose's ice recrystallization inhibition (IRI) activity significantly (Balcerzak, Febbraro, & Ben, 2013). However, increasing hydrophobicity substantially will result in aggregation and lower solubility, decreasing IRI activity. Therefore, the balance between the hydrophobic and hydrophilic domains is an important feature of IRI active molecules (Biggs et al.,

2019; Graham, Fayter, Houston, Evans, & Gibson, 2018). For example, antifreeze glycoproteins (AFGPs) interact with the ice through their hydrophobic peptide backbone while forming hydrogen bonds through their saccharide substituents (Mochizuki & Molinero, 2018).

In order to have a better understanding of IRI activity, gelatin peptides were studied in this work because their amino acid composition is approximately one-third proline and hydroxyproline, both of which contain functional groups capable of hydrogen bonding during the IRI process (Damodaran et al., 2017; Giménez, Alemán, Montero, & Gómez-Guillén, 2009). However, gelatin by itself does not provide an effective hydrophobic moiety and it has high water solubility. On the other hand, zein is rich in non-polar amino acids such as leucine and alanine (Gong, Aguirre, & Bassi, 2016), thus it is more hydrophobic and has traditionally been used to make a variety of bioactive peptides, such as ACE inhibitory peptides (Lin et al., 2011) and anti-alcoholism peptides (Laniewska-Dunaj, Jelski, Orywal, Kochanowicz, Rutkowski, & Szmitkowski, 2013). It is safe, abundant, and feasible to obtain as a by-product of corn starch isolation and ethanol production (Cheng & Jones, 2017). Thus, zein and gelatin were used as a pair of proteins with different amino acid composition and solubility profiles to study how enzyme hydrolysis and succinylation modification affect their IRI activity.

It is expected that peptide modification will improve IRI activity by modulating their hydrophilic and hydrophobic domains. As a result, succinylation was selected in this study because it can change the surface hydrophobicity (Shilpashree, Arora, Chawla, & Tomar, 2015) of most proteins, such as whey protein isolate (Pan, Li, Meng, & Zhang,

2020), to various extents. In addition, it is a generally recognized as safe (GRAS) agent according to the Food and Drug Administration, with no limitations other than good manufacturing practices (Wan, Liu, & Guo, 2018). There are two agents that can be used in succinylation: succinic anhydride (SA) and n-octylsuccinic anhydride (OSA). When peptides are modified by SA, carboxylic groups and a negative charge can be introduced to the zein peptides (Yang, Yang, Zhang, & Zhang, 2016), resulting in increased hydrophilicity. Compared to SA, OSA has an octyl group that is hydrophobic, and when it is added to the gelatin peptide, it will increase hydrophbicity. Thus, by comparing the ice crystal size of peptides succinylated with SA or OSA, we may determine the influence of hydrophobic and hydrophilic groups on IRI activity. Our hypothesis is that the balance between hydrophilicity and hydrophobicity of peptides will affect their corresponding IRI activities. Therefore, the objectives of this study were to investigate the effect of enzymatic hydrolysis and succinylation on the IRI activity of gelatin hydrolysates (GH) and zein hydrolysates (ZH), and to determine the effect of concentration and pH on activity. This study is the first to report on the comparative IRI activity of zein and gelatin hydrolysates as affected by succinylation. It is expected that this work will advance our knowledge of how to create peptides with IRI activity from easily accessible protein sources.

Materials and methods

Materials

Zein was purchased from Acros Organics (New Jersey, USA), and the protease from *Bacillus licheniformis* (Alcalase, 3.03 U/mL) was from EMD Millipore Corp

(Massachusetts, USA). Knox gelatin was purchased from a local supermarket. Polyethylene glycol 400 (PEG, M_W 380 - 420 Da) was purchased from Sigma Aldrich (Saint Louis, MO). SA was purchased from Thermo Fisher Scientific (Massachusetts, USA) and OSA was from TCI America (Oregon, USA).

Preparation of zein and gelatin hydrolysates by Alcalase

In 400 mL of 50 % ethanol, 8 g of zein was dissolved. Then, the pH of zein solution was adjusted to 8.0 with 1 N NaOH. Alcalase was then added at an enzyme-to-substrate ratio of 0.176 Anson units/g zein. The mixture was incubated at 55 ℃ for 1, 3, and 6 h. The hydrolysates were boiled for 1.5 h to remove ethanol and inactivate the enzymes. After centrifugation at 10000 x g for 10 min at room temperature, the supernatant was collected and freeze-dried before use. For the preparation of GH, gelatin (2.5 % w/v aqueous solution) was hydrolyzed using Alcalase at 55 ℃ for 0.25, 0.5, 1, and 2 h. After the pH of the solution was adjusted to 8.0 by 1 N NaOH, Alcalase was added at an enzyme-to-substrate ratio of 0.176 Anson units/g gelatin. The samples were treated the same as above, but the boiling time is just 10 min.

Quantifying the degree of hydrolysis (DH) by the o-pthaldialdehyde (OPA) method

Degree of hydrolysis of the hydrolysate samples was analyzed based on the methods of Spellman, McEvoy, O'Cuinn, and FitzGerald (2003) with slight modifications. Fresh OPA reagent was prepared by mixing 25 mL of 100 mM sodium borate, 2.5 mL of 20 % SDS solution, 1 mL of 40 mg/mL OPA dissolved in methanol, 100 μL β-mercaptoethanol, and DI water adjusting the solution to a total volume of 50 mL. The peptide samples were prepared with a concentration of 1 mg/mL in 1x PBS buffer. Ten

μL of each sample was placed in a well in a 96-well plate and filled with 200 μL of freshly prepared OPA reagent. Two blank wells were also filled with 1x PBS buffer. The absorbance was read at 340 nm after 5 min incubation. Absorbance was read using a Cambrex ELx808 Microplate Reader. DH values were calculated using the following formula:

$$DH\% = \frac{100n}{N}$$

where n is the OD value of sample, N is the OD value of totally hydrolyzed protein by HCl prepared as follows: briefly, 1 mg nonhydrolyzed protein sample was mixed with 500 μL 6 N HCl and incubated in a 110 ℃ oven overnight. After cooling to the room temperature, 500 μL 6 N NaOH was added to neutralize the system, and the same OPA procedure was applied.

Determining average molecular weight of gelatin and zein hydrolysates by size exclusion chromatography

The molecular weight distribution for each hydrolysate and protein sample was analyzed using a size exclusion (BioSep-SEC -s2000 column Phenomenex, Torrence, CA, USA) HPLC. The mobile phase consisted of a mixture of acetonitrile and ultrapure water in a proportion of 45:55 (v/v), containing 0.05 % trifluoroacetic acid. Isocratic elution was carried out using a flow rate of 1.0 mL/min for 20.0 min with sample injection volume of 20 μL. To determine the molecular weight distribution of the samples, the elution profile was compared to that of mixture of protein standards with known molecular weights (M_w) detected at 214 nm. The retention times and the log of M_w of the standards were used to construct a linear curve fit (R^2 = 0.981) and the established standard curve

equation was used to calculate the M_w of each peak in the chromatogram. The average M_w was calculated based on the percentage contribution of each peak as determined by area under the curve. When calculating the average molecular weight, the peak of M_w < 200 Da was excluded.

Measuring the surface hydrophobicity of the hydrolysate samples

The surface hydrophobicity of the hydrolysates and their modified counterparts was determined by fluorescence spectroscopy with 1-anilino-8-naphthalene sulfonate (ANS) as a probe. The hydrolysates and modified samples (5 mg) were mixed with 1 mL of 1xPBS and vortexed for 1 hour at room temperature. After centrifugation at 10000 x g for 30 min at 4 °C, the supernatants were collected and diluted with PBS to obtain a range of concentrations between 0.0156 and 0.5 mg/mL. Diluted samples were mixed with ANS reagent on a black polystyrene 96-well microplate. The fluorescence intensity was measured at excitation and emission wavelengths of 390 and 479 nm, respectively (Synergy H1, BioTek, USA). The slope of the curve of the relative fluorescence intensity as a function of protein concentration was reported as the surface hydrophobicity of the sample.

Modification of hydrolysates by succinylation reaction

ZH were modified by SA based on a procedure from previous studies with minor modifications (Shilpashree et al., 2015; Wan et al., 2018). One gram of ZH was dispersed in 125 mL ammonium bicarbonate buffer (pH = 8.0, 0.075 M). SA was added at a molar ratio (based on the reactive amino group) of 1:1. The suspension was stirred vigorously at 700 rpm and sampled periodically, and the samples were incubated in a water bath at 70

℃ to evaporate the volatile buffer salt (Smith, 1994). The optimum reaction time was determined by the amount of the residual amino group at various reaction times. The residual amino group was quantified by the OPA method as above. GH was also modified by OSA with the same procedure.

Determining secondary structure by Fourier-transform infrared spectroscopy (FTIR)

The secondary structure of hydrolysates was analyzed by FTIR (Jiang et al., 2011) using Spectrum Two FT-IR Spectrometer (PerkinElmer Inc., Waltham, MA, US). Hydrolysates and their succinylated forms were prepared in 1 x PBS solution at a concentration of 40 mg/mL. The spectra were recorded with 32 scans in the region between 1800 and 1500 cm^{-1} range with a resolution of 4 cm^{-1} and data were analyzed using PerkinElmer Spectrum IR software. The amide I band (1600-1700 cm^{-1}) in each spectrum was interpreted by Peakfit Version 4.12 (Seasolve Software Inc, San Jose, CA, USA) software to determine peptide's secondary structure.

Analyzing IRI activity of hydrolysates by splat assay

The splat assay was carried out with sample solutions containing varying concentrations (1 - 40 mg/mL) prepared by dissolving in 1x PBS buffer, 180 mM HCl, or 180 mM NaOH. Ten µL of the peptide solution was dropped from a 1.5-meter height onto a precooled microscope slide and incubated at -80 ℃. The slide was annealed at -8 ℃ using a cold-stage HCS 302 (Instec Instruments, Boulder, CO) for 10, 20, 30, 40, 50, and 60 min, with pictures taken using the microscope's built-in digital camera (Leica Microsystems, Inc, USA), through the lens of L 20x/0.40. The negative control is 40 mg/mL polyethylene glycol (PEG) (Biggs et al., 2019). All hydrolysates and succinylated

samples were prepared in duplicate (trial 1 and trial 2), and each sample was analyzed twice (2 slides). Three pictures were captured from each slide, from which the Feret's maximum diameter was averaged by ImageJ software (Saad, Fomich, Dia, & Wang, 2023).

Statistical analysis

All data were reported as average ± standard deviation and processed by Excel 2016, and SPSS 22.0, and figures were prepared using Origin 2021 Pro. The statistical significance of the data was determined using one-way analysis of variance (ANOVA) followed by the Duncan test, and the significance was established at $P < 0.05$.

Results and Discussion

Degree of hydrolysis (DH) and average molecular weight (M_w) of peptides

During hydrolysis, Alcalase cut peptide bonds randomly, resulting in the production of peptides with various molecular sizes. Therefore, the extent of the enzymatic hydrolysis was assessed by analyzing DH % and average molecular weight of all samples. As shown in **Table 2.1**, the DH % increased as hydrolysis time was prolonged while the average M_w decreased. Previous studies have demonstrated that gelatin derived peptides have antifreeze activity, and the molecular weight of these peptides is between 150 to 2500 Da (Cao, Zhao, Zhu, Xu, Yu, & Yuan, 2016; Damodaran et al., 2017; Wang, Chen, Wu, & Wang, 2015), and our GH reported in this study are within this range. Traditionally, 70 - 90 % aqueous ethanol is used to dissolve zein (Li, Li, Xia, Zhang, Wang, & Huang, 2012). However, the activity of Alcalase in this concentration range was highly reduced (Simon, Kotorman, Garab, & Laczko, 2001). In order to have a balance between the

solubility of zein and protease activity, ethanol concentration was decreased to 50% to prepare ZH. However, the protease activity was lower in such organic solvent, so the DH % of ZH was lower than that of gelatin even if the hydrolysis time was longer. At the same 1 h hydrolysis time, gelatin DH % was 2-fold higher than zein DH % (25.8 % for gelatin and 12.7 % for zein). Furthermore, the molecule fraction representing amino acid residues accounted for nearly 70 % of ZH according to the HPLC chromatogram, but that in GH accounts for less than 10%. This is because zein with high M_w tends to be less soluble and Alcalase intensively worked more on solubilized protein and peptides. As a result, the small peptide became even more hydrolyzed and possibly produces free amino acids. However, gelatin is soluble in DI water and does not have this phenomenon.

Modification of zein and gelatin hydrolysates by succinylation reactions

As shown in **Fig. 2.1**, the degree of succinylation was determined by measuring the residual amount of free amino group. The reaction of ZH and SA reached a maximum of 83.1 % at 1 h, while the reaction of GH and OSA peaked at 11 h. Based on this, reaction times were set at 1 and 11 h for SA and OSA modifications, respectively, in the subsequent experiments. The reaction time of GH by OSA (GH + OSA) is longer because OSA is hydrophobic and has a lower aqueous solubility than SA, resulting in a slower reaction. In addition, gelatin contains roughly one third of proline and hydroxyproline, which have pyrrolidine ring that can also slow the succinylation reaction of the amino nitrogen (Harrington & Von Hippel, 1962).

The sizes of the ice crystals in samples with various hydrolysis times, as well as the corresponding succinylated samples, are shown in **Fig. 2.2 A-C**. In all modified

hydrolysates, whether they come from zein or gelatin, the size of the ice crystals is about 40% that of unmodified hydrolysates with the same analyte concentration (40 mg/mL). After modification, the ZH prepared by 3 h Alcalase hydrolysis has the smallest ice crystal size compared to the other two hydrolysates prepared at different times. This difference may be due to the different amino acid sequences or peptide size of the hydrolysates from different enzymatic treatments. The ice crystal size of all GH + OSA, on the other hand, was not significantly different ($P > 0.05$), even though the average M_w decreased significantly (**Table 2.1**). This demonstrates that the size of GH after modification has no effect on IRI activity. It may be due to the amino acid composition and sequences of GH. The small peptides in GH have tripeptide repeat sequences (Damodaran et al., 2017; Giménez et al., 2009), and are rich in Pro to form hydrogen bond interactions between the ice crystal surface and water. After modification, OSA provides an alkyl side chain to stabilize the interaction (Wu, Rong, Wang, Zhou, Wang, & Zhao, 2015), and the M_w may not impact such interaction significantly. In contrast, ZH does not have a repeat sequence, and the different hydrolysates may have different amino acid sequences that affect the IRI activity.

X. Wu et al. (2021) found that some cryoprotectants, such as dimethyl sulfoxide and graphene oxide, lower the freezing point or stick to the surface of ice crystals through hydrogen bonds. Simulation also provided some evidence that hydroxyl groups contribute to the strength of the binding of the AFPs to ice (Hudait et al., 2019). Therefore, the introduction of succinyl groups on ZH contribute to an increase in carboxylic groups (Basak & Singhal, 2022), which helps to control the size of ice

crystals.

In addition, hydrophobic groups play a key role in ice recrystallization. Type I and III antifreeze proteins bind ice via methyl groups (Haymet et al., 1999; Hudait et al., 2019).When a hydrophobic dimethylfulvene residue was incorporated on the glycan-opposing face, which was hydrophilic, the IRI activity of glycopolymers was significantly increased (Graham et al., 2018). Similarly, the IRI activity of the alkylated galactose derivatives increased when the addition of hydrophobic moieties (alkyl chains) went from seven to nine carbon atoms (Trant, Biggs, Capicciotti, & Ben, 2013). Furthermore, Hudait et al. (2019) used molecular simulations to show that methyl groups slow the movement of water at the ice-binding surface and stabilize the clathrate-like water in the anchored clathrate motif that binds these proteins to ice. Based on this, the addition of an octyl group in OSA, may also contribute to the IRI activity of GH + OSA.

Physicochemical characteristics of the modified hydrolysates

ZH, treatment by Alcalase for 3 h, had the smallest ice crystal size. Therefore, it was selected for further study. However, the IRI activity of all succinylated GH by OSA is similar; GH made by Alcalase for 0.25 h was chosen for further investigation.

Fig. 2.2D depicts the effect of succinylation treatments on surface hydrophobicity. This technique involves the use of ANS as the extrinsic fluorescence probe. After modification, the surface hydrophobicity of modified ZH decreased from 7.8 to 4.2 because of the additional charge (Basak et al., 2022), whereas when the GH was modified by OSA, the surface hydrophobicity increased from 0.6 to 5.3 due to the alkyl chain added. Therefore, all succinylated samples have a better balance between hydrophobic and hydrophilic

groups than unmodified hydrolysates. This balance has been proven to correlate with IRI activity (Biggs et al., 2019; Graham et al., 2018). For example, PVA, AFPs, and AFGPs are known to be amphipathic (Biggs et al., 2019; Mitchell, Clarkson, Fox, Vipond, Scott, & Gibson, 2017; Mitchell & Gibson, 2015). Mochizuki et al. (2018) also detected the conformation structure of AFGPs and found that they can bind to the ice by hydrophobic methyl group, while hydrophilic side is important to stabilize the unique structure. Based on this, several polymers were developed, including self-assembled triplex metallohelices (Mitchell et al., 2017) and poly(Fulvo) (Graham et al., 2018), to mimic the amphiphilic structure of AFGPs and demonstrate strong IRI activity. Also, it was found that some other IRI active materials had amphiphilic structures on their faces (Mitchell et al., 2015).

The percentage of secondary structure of hydrolysates and their succinylated forms is determined and shown in **Table 2.2**, and the FT-IR spectrum at 1600-1700 cm^{-1} is shown in **Fig. 2.3**. The band regions at 1610-1640 cm^{-1} and 1670-1690 cm^{-1} were assigned as β-sheet, and the random coil and α-helix ranges were 1640-1650 cm^{-1} and 1650-1660 cm^{-1}, respectively (Yuan et al., 2018). The peaks at 1660-1670 cm^{-1} and 1690-1700 cm^{-1} were also reported to result from β-turn (Jiang et al., 2011; Yuan et al., 2018). Prior to modification, the main secondary structure of ZH and GH is the β-sheet, accounting for 53.64% and 51.47%, respectively. This is consistent with the results of Zhang, Tu, Shen, and Dai (2019): the amide I band of GH from fish scale appeared at 1631 cm^{-1}, indicating that the β-sheet is the main secondary structure of GH. However, after modification, both ZH + SA and GH + OSA showed a decrease in β-turn and an increase in random coil and β-sheet, which means that the conformation become more flexible. This is also consistent

with previous findings that SA-induced succinylation of wheat gluten resulted in a transition from β-turn to β-sheet (Liu, Zhang, Li, Yang, Yang, & Wang, 2018). This is because the introduction of succinyl groups increased the electrostatic repulsions by negatively charge (Basak et al., 2022), which then made peptides more flexible, and the peptide chains were more stretched due to the reorganized hydrogen bonding (Wang, Gan, Zhou, Cheng, & Nirasawa, 2017). However, the structure of AFPs and AFGPs are rigid, which mainly based on α-helix and polyproline II helix, respectively (Mitchell et al., 2017; Mochizuki et al., 2018). This is different from the results of this study, which may be because the samples in this study are mixtures of short peptides while those in the previous studies were whole proteins.

The effect of concentrations of succinylated hydrolysates on IRI activity

As shown in **Fig. 2.4A**, the ice crystal size of ZH and PEG solutions was similar at all concentrations. However, ZH + SA showed strong IRI activity, with a crystal size of 28.8 μm compared to that of the negative control sample (PEG), which is 50.2 μm, at the concentration of 40 mg/mL. Even if the concentration was decreased to 1 mg/mL, the ice crystal diameter was still 66.0 μm compared to that of PEG which is 73.8 μm. The IRI activity was significantly increased after modification, especially at higher concentrations. Similarly, although GH had a little IRI activity at a concentration of 40 mg/mL (its crystal size is 45.4 μm, compared to the negative control sample is 50.2 μm), this activity was lost when the concentration decreased. However, the IRI activity of its succinylated version (GH + OSA) is enhanced at all concentrations and still has smaller ice crystals at a concentration as low as 2.5 mg/mL. These endpoint concentrations (1 and

2.5 mg/mL for modified ZH and GH, respectively) are similar to that obtained from previous facially amphiphilic polymers, which slow ice growth in a range from 1 to 10 mg/mL (Biggs et al., 2019). Also, Biggs et al. (2019) found that cryoprotectants with the same mechanism had similar concentrations at which they started to inhibit the growth of ice crystals during preservation. Thus, it also provides some evidence that the IRI activity is from their amphiphilic structure. In addition, the different IRI endpoint concentrations of modified ZH and GH suggest that the intensity of IRI activity is different. For example, type III antifreeze proteins have two isoforms (SP and QAE), and the endpoint concentrations of the latter are half those of the former, which showed that the IRI activity of SP isoforms is weaker than that of QAE (Gruneberg et al., 2021). They also found that the different IRI activity is due to different ice planes' binding activities due to the structure changes. Furthermore, Hudait et al. (2019) demonstrated that both hydrogen-bonding and hydrophobic groups contribute equally but differently to ice binding. It is possible that the balance between the hydrophobic and hydrogen-bonding groups in ZH + SA and GH + OSA have contributed to their enhanced and different IRI activities.

Effect of pH on the IRI activity of SA and OSA modified zein hydrolysates

In order to analyze the effect of charge on the IRI activity of peptides, NaOH and HCl were used because the peptides will carry a relatively more positive charge in acidic solutions and a more negative charge in alkaline solutions. The ionic concentration also needed to be controlled similarly to 1xPBS, so 180 mM NaOH and 180 mM HCl solutions were used, and their pH values are 12.46 and 1.20, respectively. **Fig. 2.4C-E**

show the ice crystal size of PEG solution remains similar in different pH solutions, but that in ZH and ZH + SA decreased from 60.1 and 41.8 μm in PBS to 46.0 and 26.6 μm in 180 mM NaOH. The ice crystal size increased to 91.1 and 55.7 μm in 180 mM HCl for ZH and ZH + SA, respectively, after 60 min of incubation. It is shown that two zein hydrolysates (ZH and ZH + SA) have higher IRI activity in alkaline solutions when all of them have a net negative charge. Similarly, this phenomenon was also shown in a previous study, in which the ice-binding protein from *Marinomonas primoryensis* (MpIBP), with a pI of 4.1, only exhibited IRI activity between pH 6 and pH 12, when it carried a net negative charge (Delesky, Thomas, Charrier, Cameron, & Srubar, 2021). Also, Burkey, Riley, Wang, Hatridge, and Lynd (2018) found that polymers with hydroxyl groups, like poly(ethylene oxide) (PEO), linear polyglycerol (PG), and poly(vinyl alcohol) (PVA), have higher IRI activity at high pH solution. They speculated that this might be because the pH affects hydrogen bonding in solutions.

Conclusion

In summary, succinylation is a feasible and safe way to enhance the IRI activity of ZH and GH by changing their hydrophobic and hydrophilic balance. ZH hydrolyzed by Alcalase for 3 h and then succinylated by SA had the highest IRI activity, while OSA modified GH made by Alcalase for different times have similar IRI activity. Modified peptides showed strong IRI activity at concentration as low as 2.5 mg/mL. Furthermore, the pH of the solution affected the IRI activity of the modified ZH, which shows that the overall negative charge can contribute in controlling ice crystal growth

REFERENCES

Balcerzak, A. K., Febbraro, M., & Ben, R. N. (2013). The importance of hydrophobic moieties in ice recrystallization inhibitors. *RSC Advances, 3*(10). https://doi.org/10.1039/c3ra23220d.

Basak, S., & Singhal, R. S. (2022). Succinylation of food proteins- a concise review. *Lwt, 154*. https://doi.org/10.1016/j.lwt.2021.112866.

Biggs, C., Stubbs, C., Graham, B., Fayter, A. E. R., Hasan, M., & Gibson, M. I. (2019). Mimicking the ice recrystallization activity of biological antifreezes. when is a new polymer "active"? *Macromol Biosci, 19*(7), e1900082. https://doi.org/10.1002/mabi.201900082.

Burkey, A. A., Riley, C. L., Wang, L. K., Hatridge, T. A., & Lynd, N. A. (2018). Understanding Poly(vinyl alcohol)-Mediated Ice Recrystallization Inhibition through Ice Adsorption Measurement and pH Effects. *Biomacromolecules, 19*(1), 248-255. https://doi.org/10.1021/acs.biomac.7b01502.

Cao, H., Zhao, Y., Zhu, Y. B., Xu, F., Yu, J. S., & Yuan, M. (2016). Antifreeze and cryoprotective activities of ice-binding collagen peptides from pig skin. *Food Chemistry, 194*, 1245-1253. https://doi.org/https://doi.org/10.1016/j.foodchem.2015.08.102.

Cheng, C. J., & Jones, O. G. (2017). Stabilizing zein nanoparticle dispersions with ι-carrageenan. *Food Hydrocolloids, 69*, 28-35. https://doi.org/10.1016/j.foodhyd.2017.01.022.

Damodaran, S. (2007). Inhibition of ice crystal growth in Ice cream mix by gelatin hydrolysate. *J. Agric. Food Chem.*(55), 10918–10923.

Damodaran, S., & Wang, S. (2017). Ice crystal growth inhibition by peptides from fish gelatin hydrolysate. *Food Hydrocolloids, 70*, 46-56. https://doi.org/10.1016/j.foodhyd.2017.03.029.

Delesky, E. A., Thomas, P. E., Charrier, M., Cameron, J. C., & Srubar, W. V., 3rd. (2021). Effect of pH on the activity of ice-binding protein from Marinomonas primoryensis. *Extremophiles, 25*(1), 1-13. https://doi.org/10.1007/s00792-020-01206-9.

Giménez, B., Alemán, A., Montero, P., & Gómez-Guillén, M. C. (2009). Antioxidant and functional properties of gelatin hydrolysates obtained from skin of sole and squid. *Food Chemistry, 114*(3), 976-983. https://doi.org/10.1016/j.foodchem.2008.10.050.

Gong, M., Aguirre, A. M., & Bassi, A. (2016). Chapter 5 - Technical issues related to characterization, extraction, recovery, and purification of proteins from different waste sources. In G. Singh Dhillon (Ed.), *Protein Byproducts* (pp. 89-106): Academic Press.

Graham, B., Fayter, A. E. R., Houston, J. E., Evans, R. C., & Gibson, M. I. (2018). Facially amphipathic glycopolymers inhibit ice recrystallization. *J Am Chem Soc, 140*(17), 5682-5685. https://doi.org/10.1021/jacs.8b02066.

Gruneberg, A. K., Graham, L. A., Eves, R., Agrawal, P., Oleschuk, R. D., & Davies, P. L. (2021). Ice recrystallization inhibition activity varies with ice-binding protein

type and does not correlate with thermal hysteresis. *Cryobiology, 99*, 28-39. https://doi.org/10.1016/j.cryobiol.2021.01.017.

Harding, M. M., Anderberg, P. I., & Haymet, A. D. (2003). 'Antifreeze' glycoproteins from polar fish. *Eur J Biochem, 270*(7), 1381-1392. https://doi.org/10.1046/j.1432-1033.2003.03488.x.

Harrington, W. F., & Von Hippel, P. H. (1962). The Structure of collagen and gelatin. In C. B. Anfinsen, M. L. Anson, K. Bailey & J. T. Edsall (Eds.), *Advances in Protein Chemistry* (pp. 1-138): Academic Press.

Haymet, A. D. J., Ward, L. G., & Harding, M. M. (1999). Winter flounder "antifreeze" proteins: synthesis and ice growth inhibition of analogues that probe the relative importance of hydrophobic and hydrogen-bonding interactions. *J. Am. Chem. Soc.*

Hudait, A., Qiu, Y., Odendahl, N., & Molinero, V. (2019). Hydrogen-bonding and hydrophobic groups contribute equally to the binding of hyperactive antifreeze and ice-nucleating proteins to ice. *J Am Chem Soc, 141*(19), 7887-7898. https://doi.org/10.1021/jacs.9b02248.

Jiang, Y., Li, C., Nguyen, X., Muzammil, S., Towers, E., Gabrielson, J., & Narhi, L. (2011). Qualification of FTIR spectroscopic method for protein secondary structural analysis. *J Pharm Sci, 100*(11), 4631-4641. https://doi.org/10.1002/jps.22686.

Laniewska-Dunaj, M., Jelski, W., Orywal, K., Kochanowicz, J., Rutkowski, R., & Szmitkowski, M. (2013). The activity of class I, II, III and IV of alcohol dehydrogenase (ADH) isoenzymes and aldehyde dehydrogenase (ALDH) in brain

cancer. *Neurochemical Research, 38*(7), 1517-1521. https://doi.org/10.1007/s11064-013-1053-9.

Li, Y., Li, J., Xia, Q., Zhang, B., Wang, Q., & Huang, Q. (2012). Understanding the dissolution of α-zein in aqueous ethanol and acetic acid solutions. *The Journal of Physical Chemistry B, 116*(39), 12057-12064. https://doi.org/10.1021/jp305709y.

Lin, F., Chen, L., Liang, R., Zhang, Z., Wang, J., Cai, M., & Li, Y. (2011). Pilot-scale production of low molecular weight peptides from corn wet milling byproducts and the antihypertensive effects in vivo and in vitro. *Food Chemistry, 124*(3), 801-807. https://doi.org/https://doi.org/10.1016/j.foodchem.2010.06.099.

Liu, Y., Zhang, L., Li, Y., Yang, Y., Yang, F., & Wang, S. (2018). The functional properties and structural characteristics of deamidated and succinylated wheat gluten. *International journal of biological macromolecules, 109*, 417-423.

Mitchell, D. E., Clarkson, G., Fox, D. J., Vipond, R. A., Scott, P., & Gibson, M. I. (2017). Antifreeze protein mimetic metallohelices with potent ice recrystallization inhibition activity. *J Am Chem Soc, 139*(29), 9835-9838. https://doi.org/10.1021/jacs.7b05822.

Mitchell, D. E., & Gibson, M. I. (2015). Latent ice recrystallization inhibition activity in nonantifreeze proteins: Ca2+-activated plant lectins and cation-activated antimicrobial peptides. *Biomacromolecules, 16*(10), 3411-3416. https://doi.org/10.1021/acs.biomac.5b01118.

Mochizuki, K., & Molinero, V. (2018). Antifreeze glycoproteins bind reversibly to ice via hydrophobic groups. *J Am Chem Soc, 140*(14), 4803-4811. https://doi.org/10.1021/jacs.7b13630.

Pan, Y., Li, X. M., Meng, R., & Zhang, B. (2020). Exploration of the stabilization mechanism and curcumin bioaccessibility of emulsions stabilized by whey protein hydrolysates after succinylation and glycation in different orders. *J Agric Food Chem, 68*(2), 623-632. https://doi.org/10.1021/acs.jafc.9b07350.

Shilpashree, B. G., Arora, S., Chawla, P., & Tomar, S. K. (2015). Effect of succinylation on physicochemical and functional properties of milk protein concentrate. *Food Research International, 72*, 223-230. https://doi.org/10.1016/j.foodres.2015.04.008.

Simon, L. M., Kotorman, M., Garab, G., & Laczko, I. (2001). Structure and activity of alpha-chymotrypsin and trypsin in aqueous organic media. *Biochem Biophys Res Commun, 280*(5), 1367-1371. https://doi.org/10.1006/bbrc.2001.4282.

Smith, B. J. (1994). Enzymatic methods for cleaving proteins. *Basic protein and peptide protocols*, 289-296.

Spellman, D., McEvoy, E., O'Cuinn, G., & FitzGerald, R. J. (2003). Proteinase and exopeptidase hydrolysis of whey protein: Comparison of the TNBS, OPA and pH stat methods for quantification of degree of hydrolysis. *International Dairy Journal, 13*(6), 447-453. https://doi.org/10.1016/s0958-6946(03)00053-0.

Trant, J. F., Biggs, R. A., Capicciotti, C. J., & Ben, R. N. (2013). Developing highly active small molecule ice recrystallization inhibitors based upon C-linked

antifreeze glycoprotein analogues. *RSC Advances, 3*(48). https://doi.org/10.1039/c3ra43835j.

Wan, Y., Liu, J., & Guo, S. (2018). Effects of succinylation on the structure and thermal aggregation of soy protein isolate. *Food Chem, 245*, 542-550. https://doi.org/10.1016/j.foodchem.2017.10.137.

Wang, W., Chen, M., Wu, J., & Wang, S. (2015). Hypothermia protection effect of antifreeze peptides from pigskin collagen on freeze-dried Streptococcus thermophiles and its possible action mechanism. *LWT - Food Science and Technology*, *63*(2), 878-885. https://doi.org/https://doi.org/10.1016/j.lwt.2015.04.007.

Wang, Y., Gan, J., Zhou, Y., Cheng, Y., & Nirasawa, S. (2017). Improving solubility and emulsifying property of wheat gluten by deamidation with four different acids: Effect of replacement of folded conformation by extended structure. *Food Hydrocolloids, 72*, 105-114. https://doi.org/https://doi.org/10.1016/j.foodhyd.2017.04.013.

Wu, J., Rong, Y., Wang, Z., Zhou, Y., Wang, S., & Zhao, B. (2015). Isolation and characterisation of sericin antifreeze peptides and molecular dynamics modelling of their ice-binding interaction. *Food Chemistry, 174*, 621-629. https://doi.org/https://doi.org/10.1016/j.foodchem.2014.11.100.

Wu, X., Yao, F., Zhang, H., & Li, J. (2021). Antifreeze proteins and their biomimetics for cell cryopreservation: Mechanism, function and application-A review. *Int J Biol Macromol, 192*, 1276-1291. https://doi.org/10.1016/j.ijbiomac.2021.09.211.

Yang, M., Yang, J., Zhang, Y., & Zhang, W. (2016). Influence of succinylation on physicochemical property of yak casein micelles. *Food Chemistry, 190*, 836-842. https://doi.org/https://doi.org/10.1016/j.foodchem.2015.06.030.

Yuan, H., Lv, J., Gong, J., Xiao, G., Zhu, R., Li, L., & Qiu, J. (2018). Secondary structures and their effects on antioxidant capacity of antioxidant peptides in yogurt. *International Journal of Food Properties*, *21*(1), 2167-2180. https://doi.org/10.1080/10942912.2018.1501700.

Zhang, Y., Tu, D., Shen, Q., & Dai, Z. (2019). Fish scale valorization by hydrothermal pretreatment followed by enzymatic hydrolysis for gelatin hydrolysate production. *Molecules, 24*(16). https://doi.org/10.3390/molecules24162998.

APPENDIX

Table 2.1. Degree of hydrolysis (DH) and average molecular weight (M_w) of protein hydrolysates generated by Alcalase treatment at different times.

Protein	Hydrolysis time (h)	DH (%) *	Average M_w (g/mol)
Zein	1	12.7±3.8	887.6±9.9[a]
	3	14.2±2.2	832.6±27.3[b]
	6	15.4±2.9	814.8±35.7[b]
Gelatin	0.25	20.3±1.2[b]	1784.4±71.2[a]
	0.5	22.0±1.6[b]	1181.6±108.0[b]
	1	25.8±0.8[ab]	973.0±91.7[c]
	2	29.4±1.8[a]	937.9±129.1[c]

*DH: degree of hydrolysis. Different superscripts in the same column indicate significant differences ($P < 0.05$).

Table 2.2. Secondary structure profiles of different hydrolysates as determined by FTIR.

samples	Secondary structure (%)			
	β-sheet	**random coil**	**α-helix**	**β-turn**
ZH	53.1±0.1	8.1±2.6	16.8±2.3	20.3±2.7
ZH + SA	61.7±0.8	10.1±0.5	19.0±1.9	9.3±2.0
GH	52.3±1.1	1.3±0.1	18.6±0.7	28.3±2.4
GH + OSA	63.4±0.7	6.8±0.2	14.7±0.5	15.2±0.4

ZH: zein hydrolysates made by Alcalase for 3 h, ZH + SA: zein hydrolysates made by Alcalase for 3 h and then succinylated by SA, GH: gelatin hydrolysates made by Alcalase for 0.25 h, GH+OSA: gelatin hydrolysates made by Alcalase for 0.25 h and then modified by OSA.

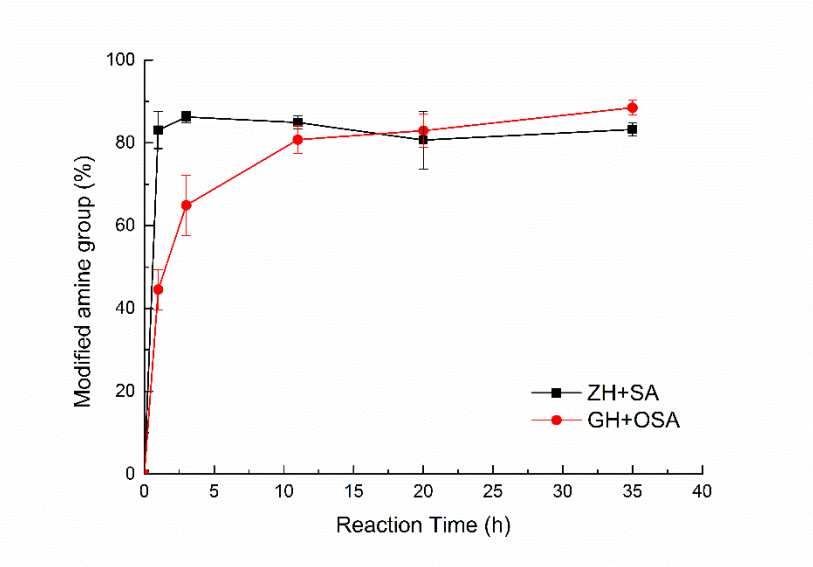

Figure 2.1. The degree of modification of zein hydrolysate (3 h) modified by SA (ZH + SA), and gelatin hydrolysates (0.25 h) modified by OSA (GH + OSA) during 35 h reaction at room temperature.

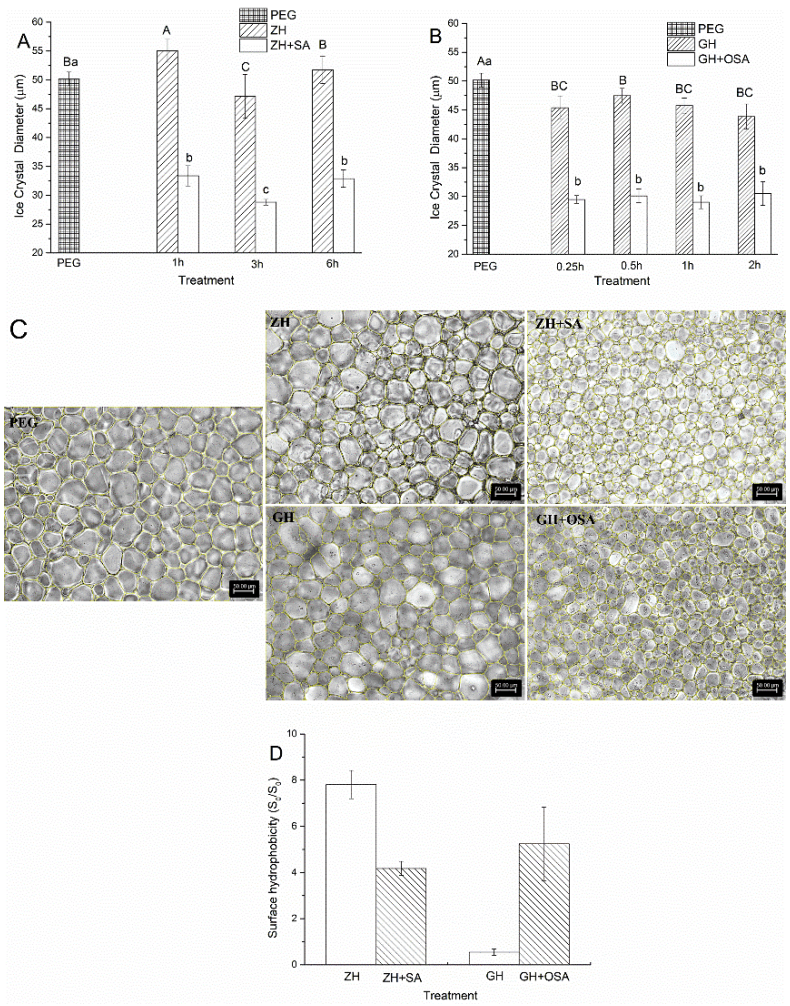

Figure 2.2. (A-B) Effect of hydrolysis time and succinylation modification on average Feret's diameter of ice crystal as affected by 40 mg/mL zein (A) and gelatin (B) and their succinylated forms. Different lowercase letters represent significantly different means of unmodified hydrolysates and capital letters represent significantly different means of succinylated samples ($p < 0.05$). (C) Microscopic images of PEG, ZH (3 h), ZH + SA, GH (0.25 h), and GH + OSA solution at 40 mg/mL concentration after annealing for 30 min at -8 °C under 20x/0.40 lens (scale = 50 μm). (D) The surface hydrophobicity of hydrolysates and their corresponding modified samples. The data were shown as the ratio of hydrolysates or modified hydrolysates to their corresponding protein.

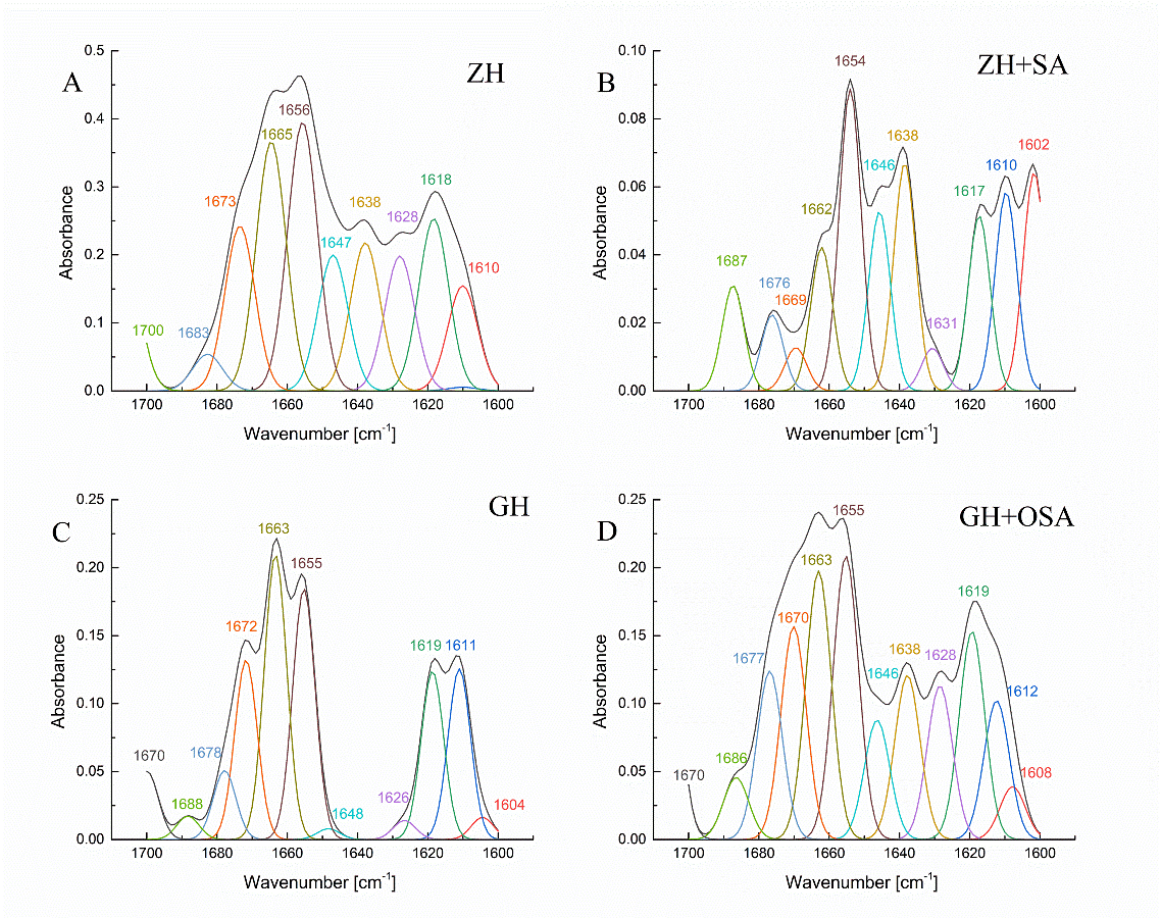

Figure 2.3. The FTIR spectra of amide I band (1700-1600 cm-1) of ZH (A), ZH + SA (B), GH (C) and GH + OSA (D) in 1xPBS buffer at 40 mg/mL concentration and at room temperature.

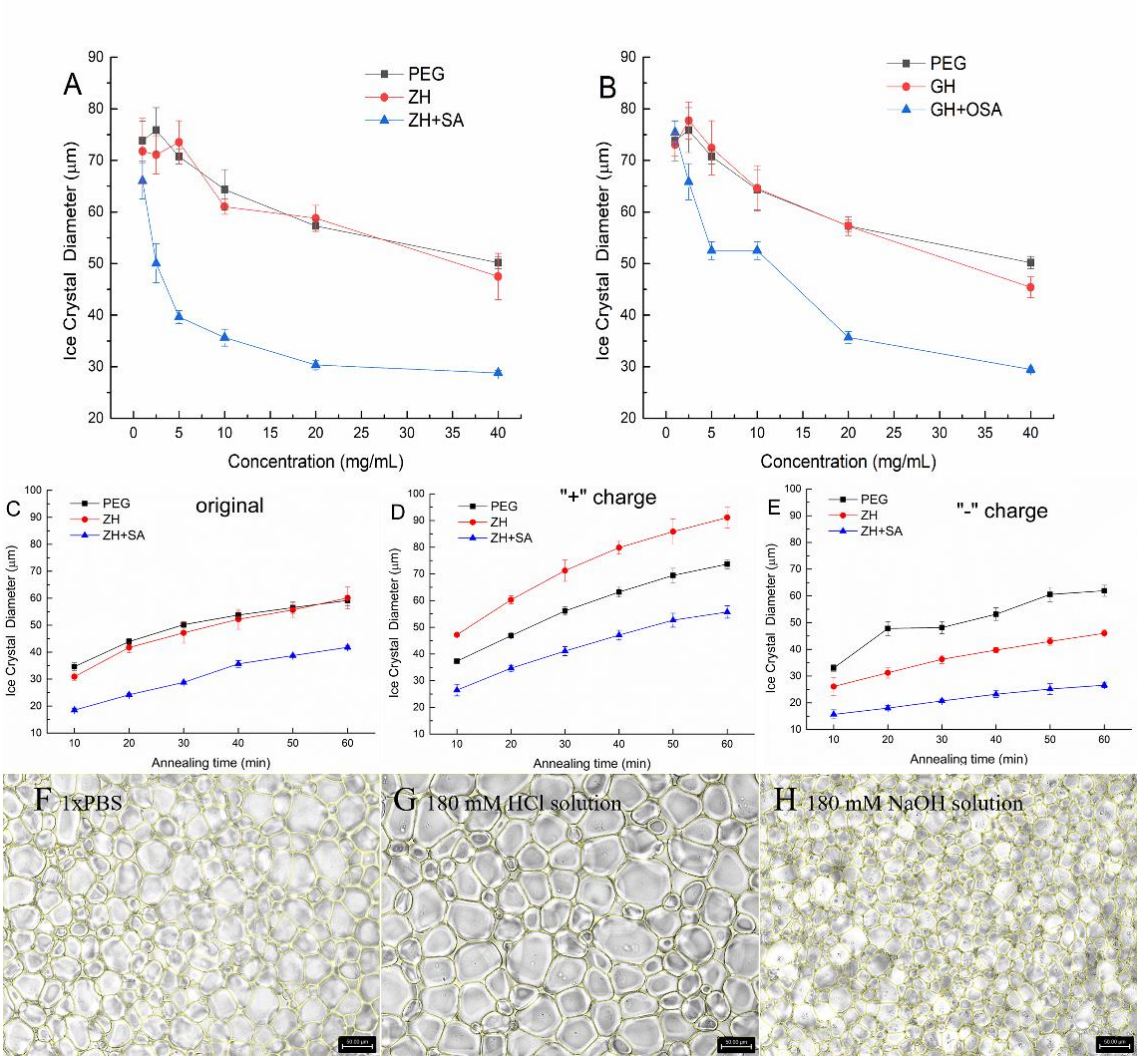

Figure 2.4. (A-B) Average Feret's diameter of ice crystals affected by succinylated ZH (3 h) and gelatin (0.25 h) hydrolysates by SA (A) and OSA (B) analyzed by splat assay in 1xPBS at different concentrations after 60 min at -8 °C annealing. (C-E) Average Feret's diameter of ZH and ZH + SA ice crystals measured by splat assay in 1xPBS (pH = 7.3) (C), 180 mm HCl (pH = 1.20) (D), and 180 mM NaOH (pH = 12.46) (E) solutions at 40 mg/mL (w/v) for 60 min. (F-H) Microscope images of ZH + SA in 1xPBS (pH = 7.3) (F), 180 mm HCl (pH = 1.20) (G), and 180 mM NaOH (pH = 12.46) (H) solution (c = 40 mg/mL) after annealing for 60 minutes at -8°C under 20x/0.40 lens (scale = 50 μm).

CHAPTER THREE

THE ICE RECRYSTALLIZATION INHIBITION ACTIVITY OF WHEAT GLUTENIN HYDROLYSATES AND EFFECT OF SALT ON THEIR ACTIVITY

A version of this chapter was originally published by Yuan Yuan, Vermont P. Dia, and Tong Wang.

Vera:

Yuan, Y., Dia, V. P., & Wang, T. (2024). The ice recrystallization inhibition activity of wheat glutenin hydrolysates and effect of salt on their activity. Food Hydrocolloids, 154, 110153.

Abstract

This study aimed to investigate the antifreeze activity of wheat glutenin hydrolysates produced by Alcalase and trypsin at varying degrees of hydrolysis. The influence of salt concentrations of two solutions (phosphate-buffered saline, PBS, and NaCl) and types of cations (NaCl and $CaCl_2$) in the dispersing media on hydrolysates was further analyzed. The results revealed a consistently higher ice recrystallization inhibition (IRI) activity for all hydrolysates dispersed in 0.1 x PBS than in 1 x PBS. Interestingly, glutenin hydrolysates exhibited better IRI activity in $CaCl_2$ than in NaCl solution under the same ionic strength. Furthermore, trypsin-derived hydrolysates (with a molar mass about 10 kDa) consistently had better IRI activity than those produced by Alcalase (with a molar mass less than 1 kDa), regardless of the dispersing media. The observed increase in IRI activity was associated with alterations in the secondary structure, characterized by a higher α-helix and lower β-turns content. This suggests that structural rigidity of the molecules plays a significant role in enhancing the antifreeze activity of peptides. Additionally, the scores plot of the partial least-squares discriminant analysis model indicates that salt concentration had a more significant impact than salt type on the IRI

activity of glutenin hydrolysates. In conclusion, our findings provide insights into the factors influencing the IRI activity of protein hydrolysates.

Introduction

Antifreeze peptides have long been studied for their potential applications in frozen food, as they can control the formation and growth of ice crystals (Biggs, Stubbs, Graham, Fayter, Hasan, & Gibson, 2019). Although the mechanism of these peptides is still elusive, some characteristics have been identified. Firstly, hydrophobic groups were reported to be associated with stronger antifreeze activity. For example, antifreeze glycoproteins can bind to ice through their hydrophobic methyl groups (Mochizuki & Molinero, 2018). Secondly, many antifreeze peptides contain proline residues (Damodaran & Wang, 2017; Kim., Damodaran., & Yethiraj., 2009; Yang et al., 2022). Computational modeling also showed that tetrapeptide with proline residues is more effective in retarding crystal growth compared to glycine (Kim. et al., 2009). Additionally, peptides with acidic amino acid residues like glutamic acid often exhibit superior antifreeze activity compared to peptides from other sources (Luo et al., 2023; Yang et al., 2022).

Wheat flour typically contains 10 - 15 % protein (Wieser, Koehler, & Scherf, 2022), with approximately 35 % of its amino acids being hydrophobic and proline-rich (Sivam, Sun-Waterhouse, Quek, & Perera, 2010). However, wheat protein is a complex mixture, and it is classified into four groups, namely albumin, globulin, gliadin, and glutenin, according to their solubilities in various solvents (Lookhart, 1995). The first two fractions are non-gluten proteins, constituting around 15 - 20 % of total wheat protein, while the latter two fractions, gliadin and glutenin, are classified as gluten proteins, accounting for approximately 80 - 85 % of the total wheat protein (Thewissen, Celus, Brijs, & Delcour,

2011). These fractions exhibit distinct molecular size, amino acid composition, and functionality. Gluten hydrolysates have demonstrated cryoprotective properties on frozen dough (Yanyan Zhang, Wang, Liu, Liu, Wang, & Zhang, 2022). However, the specific proteins or molecular characteristics of the protein hydrolysates responsible for this activity have not been elucidated in previous studies. Given that glutenin, the largest component of gluten (Urade, Sato, & Sugiyama, 2018), is hydrophobic and rich in proline and glutamic acid, the use of proteases to generate hydrolysates as antifreeze agents becomes pertinent. These hydrolysates, enriched with glutamic acid and proline residues, hold the potential to inhibit ice crystal growth originating from a common food protein.

The standard splat assay is a commonly used method for detecting ice recrystallization inhibition (IRI) activity (Delesky & Srubar, 2022). Typically, this assay is conducted in the presence of >2 mM NaCl or 1 x phosphate-buffered saline (PBS), which contains NaCl, KCl, Na_2HPO_4, and KH_2PO_4, to prevent false positives results (Voets, 2017). Despite its frequent use, few studies have investigated how different salt types and concentrations in dispersing media influence the IRI activity of peptides. In a study by Leiter, Rau, Winger, Muhle-Goll, Luy, and Gaukel (2016), the addition of 30 mM NaCl showed a synergetic effect with antifreeze protein (AFP) III under a 49 % sucrose solution condition. However, they did not explain the reason, and the sucrose concentration may be too high to accurately describe the effect of salt. Moreover, the choice of salt in the dispersing media can also influence the IRI effects of peptides. For example, Suris-Valls and Voets (2019) compared the ice crystal size of antifreeze

glycoprotein $(AFGP)_{1-5}$ and type III AFP in sodium nitrate, sodium chloride, sodium borate, sodium phosphate, and sodium citrate buffers and discovered that the citrate buffer consistently led to higher IRI activity for both proteins. In addition, certain Ca^{2+} ions have an additional impact on the antifreeze activity of proteins. For example, type II AFP exhibits Ca^{2+} dependent activity (Arai, Nishimiya, Ohyama, Kondo, & Tsuda, 2019).

Therefore, the choice of salts in dispersing media is not only crucial for IRI activity but also has a significant impact on the conformation of proteins. Salt at a low concentration stabilizes the proteins and hence impacts their conformation (Tsumoto, Ejima, Senczuk, Kita, & Arakawa, 2007). Moreover, different ions can influence the conformation of peptides, as observed in the orientation of Ca^{2+} binding residues in type II AFP in the presence of Ca^{2+} (Arai et al., 2019), which affects its ice-binding activity. The antifreeze activity of proteins is known to correlate with their rigid conformation (Patel & Graether, 2010). AFPs and AFGPs, known for their high IRI activity, possess rigid structures primarily due to α-helix and polyproline II helix, respectively (Mochizuki et al., 2018; Nishimiya et al., 2006; Sicheri & Yang, 1996). This characteristic has been used in the synthesis of triplex metallohelices, demonstrating potent IRI activity that emphasizes the importance of rigid helix structures on effective ice interaction (Mitchell, Clarkson, Fox, Vipond, Scott, & Gibson, 2017). In addition to IRI activity, peptides with a high α-helix structure also tend to exhibit higher thermal hysteresis activity (Rojas, Aróstica, Carvajal-Rondanelli, Albericio, Guzmán, & Cárdenas, 2022), which can related to antifreeze activity. Furthermore, antifreeze peptides from shrimp (Zhu, Zheng, & Dai, 2022), silver

carp (Wang et al., 2021), *Taki Fugu obscurus* skin (Yang et al., 2022), and Antarctic yeast protein (Shah et al., 2012) are all characterized by an α-helix structure. Peptides with an α-helix may have a more stable conformation, which is related to antifreeze activity (Zhang, Liu, Li, Gutowski, Yin, & Wang, 2018).

Based on these findings, our hypothesis is that wheat glutenin hydrolysates may exhibit potent IRI activity due to their unique amino acid profile, and the strength of this activity may be influenced by molecular size, secondary structure, and condition of dispersing media that modify their conformations. The objective of this study is to evaluate the IRI activity of wheat glutenin hydrolysates under different salt concentrations (0.1 x PBS and 1 x PBS) and salt solutions (NaCl and $CaCl_2$ solution) and correlate this to their secondary structure.

Materials and methods

Materials

Wheat flour (Bob's Red Mill) was purchased from the local grocery store. The Alcalase from *Bacillus licheniformis* (3.03 U/mL) was purchased from EMD Millipore Corp (Massachusetts, USA), and trypsin from porcine pancreas was purchased from Sigma-Aldrich company (Missouri, USA).

Glutenin hydrolysates preparation

The extraction of glutenin from wheat flour followed the Osborne fractionation method as outlined by Lookhart (1995) with a slight modification. In brief, 100 g of wheat flour underwent sequential extractions with DI water, 0.5 M NaCl, and 70% ethanol to eliminate albumin, globulin, and gliadin. Subsequently, the residual material was initially

combined with 400 mL of 50% 2-propanol (containing 1 % dithiothreitol) to disrupt disulfide bonds. After centrifugation at 5000 x g for 10 minutes, the precipitate was extracted with 400 mL of 0.05 M NaOH solution for three times. The extracted glutenin supernatant was dialyzed (3.5 kDa) and subsequently lyophilized. Given that glutenin is not soluble in aqueous 30 min. In the case of trypsin hydrolysis, the enzyme was introduced at a concentration of 180 units per gram of glutenin powder, and the pH was adjusted to 8.0 using 0.5 M NaOH. The hydrolysis times were 1, 2, 3, and 4 h. After completion of the hydrolysis process, all samples were boiled for 10 min to deactivate the enzyme. Subsequently, all samples were centrifuged for 5 min at 5000 x g, and the resulting supernatant was freeze-dried for further characterization and analysis. The yield of glutenin hydrolysates was calculated by the mass of freeze-dried supernatant relative to the mass of initial glutenin powder.

Amino acid composition and protein content determination

The method used was that of Akhlaghi, Ghaffari, Attar, and Alamir Hoor (2015), with slight modifications. Samples (1 mg/mL) were hydrolyzed by 6 M HCl at 150 °C for 30 min. After hydrolysis, the samples were dried under vacuum at 50 - 60 °C overnight, then sample buffer (50 mM $NaHCO_3$, pH = 8.4) was used to dissolve and dilute the sample. Subsequently, 200 µL of the diluted samples were mixed with 300 µL of 4 mM dabsyl chloride and vortexed for 30 seconds. The mixture was then heated at 70 °C for 20 min. Next, 500 µL of diluent solution, consisting of a mixture of 50 mM sodium phosphate buffer (pH = 7.0) and HPLC-grade ethanol was added. The resulting solutions were filtered by a 0.45 µm Nylon filter for HPLC analysis. HPLC analysis was performed

using a Zorbax Eclipse Plus C18 column under the following condition: 10 μL of injection volume, a flow rate of 1 mL/min, and a column temperature of 40 °C. The UV-Vis detector wavelength was 436 nm. Sodium acetate buffer (25 mM, pH = 6.5) containing 4 % dimethylformamide was used as mobile phase A, and acetonitrile was used as mobile phase B. A gradient elution program was employed with the following time (min)/percentage B values: 0/15, 20/40, 32/70, 34/70, 35/15, 45/15. To construct the standard curve, an amino acid (AA) standard mixture (Sigma, AA-S-18) containing 17 AA standards was utilized. The standards were prepared by diluting the standard mixture to concentrations of 1.56, 3.13, 6.25, 12.50, and 25.00 nanomoles of all amino acid standards in tubes using the sample buffer. The protein content determination was calculated by adding up the weights of all amino acids.

Phenol-sulfuric acid method for total carbohydrates assay

The method of Nielsen (2017) was used with slight modifications. Briefly, 1 mL sample (1 mg/mL) was mixed with 25 μL of 80 % phenol solution and 2.5 mL of concentrated sulfuric acid, and left to stand for 10 min. After cooling to room temperature, the absorbance was measured at 490 nm. Glucose was used as standard for qualification.

Size exclusion chromatography for average molecular weight determination

The molecular weight of glutenin and its corresponding hydrolysates was analyzed by a BioSep-SEC-s2000 column (Phenomenex, Torrance, CA, USA), with the mobile phase comprised of a 45:55 (v/v) mixture of acetonitrile and HPLC-grade water with 0.05 % trifluoroacetic acid. The molecular weight distribution was determined by comparing the elution profile with a mixture of protein standards with known molecular weights (M_w)

detected at 214 nm. Retention times and the logarithm of M_w for standards (albumin, aprotinin, bradykinin acetate, bradykinin fragment 1–5, glutathione, and glycine) were employed to construct a linear standard curve ($R^2 = 0.992$). The established standard curve equation was then utilized to calculate the M_w of each peak in the chromatogram. The average M_w was computed based on the percentage contribution of each peak, as determined by the area under the curve.

O-pthaldialdehyde (OPA) method for determining relative degree of hydrolysis

The degree of hydrolysis (DH) of hydrolysates was analyzed following a previous study (Spellman, McEvoy, O'Cuinn, & FitzGerald, 2003) with minor modifications. The fresh OPA reagent was prepared by combining 25 mL of 100 mM borax, 2.5 mL of a 20 % SDS solution, a solution containing 40 mg of OPA dissolved in 1 mL of methanol, 100 μL of β-mercaptoethanol, and DI water, adjusting the solution to a final volume of 50 mL. The hydrolysates were dissolved in 1x PBS solution at a concentration of 1 mg/mL. Ten μL of each sample was placed in a well in a 96-well plate and filled with 200 μL of the freshly prepared OPA reagent. A fully hydrolyzed glutenin was prepared by dissolving it in 6 M HCl at 110 °C overnight at a concentration of 1 mg/mL. Absorbance was read using a Cambrex ELx808 Microplate Reader at 340 nm after incubating for 5 min. The DH values were calculated using the following formula:

Splat assay for IRI activity

The splat assay was carried out as previously reported (Knight, Hallett, & DeVries, 1988) and calculated as we previously reported (Yuan, Fomich, Dia, & Wang, 2023), with sample solutions containing varying concentrations (1 - 40 mg/mL) prepared by

dissolving in 1x PBS, 0.1 x PBS, 10 mM NaCl, 10 mM $CaCl_2$, and 30 mM NaCl. Samples were prepared in duplicate and each sample was analyzed twice in independent slides. Three pictures were captured from each slide, from which the Feret's maximum diameter was averaged by ImageJ software (Saad, Fomich, Dia, & Wang, 2023).

Fourier transform infrared (FTIR) for secondary structure analysis of hydrolysates

The secondary structure of hydrolysates was analyzed by FTIR using Spectrum Two FT-IR Spectrometer (PerkinElmer Inc., Waltham, MA, US). Hydrolysates were prepared in 1 x PBS, 0.1 x PBS, 10 mM NaCl, 10 mM $CaCl_2$, and 30 mM NaCl solution at a concentration of 40 mg/mL. The spectra were recorded with 32 scans in the region between 1800 and 1500 cm^{-1} range with a resolution of 4 cm^{-1} and data were analyzed using PerkinElmer Spectrum IR software (Sadat & Joye, 2020). The amide I band (1600-1700 cm^{-1}) in each spectrum was interpreted by Origin 2021 Pro software to determine peptide's secondary structure. The band regions at 1610-1640 cm^{-1} and 1670-1690 cm^{-1} were assigned as β-sheet, and the random coil and α-helix ranges were 1640-1650 cm^{-1} and 1650-1660 cm^{-1}, respectively. The peaks at 1660-1670 cm^{-1} and 1690-1700 cm^{-1} were also reported to result from β-turn (Yuan et al., 2023).

Statistical analysis

The statistical analysis was performed based on the results of two independent trials of the experiment, and each trial was repeated 3 times. All data were reported as average ± standard deviation and processed by Excel 2016, and SPSS 22.0, and figures were prepared using Origin 2021 Pro. Principal component analysis (PCA) was created using Origin Pro apps, and partial least-squares discriminant analysis (PLS-DA) score plots

were derived with the SIMCA-P software (Version 14.1, Umetrics AB, Umea, Sweden). The statistical significance of the data was determined using one-way analysis of variance (ANOVA) followed by the Duncan test, and the significance was established at $P < 0.05$.

Results and discussion

Effect of enzyme type and hydrolysis time on peptides' size and IRI activity

After Osborne fractionation, the yield of glutenin is 7.6 % based on dry wheat flour powder. The protein content of the isolated glutenin accounted for 83.9 %, with 16.9 % carbohydrates. This result indicates that the extracted glutenin samples contain sufficient protein for further analysis. However, glutenin is not water-soluble, so proteases (Alcalase and trypsin) were used to increase its solubility. As the hydrolysis time increased, a rise in the yield of glutenin hydrolysates was observed, indicating a more solubilized mass over prolonged hydrolysis time. This trend is corroborated by the corresponding decrease in the average molecular weight of the hydrolysates, as shown in **Table 3.1**. The observed pattern suggests an increasing efficiency in the enzymatic treatment with extended hydrolysis times.

It is crucial to note the significant disparity in the hydrolytic capabilities of Alcalase and trypsin. The mass yield of Alcalase hydrolysates consistently exceeded 60 % within a short timeframe, typically less than half an hour. In contrast, trypsin hydrolysates, even with extended hydrolysis times of up to 4 hours, only reached a maximum yield of 50 %. Additionally, there is a substantial difference in the average molecular weight, with Alcalase hydrolysates typically falling below 1 kDa, while trypsin hydrolysates tend to be around 10 kDa. This difference arises from the fact that trypsin only cleaves peptide

bonds between Arg or Lys and the adjacent amino acid, while Alcalase can work on all types of peptide bond.

Despite all hydrolysates exhibiting weak IRI activity in the 1 x PBS solution compared to the negative polyethylene glycol (PEG) control, trypsin hydrolysates demonstrate significantly higher IRI activity compared to Alcalase hydrolysates. Specifically, the former inhibited the ice crystal size by approximately 30 %, while the latter showed less than a 20 % reduction, compared to negative control samples. It is significant, however, that previous studies on pig skin collagen, fish gelatin, and silver carp have consistently indicated that antifreeze peptides with molecular masses less than 3 kDa exhibited higher activity than those with molecular weights greater than 3 kDa (Chen, Wu, Cai, & Wang, 2021; Damodaran et al., 2017; Luo et al., 2023). It is important to recognize that these studies focused on animal-derived materials, while glutenin, being a plant protein, may exhibit different activity profiles. In addition, the profiles of peptides from different enzymes are distinct, which may contribute to the observed differences in activity.

Effect of amino acid profile on IRI activity

To analyze the effect of amino acid composition on IRI activity, four different glutenin hydrolysates generated with different enzymes and hydrolysis times (Try 1h, Try 2h, Alc 5m, and Alc 30m) were selected for further analysis. **Table 3.2** displays the amino acid profile of these glutenin hydrolysates. Notably, Glu constitutes a significant portion, accounting for over 60 % of the total amino acids. Additionally, Pro content is substantial, ranking second. This difference in amino acid composition is an important factor that can influence the antifreeze activity of peptides (Chen et al., 2021).

The correlation between Glu and Pro with IRI activity is supported by previous studies. Polymers, composed of glutamic acids, such as oligo- and poly(glutamic acid)s, have demonstrated antifreeze activity (Mitsuiki, Mizuno, Tanimoto, & Motoki, 1998). Additionally, Wang et al. (2021) identified seven antifreeze peptides from silver carp sharing the same Glu-Glu sequences, proposing that this sequence might be linked to ice binding sites. Molecular simulations conducted by Luo et al. (2023) may provide further evidence, showing that Glu and Asp residues in peptides from silver carp can bind more free water, effectively inhibiting the formation and nucleation of ice crystals. Moreover, the presence of acidic amino acids, including Glu and Asp, introduces a negative charge in neutral conditions, and this negative charge has been linked to higher antifreeze activity (Yuan et al., 2023). Furthermore, proline has been previously linked to cryoprotective activity. L-proline, for example, has proven useful in the cryopreservation of cells (Liu et al., 2023). Peptides rich in proline, such as gelatin (Damodaran et al., 2017), or those containing Pro (Kim. et al., 2009), have demonstrated the ability to inhibit the growth of ice crystals. Studies by Rojas et al. (2022) also indicated that polyproline peptides exhibit higher thermal hysteresis activity compared to other homopeptides, such as Arg and Lys.

Effect of salt concentration in dispersing media on IRI activity

Fig. 3.1 shows that all four hydrolysates exhibit higher antifreeze activity at 0.1 x PBS than 1 x PBS. Notably, hydrolysates produced by trypsin consistently show superior activity compared to those generated by Alcalase at 0.1 x PBS. Specifically, the ice crystal size of Try 1h and Try 2h is too small to be analyzed by the automated images

analysis program at the concentration of 40 mg/mL, and their ice crystal size relative to the same concentration of PEG (ICS %) values are 63.9 % and 70.9 %, respectively, even at a low concentration of 5 mg/mL. Additionally, the hydrolysate produced by Alcalase for 30 min exhibits significantly higher activity compared to the one produced for 5 min, particularly in the 0.1 x PBS solution. One interesting finding was the increase in hydrolysates' IRI activity as salt concentration decreased, observed in both PBS and NaCl solution. For example, ICS of Alcalase 5 min and Alcalase 30 min decreased by 26 % and 46 %, respectively, compared to the control. However, no significant difference in ice crystal size reduction is observed between the two trypsin samples, suggesting that salt concentration may have different impacts on glutenin peptides with different average molar masses.

The relationship between salt concentration and the IRI activity of antifreeze polymers is intricate and seemingly contradictory. Various studies have illustrated a synergistic effect between salt concentration and IRI activity. For instance, Leiter et al. (2016) observed an enhancement in the activity of antifreeze protein III (AFP III) with the addition of 30 mM NaCl. Similarly, Hayakari and Hagiwara (2012) reported that the interaction between winter flounder antifreeze proteins and the ice surface was intensified by adding 147 mM NaCl. Conversely, Delesky (2020) found that the addition of 151 mM salts such as $CaCl_2$, $MgCl_2$, $CuCl_2$, or $AlCl_3$ reduced the IRI activity of poly(2-hydroxypropylmethacrylamide) and eliminated the IRI activity of polythreonine. However, the underlying mechanisms of these effects remain unexplored. Building on these observations, Wu et al. (2017) compared the impact of various salt solutions,

without the presence of polymers, on the final crystal size at different salt concentrations. Their research showed the significant role of the Hofmeister series in final ice crystals size, although the study did not focus on the effects on materials active in IRI. Generally, the Hofmeister series seems to influence ice recrystallization, suggesting that the previous contradictory results may come from the differences in salt type. However, further research is needed to elucidate these interactions more clearly.

Effect of different cations on the IRI activity of wheat glutenin hydrolysates

In Fig. 3.2, the data for trypsin hydrolysates at 4 % were not included in the figure due to its unrecognizable small ice particles. Trypsin hydrolysates still displayed higher IRI activity than Alcalase hydrolysates in the $CaCl_2$ solution. In addition, all samples exhibited greater IRI activity in NaCl solutions compared to $CaCl_2$ solutions at the same concentration. However, the difference in antifreeze activity in trypsin hydrolysates was more pronounced than that in Alcalase hydrolysates.

It is important to note that the ionic strength of 10 mM NaCl and $CaCl_2$ solutions differs, and this variance in ionic strength could impact IRI activity. To ensure a fair comparison, we selected a 30 mM NaCl solution to equate the ionic strength of 10 mM $CaCl_2$. Interestingly, the ICS % of all hydrolysates is lower in the presence of Ca^{2+} at the same ionic strength (**Fig. 3.2**). Specifically, all four samples showed an ICS reduction of approximately 10 mM in $CaCl_2$ solution compared to NaCl solution at a concentration of 40 mg/mL, indicating that the type of cation also has an impact on IRI activity.

This suggests that Ca^{2+} can promote the IRI of glutenin hydrolysates compared to Na^{+}. A similar phenomenon was observed in Ca^{2+} dependent type II AFP, where Ca^{2+} binding

residues are preferable to binding ice only in the Ca^{2+}-bound state. The presence of ice-like clathrate waters induced by Ca^{2+} binding facilitates the ice-binding capability of these proteins as well (Arai et al., 2019). This Ca^{2+} promoted IRI activity was also shared in other Ca^{2+} dependent antifreeze proteins (Vance, Olijve, Campbell, Voets, Davies, & Guo, 2014) and certain lectins, such as soybean agglutinin, *R. communis* agglutinin, and human c-type lectins (Mitchell & Gibson, 2015). Despite being homologous to type II AFPs, these lectins are not inherent in antifreeze activity. However, the existence of Ca^{2+} ions could effectively switch on and off their IRI activity. However, glutenin is neither a Ca^{2+} dependent protein nor homologous to type II AFPs, so the reason for this phenomenon remains unclear. Wu et al. (2017) suggested that high charge density ions preferentially reside at the ice-water interface, inhibiting ice growth, whereas ions with relatively low anions charge density do not. Although this observation was specifically related to anions, cations might follow a similar pattern. Given that Ca^{2+} has a higher charge density than Na^{+}, this characteristic could be a contributing factor to the superior IRI activity of wheat glutenin hydrolysates in 10 mM $CaCl_2$ dispersing media.

Effect of dispersing medium on IRI activity of peptides

The FT-IR spectrum in the 1600-1700 cm^{-1} regions is shown in **Fig. 3.3**, and **Fig. 3.4** summarizes the secondary structure of hydrolysates in different dispersing media. Both figures showed that the salt concentration and types in the dispersing medium significantly influenced the secondary structure of peptides. Notably, a common trend across all hydrolysates was observed: lower salt concentrations (10-30 mM) led to an increase in α-helix content and a decrease in β-turn content compared to the 1 x PBS

solution with a concentration of about 150 mM. Furthermore, trypsin hydrolysates displayed a lower content of β-sheet structure in 0.1 x PBS than in 1 x PBS, whereas Alcalase hydrolysates did not exhibit this phenomenon. Additionally, the type of salt was found to impact the secondary structure. Under the same ionic strength, the content of α-helix in all four hydrolysates in a 10 mM $CaCl_2$ solution was higher than that in a 30 mM NaCl solution. In NaCl solutions, all hydrolysates tend to have minimal content of random coil, particularly in 30 mM NaCl. However, the secondary structure data for all samples in 10 mM $CaCl_2$ and NaCl solutions, on the other hand, were more like those in the 0.1 x PBS solution than the 1 x PBS solution. This suggests that salt concentration has a more significant influence than salt type on the conformation of peptides. Moreover, **Fig. 3.4** also demonstrated that two trypsin hydrolysates exhibited a higher content of α-helix than Alcalase hydrolysates in 1 x PBS and 0.1 x PBS solutions. Considering the relationship between the structure rigidity and IRI activity, this higher content of α-helix may provide an explanation for the higher IRI activity of trypsin hydrolysates (**Table 3.1**).

From Fig. 3.5, a significant negative correlation ($P < 0.001$) is evident between the α-helix content and the ICS %, with an R value of -0.56. Conversely, there is a significant positive correlation ($P = 0.005$) between the β-turn content and the ICS %, with an R value of 0.43. These findings suggest that as the α-helix content increases and the β-turn content decreases, there is a corresponding increase in the IRI activity for glutenin hydrolysates. The rise in α-helix content and the decline in β-turn content typically signify an increase in structural rigidity, a characteristic associated with higher antifreeze

activity (Patel, et al., 2010). Because of this, the observed changes in conformation, especially the higher amount of α-helix in the dispersing media, may help explain the improvement in the IRI activity.

The importance of dispersing medium on IRI activity of glutenin hydrolysates

To discern discrimination in various dispersing media, PCA and PLS-DA methods were employed. A total of 40 data sets obtained from four glutenin hydrolysates (Alc 5m, Alc 30m, Try 1h, and Try 2h) dispersed in five different media (1 x PBS, 0.1 x PBS, 10 mM NaCl, 10 mM $CaCl_2$, 30 mM NaCl) were analyzed. In the PCA model, the first principal component contributed 50.6 %, and the second principal component contributed 28.7 % of the variance. The PCA score plot aimed to demonstrate if the glutenin hydrolysates could be categorized based on different dispersing media. The greater the distance between groups, the more distinct the samples are. **Fig. 3.6** displayed 95 % confidence ellipses overlapping with each cluster, indicating inadequate separation among groups, and suggesting that the PCA model did not effectively differentiate among the various dispersing media. However, it is noteworthy that the cluster of 1 x PBS exhibited relatively greater separation from the other groups, implying a more distinct profile in comparison. In addition, the direction of the arrows explained the correlation between the variables (Guo et al., 2023). Briefly, arrows pointing in the same direction indicate a positive correlation between the represented variables, while arrows pointing in opposite directions indicate a negative correlation. Among different secondary structures, there is an evident correlation between α-helix and antifreeze activity.

Fig 7B was used to validate the PLS-DA model reliability. According to established conventions, R2 is not to exceed 0.3-0.4, and Q2 should below 0.05, indicating the model does not suffering from overfitting (Eriksson, Byrne, Johansson, Trygg, & Vikström, 2013). However, adopting a more stringent criterion, all points on the left side should be below the right points, respectively, providing evidence of the model's reliability. The left data points represent Q_2 and R_2 values derived from 200 permutation tests, while the right two points illustrate Q_2 and R_2 values of the actual model (Eriksson et al., 2013; Li, Wang, Zeng, Liu, Huang, & Mei, 2018). In **Fig. 3.7A**, the PLS-DA plot illustrates a distinct separation between samples with 1 x PBS and those with lower concentration solutions. The solid points representing 1 x PBS are notably distant from other groups at low salt concentrations, underscoring the substantial influence of salt concentration compared to salt type. Furthermore, under similar salt concentrations, the position of the composite salt solution (0.1 x PBS) is slightly distant from the other three salt solutions with only one type of salt present. Samples in two different concentrations of NaCl solutions are closely grouped together, indicating that salt type still has an impact on the properties of gluten in hydrolysates, but this impact is less pronounced than the effect of salt concentration.

Conclusion

In summary, wheat glutenin hydrolysates, generated using Alcalase and trypsin, exhibited modest IRI activity in a 1 x PBS solution, potentially linked to their high content of Glu and Pro. Notably, trypsin-derived hydrolysates consistently demonstrated superior antifreeze properties compared to those produced by Alcalase in different dispersing

media, and these differences may stem from variations in molecular mass or peptide residues. One interesting finding was the increase in hydrolysates' IRI activity as salt concentration decreased, observed in both PBS and NaCl solution. Additionally, all hydrolysates showed higher IRI activity in $CaCl_2$ solution than in NaCl solution, under the same ionic strength, indicating that the type of cation also has an impact on IRI activity. However, salt concentration appears to have a more significant impact than salt type on IRI activity. The observed improvement in activity in different solutions correlated with changes in secondary structure, characterized by increased α-helix content and reduced β-turns. These findings suggest that the observed improvement in IRI activity for glutenin hydrolysates is associated with increased structural rigidity.

REFERENCES

Akhlaghi, Y., Ghaffari, S., Attar, H., & Alamir Hoor, A. (2015). A rapid hydrolysis method and DABS-Cl derivatization for complete amino acid analysis of octreotide acetate by reversed phase HPLC. *Amino Acids, 47*(11), 2255-2263. https://doi.org/10.1007/s00726-015-1999-9.

Arai, T., Nishimiya, Y., Ohyama, Y., Kondo, H., & Tsuda, S. (2019). Calcium-binding generates the semi-clathrate waters on a type II antifreeze protein to adsorb onto an ice crystal surface. *Biomolecules, 9*(5). https://doi.org/10.3390/biom9050162.

Biggs, C., Stubbs, C., Graham, B., Fayter, A. E. R., Hasan, M., & Gibson, M. I. (2019). Mimicking the ice recrystallization activity of biological antifreezes. when is a new polymer "active"? *Macromol Biosci, 19*(7), e1900082. https://doi.org/10.1002/mabi.201900082.

Chen, X., Wu, J., Cai, X., & Wang, S. (2021). Production, structure-function relationships, mechanisms, and applications of antifreeze peptides. *Compr Rev Food Sci Food Saf, 20*(1), 542-562. https://doi.org/10.1111/1541-4337.12655.

Damodaran, S., & Wang, S. (2017). Ice crystal growth inhibition by peptides from fish gelatin hydrolysate. *Food Hydrocolloids, 70*, 46-56. https://doi.org/10.1016/j.foodhyd.2017.03.029.

Delesky, E. A. (2020). Ice recrystallization inhibition of ice-binding proteins and bioinspired synthetic mimics in non-physiological environments. University of Colorado at Boulder.

Delesky, E. A., & Srubar, W. V., 3rd. (2022). Ice-binding proteins and bioinspired synthetic mimics in non-physiological environments. *iScience, 25*(5), 104286. https://doi.org/10.1016/j.isci.2022.104286.

Eriksson, L., Byrne, T., Johansson, E., Trygg, J., & Vikström, C. (2013). *Multi-and megavariate data analysis basic principles and applications*: Umetrics Academy.

Guo, H., Zheng, Y.-J., Wu, D.-T., Du, X., Gao, H., Ayyash, M., . . . Gan, R.-Y. (2023). Quality evaluation of citrus varieties based on phytochemical profiles and nutritional properties. *Frontiers in Nutrition, 10*, 1165841.

Hayakari, K., & Hagiwara, Y. (2012). Effects of ions on winter flounder antifreeze protein and water molecules near an ice/water interface. *Molecular Simulation, 38*(1), 26-37.

Kim., J. S., Damodaran., S., & Yethiraj., A. (2009). Retardation of ice crystallization by short peptides. *J. Phys. Chem. A*(113), 4403–4407.

Knight, C. A., Hallett, J., & DeVries, A. (1988). Solute effects on ice recrystallization: an assessment technique. *Cryobiology, 25*(1), 55-60.

Leiter, A., Rau, S., Winger, S., Muhle-Goll, C., Luy, B., & Gaukel, V. (2016). Influence of heating temperature, pressure and pH on recrystallization inhibition activity of antifreeze protein type III. *Journal of Food Engineering, 187*, 53-61. https://doi.org/10.1016/j.jfoodeng.2016.04.019.

Li, Y., Wang, D., Zeng, C., Liu, Y., Huang, G., & Mei, Z. (2018). Salivary metabolomics profile of patients with recurrent aphthous ulcer as revealed by liquid

chromatography–tandem mass spectrometry. *Journal of International Medical Research, 46*(3), 1052-1062. https://doi.org/10.1177/0300060517745388.

Liu, C., Feng, H., Han, J., Zhou, H., Yuan, L., Pan, H., . . . Li, X. (2023). Effect of L-proline on sperm quality during cryopreservation of boar semen. *Animal Reproduction Science, 258*, 107359. https://doi.org/https://doi.org/10.1016/j.anireprosci.2023.107359.

Lookhart, G. E. O. R., and Scott Bean. (1995). Separation and characterization of wheat protein fractions by high-performance capillary electrophoresis. *Cereal Chemistry, 72*(6), 527-532.

Luo, W., Yuan, C., Wu, J., Liu, Y., Wang, F., Li, X., & Wang, S. (2023). Inhibition mechanism of membrane-separated silver carp hydrolysates on ice crystal growth obtained through experiments and molecular dynamics simulation. *Food Chem, 414*, 135695. https://doi.org/10.1016/j.foodchem.2023.135695.

Mitchell, D. E., Clarkson, G., Fox, D. J., Vipond, R. A., Scott, P., & Gibson, M. I. (2017). Antifreeze protein mimetic metallohelices with potent ice recrystallization inhibition activity. *J Am Chem Soc, 139*(29), 9835-9838. https://doi.org/10.1021/jacs.7b05822.

Mitchell, D. E., & Gibson, M. I. (2015). Latent ice recrystallization inhibition activity in nonantifreeze proteins: Ca2+-activated plant lectins and cation-activated antimicrobial peptides. *Biomacromolecules, 16*(10), 3411-3416. https://doi.org/10.1021/acs.biomac.5b01118.

Mitsuiki, M., Mizuno, A., Tanimoto, H., & Motoki, M. (1998). Relationship between the antifreeze activities and the chemical structures of oligo- and poly(glutamic acid)s. *Journal of Agricultural and Food Chemistry, 46*(3), 891-895. https://doi.org/10.1021/jf970797m.

Mochizuki, K., & Molinero, V. (2018). Antifreeze glycoproteins bind reversibly to ice via hydrophobic groups. *J Am Chem Soc, 140*(14), 4803-4811. https://doi.org/10.1021/jacs.7b13630.

Nielsen, S. S. (2017). *Food analysis laboratory manual*: Springer.

Nishimiya, Y., Kondo, H., Yasui, M., Sugimoto, H., Noro, N., Sato, R., . . . Tsuda, S. (2006). Crystallization and preliminary X-ray crystallographic analysis of Ca2+-independent and Ca2+-dependent species of the type II antifreeze protein. *Acta Crystallographica Section F: Structural Biology and Crystallization Communications, 62*(6), 538-541.

Patel, S. N., & Graether, S. P. (2010). Increased flexibility decreases antifreeze protein activity. *Protein Sci, 19*(12), 2356-2365. https://doi.org/10.1002/pro.516.

Rojas, R., Aróstica, M., Carvajal-Rondanelli, P., Albericio, F., Guzmán, F., & Cárdenas, C. (2022). Relationship between type II polyproline helix secondary structure and thermal hysteresis activity of short homopeptides. *Electronic Journal of Biotechnology, 59*, 62-73. https://doi.org/10.1016/j.ejbt.2022.08.003.

Sadat, A., & Joye, I. J. (2020). Peak fitting applied to fourier transform infrared and raman spectroscopic analysis of proteins. *Applied Sciences, 10*(17). https://doi.org/10.3390/app10175918.

Shah, S. H., Kar, R. K., Asmawi, A. A., Rahman, M. B., Murad, A. M., Mahadi, N. M., . . . Bhunia, A. (2012). Solution structures, dynamics, and ice growth inhibitory activity of peptide fragments derived from an antarctic yeast protein. *PLoS One, 7*(11), e49788. https://doi.org/10.1371/journal.pone.0049788.

Sicheri, F., & Yang, D. (1996). Structure determination of a lone α-helical antifreeze protein from winter flounder. *Acta Crystallographica Section D: Biological Crystallography, 52*(3), 486-498.

Sivam, A. S., Sun-Waterhouse, D., Quek, S., & Perera, C. O. (2010). Properties of bread dough with added fiber polysaccharides and phenolic antioxidants: a review. *J Food Sci, 75*(8), R163-174. https://doi.org/10.1111/j.1750-3841.2010.01815.x.

Spellman, D., McEvoy, E., O'Cuinn, G., & FitzGerald, R. J. (2003). Proteinase and exopeptidase hydrolysis of whey protein: Comparison of the TNBS, OPA and pH stat methods for quantification of degree of hydrolysis. *International Dairy Journal, 13*(6), 447-453. https://doi.org/10.1016/s0958-6946(03)00053-0.

Suris-Valls, R., & Voets, I. K. (2019). The impact of salts on the ice recrystallization inhibition activity of antifreeze (glyco)proteins. *Biomolecules, 9*(8). https://doi.org/10.3390/biom9080347.

Thewissen, B. G., Celus, I., Brijs, K., & Delcour, J. A. (2011). Foaming properties of wheat gliadin. *J Agric Food Chem, 59*(4), 1370-1375. https://doi.org/10.1021/jf103473d.

Tsumoto, K., Ejima, D., Senczuk, A. M., Kita, Y., & Arakawa, T. (2007). Effects of salts on protein-surface interactions: applications for column chromatography. *J Pharm Sci, 96*(7), 1677-1690. https://doi.org/10.1002/jps.20821.

Urade, R., Sato, N., & Sugiyama, M. (2018). Gliadins from wheat grain: an overview, from primary structure to nanostructures of aggregates. *Biophys Rev, 10*(2), 435-443. https://doi.org/10.1007/s12551-017-0367-2.

Vance, T. D., Olijve, L. L., Campbell, R. L., Voets, I. K., Davies, P. L., & Guo, S. (2014). Ca2+-stabilized adhesin helps an Antarctic bacterium reach out and bind ice. *Biosci Rep, 34*(4). https://doi.org/10.1042/bsr20140083.

Voets, I. K. (2017). From ice-binding proteins to bio-inspired antifreeze materials. *Soft Matter, 13*(28), 4808-4823. https://doi.org/10.1039/c6sm02867e.

Wang, F., Cui, M., Liu, H., Li, X., Yu, J., Huang, Y., & Liu, Y. (2021). Characterization and identification of a fraction from silver carp (Hypophthalmichthys molitrix) muscle hydrolysates with cryoprotective effects on yeast. *LWT, 137*. https://doi.org/10.1016/j.lwt.2020.110388.

Wieser, H., Koehler, P., & Scherf, K. A. (2022). Chemistry of wheat gluten proteins: Quantitative composition. *Cereal Chemistry, 100*(1), 36-55. https://doi.org/10.1002/cche.10553.

Wu, S., Zhu, C., He, Z., Xue, H., Fan, Q., Song, Y., . . . Wang, J. (2017). Ion-specific ice recrystallization provides a facile approach for the fabrication of porous materials. *Nat Commun, 8*, 15154. https://doi.org/10.1038/ncomms15154.

Yang, F., Jiang, W., Chen, X., Chen, X., Wu, J., Huang, J., . . . Wang, S. (2022). Identification of novel antifreeze peptides from takifugu obscurus skin and molecular mechanism in inhibiting ice crystal growth. *J Agric Food Chem, 70*(44), 14148-14156. https://doi.org/10.1021/acs.jafc.2c04393.

Yuan, Y., Fomich, M., Dia, V. P., & Wang, T. (2023). Succinylation of zein and gelatin hydrolysates improved their ice recrystallization inhibition activity. *Food Chem, 424*, 136431. https://doi.org/10.1016/j.foodchem.2023.136431.

Zhang, Y., Liu, K., Li, K., Gutowski, V., Yin, Y., & Wang, J. (2018). Fabrication of anti-icing surfaces by short alpha-helical peptides. *ACS Appl Mater Interfaces, 10*(2), 1957-1962. https://doi.org/10.1021/acsami.7b13130.

Zhang, Y., Wang, W., Liu, Y., Liu, X., Wang, H., & Zhang, H. (2022). Cryoprotective effect of wheat gluten enzymatic hydrolysate on fermentation properties of frozen dough. *Journal of Cereal Science, 104*. https://doi.org/10.1016/j.jcs.2022.103423.

Zhu, K., Zheng, Z., & Dai, Z. (2022). Identification of antifreeze peptides in shrimp byproducts autolysate using peptidomics and bioinformatics. *Food Chem, 383*, 132568. https://doi.org/10.1016/j.foodchem.2022.132568.

APPENDIX

Table 3.1. Yield and property of hydrolysates of wheat glutenin made by two proteases.

Protease	Hydrolysis time (min)	DH (%)	Average M_w (KDa)	Yield (%) *	ICS (%) **
Alcalase	5	15.2±1.5^{b}	0.8±0.1 ^{a}	63.8±4.0	88.4±2.6
	15	26.9±3.5^{a}	0.6±0.1^{ab}	66.1±0.9	83.7±8.4
	30	31.3±4.1^{a}	0.5±0.0 ^{b}	71.8±6.5	84.5±5.2
Trypsin	60	12.3±1.4^{b}	15.1±1.6 ^{a}	37.9±1.5 ^{c}	71.1±1.3^{bc}
	120	15.4±1.8^{b}	13.7±0.1^{ab}	45.7±0.8 ^{b}	77.0±3.6 ^{a}
	180	15.7±2.0^{b}	9.8±1.0 ^{b}	46.5±0.2^{ab}	68.3±3.4 ^{c}
	240	21.8±3.4^{a}	9.8±1.6 ^{b}	50.9±1.7 ^{a}	73.8±1.4^{ab}

Different lowercase letter in the same column and enzyme indicates significant differences among means ($P < 0.05$)

* The mass balance was relative to the starting dry glutenin powder obtained by Osborne fractionation.

** The IRI activity was expressed as the average ice crystal size (ICS) relative to the same concentration (40 mg/mL) of PEG negative control in 1 x PBS, with lower values representing higher activity

Table 3.2. The amino acid composition of the isolated glutenin fraction and its hydrolysates

Amino acid	Content (mg/100 total protein mg, %)				
	Glutenin	**Alc 5m**	**Alc 30m**	**Try 1h**	**Try 2h**
Asp	4.4 ± 0.0	3.5±0.0	2.9±0.1	2.2±0.2	2.6±0.3
Glu	40.1 ± 0.0	68.7±1.7	64.6±3.8	66.7±1.6	70.4±3.4
Ser	6.0 ± 0.1	1.2±0.1	0.7±0.1	0.1±0.1	0.1±0.1
Thr	2.6 ± 0.0	1.5±0.1	2.6±1.0	4.1±0.1	2.2±0.2
Gly	5.2 ± 0.4	0.9±0.1	1.0±0.2	0.9±0.1	0.8±0.1
Ala	2.1 ± 0.1	4.6±0.1	5.2±0.3	4.2±0.0	4.1±0.1
Arg	6.5 ± 0.6	2.9±0.2	3.5±0.8	2.8±0.2	2.4±0.3
Pro	10.4 ± 0.5	5.7±0.3	7.1±0.4	6.7±0.5	6.4±0.7
Val	1.8 ± 0.7	0.0±0.0	0.3±0.0	0.2±0.0	0.0±0.0
Met	2.2 ± 0.5	2.0±0.1	2.5±0.6	2.4±0.2	2.2±0.4
Lle	5.5 ± 0.4	1.3±0.1	1.4±0.2	1.1±0.0	0.7±0.2
Leu	2.8 ± 0.2	1.1±0.1	1.3±0.3	1.3±0.3	1.0±0.2
Phe	1.1 ± 0.1	5.4±0.6	5.8±0.9	5.6±0.2	5.4±0.5
Cys	0.8 ± 0.0	0.2±0.0	0.2±0.0	0.3±0.3	0.3±0.0
Lys	2.0 ± 0.1	0.0±0.0	0.0±0.0	0.0±0.0	0.0±0.0
His	3.4 ± 0.1	0.0±0.0	0.0±0.0	0.1±0.1	0.0±0.0
Tyr	3.1± 0.3	1.0±0.0	0.9±0.3	0.8±0.0	0.9±0.1
Total protein content (mg protein/mg sample)	83.9 ± 5.3	96.5±2.1	89.8±1.1	100.1±4.9	100.2±1.3

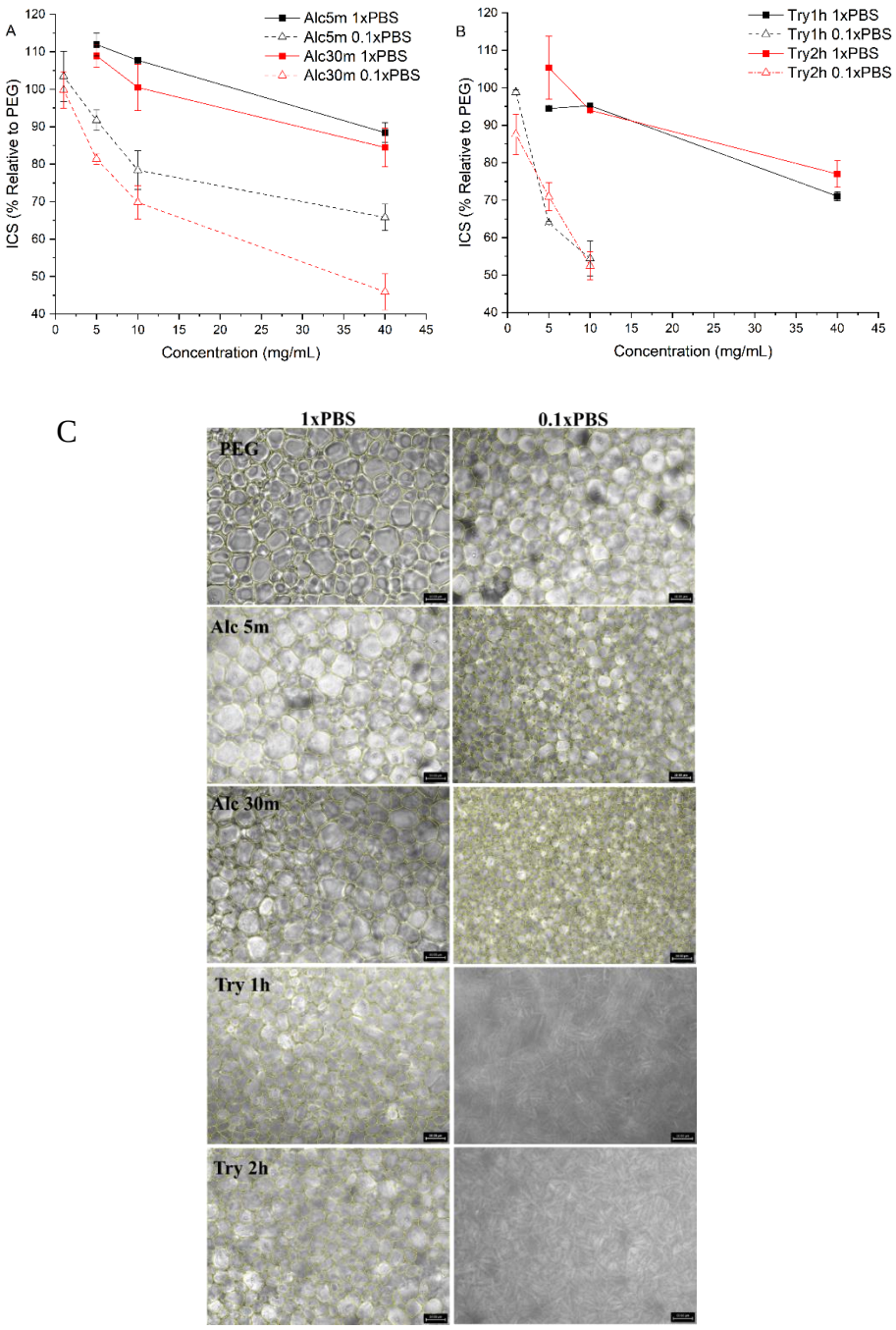

Figure 3.1. Enzymatic hydrolysis and PBS concentration affected the IRI activity of wheat glutenin. A) IRI activity of Alcalase hydrolysates, B) IRI activity of trypsin hydrolysates, and C) representative ice images as affected by PBS concentration.

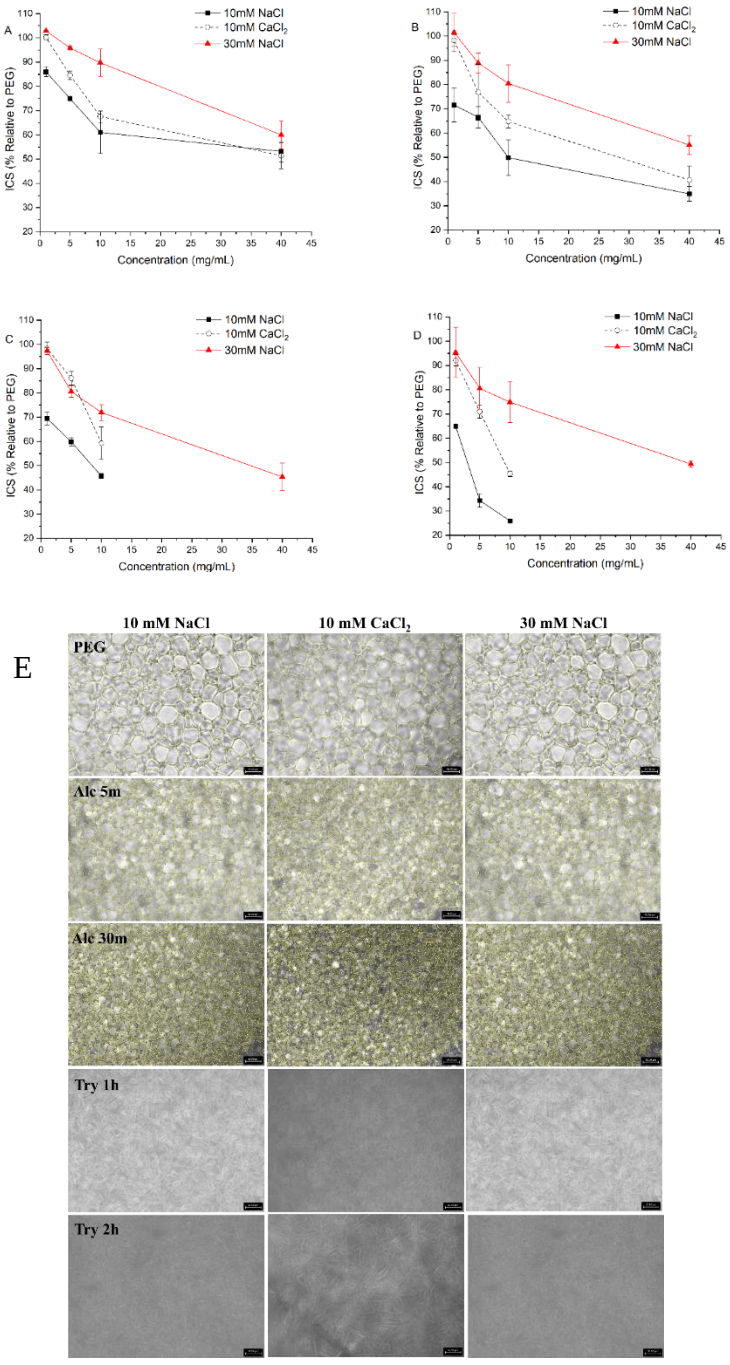

Figure 3.2. Ionic strength and cation type affected the IRI activity of wheat glutenin hydrolysates (A: Alc 5m; B: Alc 30m; C: Try 1h; D: Try 2h, E: representative ice crystal images).

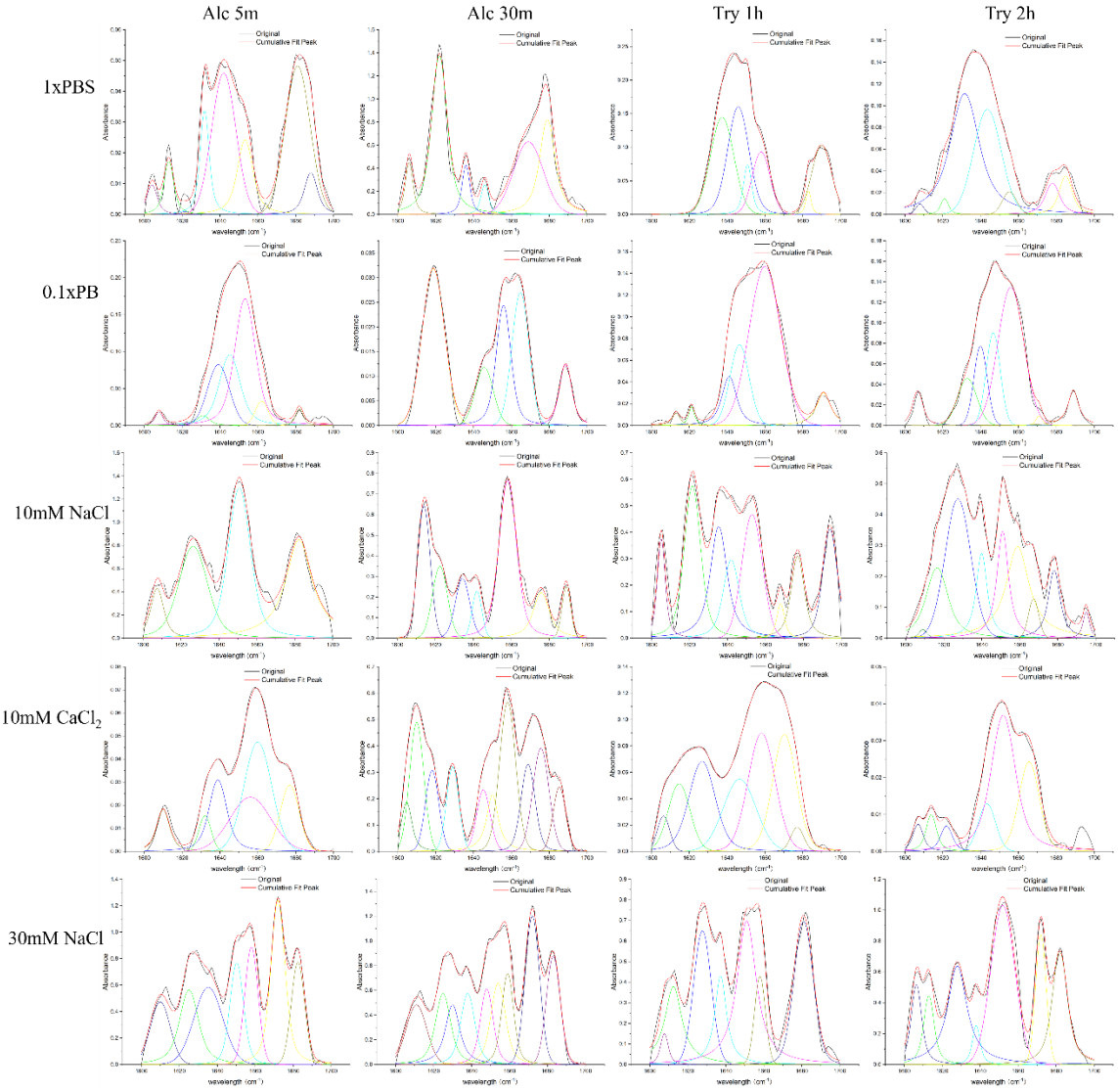

Figure 3.3. The FTIR spectra of amide I band (1700-1600 cm-1) of glutenin hydrolysates in different dispersing media at 40 mg/mL concentration and at room temperature.

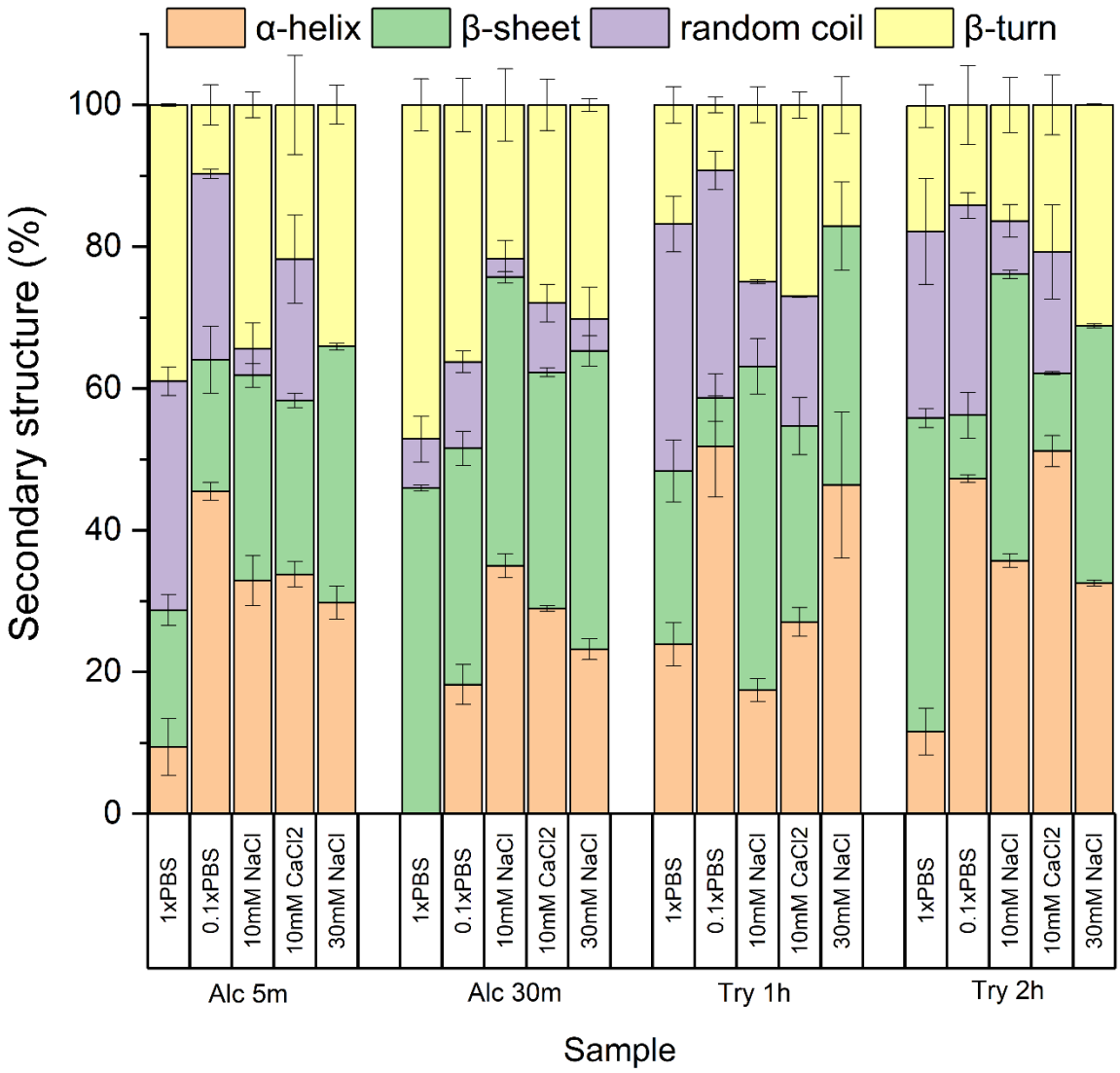

Figure 3.4. The effect of dispersing media on secondary structure of glutenin hydrolysates

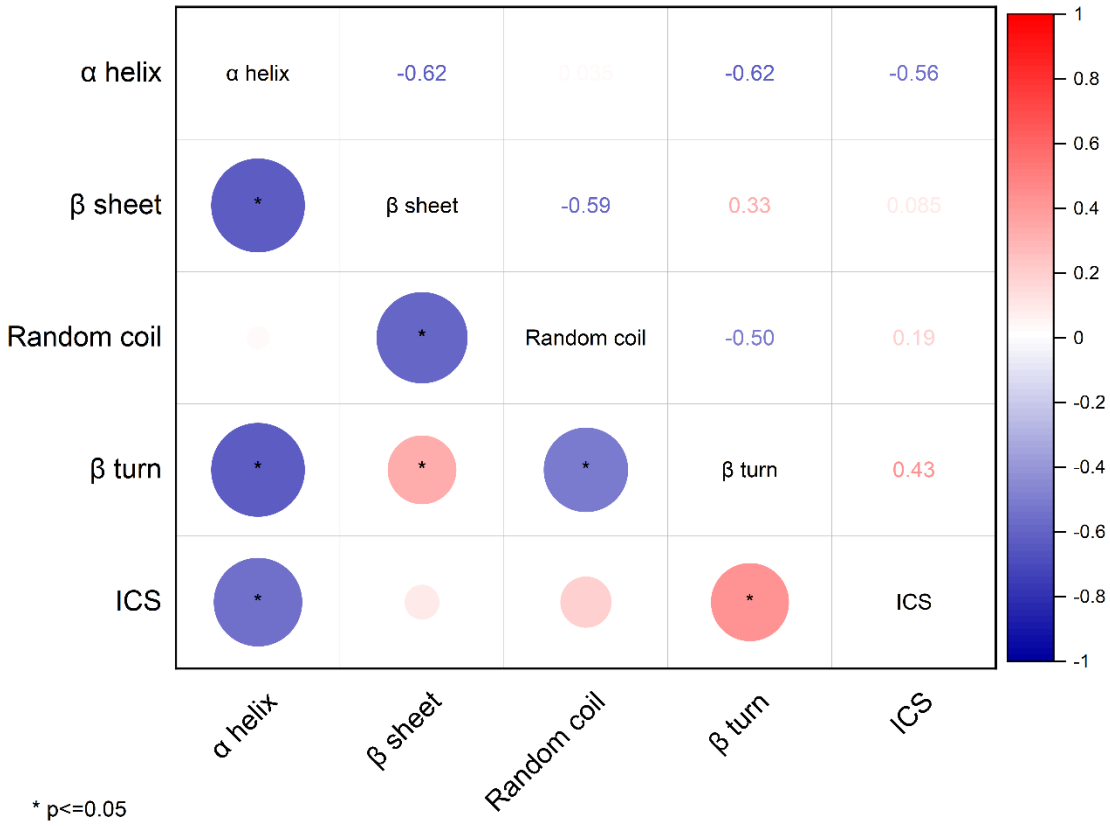

Figure 3.5. Pearson's correlation coefficients for the secondary structure and IRI activity of glutenin hydrolysates in different dispersing media.

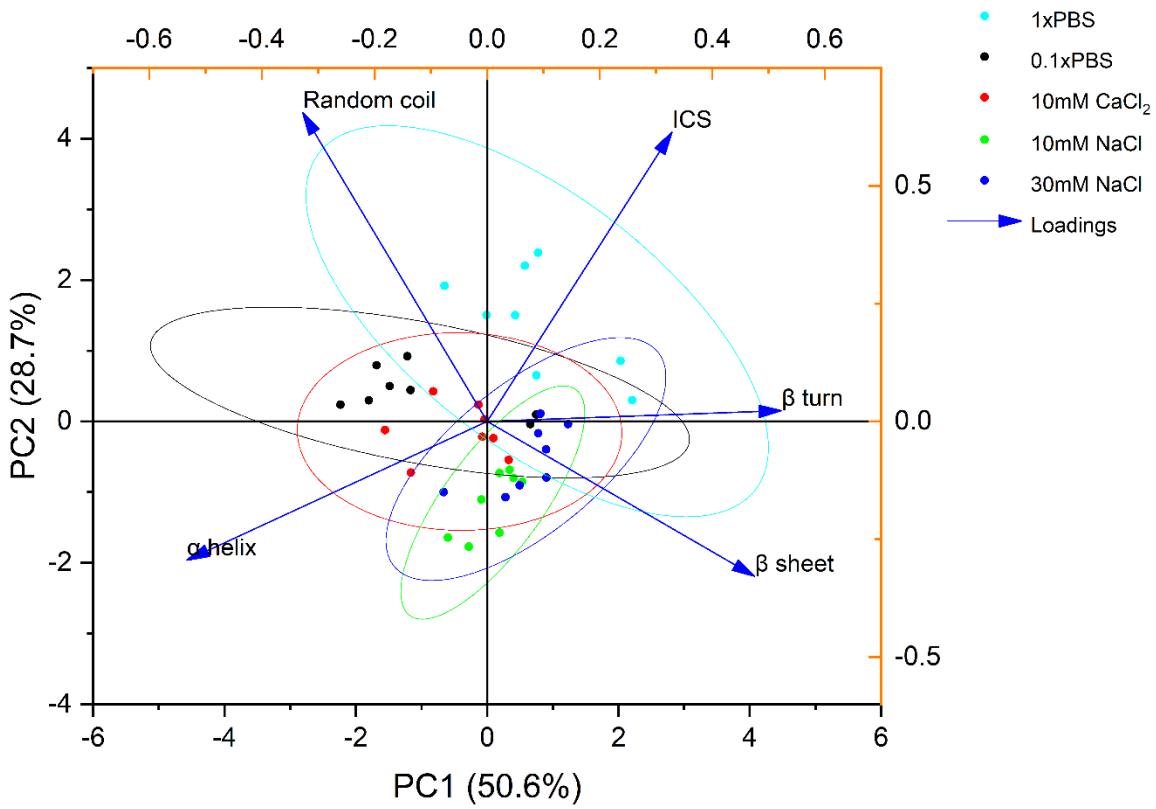

Figure 3.6. Discriminant analysis of glutenin hydrolysates in various dispersing media (blue: 1 x PBS, black: 0.1 x PBS, green: 10 mM NaCl, red: 10 mM CaCl2, and navy blue: 30 mM NaCl): a PCA-based classification model using scores plot and loading plots with 95% confidence ellipses.

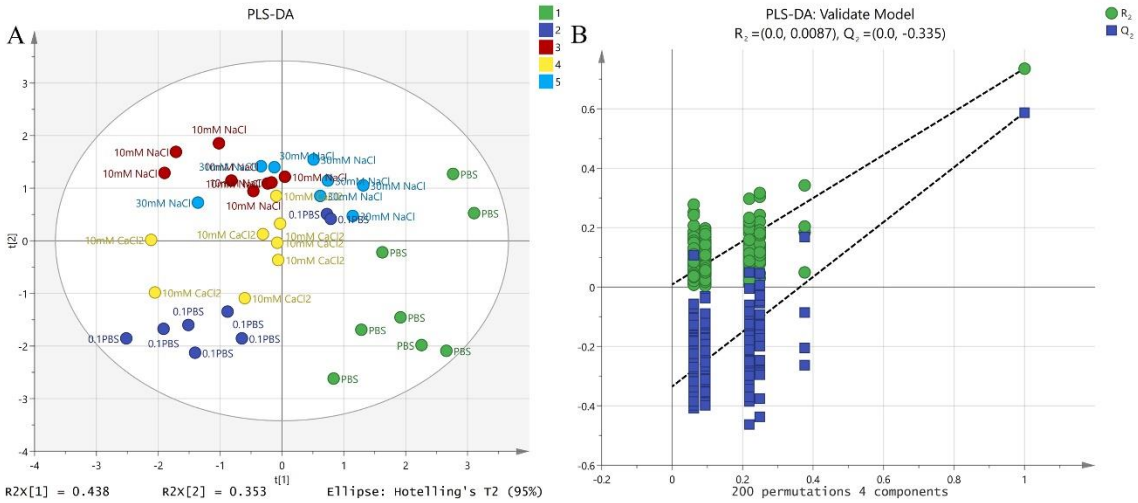

Figure 3.7. Score plots (A), and 200 permutation tests (B) for the PLS-DA model of glutenin hydrolysates in different dispersing media.

CHAPTER FOUR

IDENTIFICATION OF ANTIFREEZE ALBUMIN PROTEIN FROM WHEAT FLOUR AND INSIGHTS FROM MOLECULAR DYNAMICS SIMULATION

A version of this chapter was submitted to Food Hydrocolloids journal and is currently under review.

Abstract

Biobased antifreeze agents, particularly those derived from food sources, are increasingly in demand for their applications in food and biomedical industries. This study focuses on the extraction, purification, and identification of amylase trypsin inhibitors from wheat flour, which demonstrate ice recrystallization inhibition (IRI) activity. After Osborne fractionation and gel filtration chromatography of the albumin fraction, the isolated proteins from the wheat albumin fraction exhibited high IRI activity. Then, the fractions displaying the most potent IRI activity, specifically F1 and F2 fractions, were subsequently analyzed by LC/MS, leading to the identification of 26 proteins. From these, two dominant proteins, dimeric alpha-amylase inhibitor (AAI) and alpha-amylase inhibitor WDAI-3 (WDAI-3) were selected based on abundance and homology for detailed molecular dynamic (MD) simulations under freezing conditions. Trypsin inhibitor from soybeans, which lacks IRI activity but shares similar molecular weight and biochemical properties was used as a control. The study found that the WDAI-3 exhibits the highest IRI activity, while the AAI and soybean protein show negligible activity. Therefore, MD results provide strong support for experimental observations.

Introduction

Cryopreservation is critical for extending the shelf life of food and biomedical materials. However, the sensory quality of frozen food and cell viability can deteriorate due to ice recrystallization, a phenomenon caused by Ostwald ripening during cold storage (Ghalamara, Silva, Brazinha, & Pintado, 2022). To address this issue, researchers have identified certain food-derived peptides with antifreeze activity that may serve as cryoprotective additives. For instance, soybean hydrolysates (Fomich, Día, Premadasa, Doughty, Krishnan, & Wang, 2023), fish gelatin hydrolysates (Damodaran & Wang, 2017), and hydrolysates from Silver Carp (Zhou, Wang, Yu, Li, & Liu, 2019) have been found to control the growth of ice crystals by demonstrating ice recrystallization inhibition (IRI) activity.

Wheat flour is a common food material across the world, and its proteins can be classified into two groups: gluten and non-gluten proteins (Lookhart, 1995). While wheat gluten and glutenin hydrolysate have been reported to show antifreeze activity in previous studies (Yuan Yuan, Dia, & Wang, 2024; Zhang, Wang, Liu, Liu, Wang, & Zhang, 2022), the potential of non-gluten proteins, which include water-soluble albumins and globulins, remains unexplored. These proteins could be particularly valuable as antifreezing ingredients for gluten-intolerant populations, offering potentially versatile applications.

In our preliminary study, high antifreeze activity of water-soluble wheat protein was identified. However, wheat albumin is a mixture that can be further divided into a high molecular weight fraction, which contains enzymes involved in metabolic activity

(Piergiovanni, 2007) and a low molecular weight fraction including α-amylase inhibitors and other proteins involved in plant defense (Silano, Pocchiari, & Kasarda, 1973). Among these, α-amylase inhibitors are the most abundant proteins in the albumin fraction of wheat (Geisslitz et al., 2022). Since molecular weight appears to be a significant factor influencing IRI activity of peptides and proteins, for example, gelatin hydrolysates ranging from 700-1400 Da have been shown to significantly inhibit ice crystal growth more effectively than other peptides (Wang, Agyare, & Damodaran, 2009), hydrolysates from tilapia scales, with sizes below 2000 Da, have demonstrated cryoprotectant activity in preserving *S. thermophilus* (Xu Chen, Li, Yang, Wu, & Wang, 2020), the low molecular weight wheat albumin fraction was evaluated for it potential IRI activity. Research by Fu et al. (2019) also demonstrated that hydrolysates produced by alkaline protease from *Scomberomorus niphonius*, showed substantial antifreeze ability when their molecular weight is from 1426 to 1810 Da. However, these studies predominantly focus on peptides, and a comparative analysis of antifreeze activity among proteins from the same origin but of varying sizes, such as different fractions of wheat albumin, has yet to be explored.

While experimental observations can provide valuable evidence of antifreeze activity, understanding the structural or conformational changes of antifreeze polymers under freezing conditions and their molecular interactions with ice and water molecules are crucial for providing molecular basis and support. Molecular dynamics (MD) simulations have emerged as a powerful tool in this regard. For example, Midya and Bandyopadhyay (2014) found that conformational rigidity is important for *Tenebrio molitor* (insect)

antifreeze protein because its ice binding surface (IBS) is relatively more rigid than the non-ice binding surface (NIBS). Meanwhile, IBS exhibits structured and ordered water arrangements in solvation shells, while NIBS does not have it even at lower temperatures. Similarly, Mochizuki and Molinero (2018) also used MD to illustrate that the presence of unusual polyproline II helix (PPII helix) secondary structure of antifreeze glycoprotein ($AFGP_8$) may be vital for its ice binding activity. Beyond proteins and peptides, the polymer poly(vinyl)alcohol has also been shown to exhibit the ability to inhibit ice formation, and this inhibition was correlated with a matching of the polymer interactions at the ice lattice, specifically interactions between the polymer's hydroxyl groups and adjacent water-molecules within the ice-lattice (Naullage & Molinero, 2020). These past simulations studies highlighted the usefulness of computational methods to explore the mechanism of IRI activity of proteins from similar origin but with different molecular weights or structural features, since detailed molecular-level information is often challenging to obtain through experimental methods alone.

Based on these prior studies, we hypothesized that the albumin portions of wheat, specifically a subset of particularly some types of albumin proteins, may exhibit antifreeze properties analogous to those found in wheat gluten. To verify this hypothesis, the initial step involved the purification and characterization of albumin proteins. Following this, specific proteins were identified based on the coverage of amino acid sequences, derived from liquid chromatography-mass spectrometry (LC-MS) analysis. Subsequently, MD simulations were employed to investigate the interactions of each protein with water under freezing conditions. These allow the examination of both the

conformational responses of the proteins under these conditions and quantification of both free-water and ice interactions. Hence, the potential molecular mechanisms underpinning observed differences in IRI activity of wheat albumin proteins are explored and discussed.

Materials and methods

Materials.

Wheat flour (Bob's Red Mill, OR, USA) was purchased from a local grocery store. Polyethylene glycol 400 (PEG, MW 380 - 420 Da) was purchased from Sigma Aldrich (Saint Louis, MO). Alcalase, derived from *Bacillus licheniformis* with an activity of 3.03 U/mL, was acquired from EMD Millipore Corp (Massachusetts, USA). Cellulase from *Aspergillus niger* was purchased from MP Biomedicals (Solon, Ohio, USA).

Extraction of albumin from wheat flour.

To extract albumin, 100 g of wheat flour was mixed with 400 mL of deionized (DI) water for 30 minutes, followed by centrifugation at 5000 x g for 5 minutes to collect the supernatant. This process was repeated three times, with the DI water volume reduced to 300 mL for the subsequent two cycles. The supernatants from all three cycles were combined and subjected to freeze-drying.

Removal of protein or polysaccharides from crude albumin to identify the IRI activity.

The lyophilized powder of crude albumin was reconstituted in DI water to a 5% (w/w) concentration. The pH of the mixture was adjusted to 8.0 using 0.1 M NaOH. Alcalase was then added at an enzyme-to-substrate ratio of 0.176 Anson units per gram of powder, and the mixture was incubated at 55 °C for 0.5, 1, and 24 hours. For cellulase hydrolysis,

the pH was adjusted to 4-5 using 0.1 M HCl, and the mixture was incubated at 50 °C for 12, 24, and 48 hours. The enzyme concentration was 0.1 % of the sample weight. After hydrolysis, all samples were boiled for 10 minutes to inactivate the enzymes. The hydrolyzed samples were then transferred to dialysis tubes with a molecular weight cut-off of 3.5 kDa and dialyzed for three days to remove small molecules. For comparison, control samples without enzymatic treatment were prepared by dialyzing a solution of the same albumin crude extract under identical conditions.

Fractionation of wheat albumin using gel filtration chromatography.

The crude albumin extract was prepared by dissolving lyophilized crude albumin extracted in 100 mM ammonium bicarbonate buffer to a final concentration of 50 mg/mL, followed by filtration through a 0.22 μm (PVDF) syringe filter. The fractionation process was carried out using an AKTA protein purification system (General Electric, Boston, MA) equipped with a UV detector set at 280 nm. Five milliliters of the sample was loaded onto a HiLoad 16/600 Superdex 30 pg column (with a molecular weight range of 1-10 kDa, General Electric, Boston, MA) and eluted at a flow rate of 1 mL/min over 180 minutes. The eluted samples were collected using an F9-R fraction collector (General Electric, Boston, MA) and divided into seven fractions (F1-F7) based on UV absorbance. To remove ammonium bicarbonate, the fractions were incubated at 65 °C overnight, followed by freeze-drying. To collect sufficient samples, multiple injections were performed for each independent fractionation experiment. The LC fractionation process was repeated twice in this study.

Determination of molecular weight of albumin extract and their fractions.

The molecular weight of samples was analyzed using a BioSep-SEC-s2000 column (Phenomenex, Torrance, CA, USA) (Yuan Yuan et al., 2024). A mobile phase composed of a 45:55 (v/v) mixture of acetonitrile and HPLC-grade water containing 0.05 % trifluoroacetic acid was utilized for the separation. Molecular weight distribution was determined by comparing the elution pattern with a series of protein standards of known molecular weights (M_w), detected at 214 nm. A linear standard curve was established using the retention times and the logarithm of M_w for the standards (albumin, aprotinin, bradykinin acetate, bradykinin fragment 1-5, glutathione, and glycine). Subsequently, this curve equation was employed to calculate the M_w of individual peaks in the chromatogram. The average M_w was computed based on the proportional contribution of each peak, determined from the area under the curve.

Determination of protein content by total amino acid composition analysis.

The protein content determination involved the treatment of samples at a concentration of 1 mg/mL with 6 M HCl at 150 °C for 30 minutes (Akhlaghi, Ghaffari, Attar, & Alamir Hoor, 2015). Post-hydrolysis, the samples underwent vacuum drying at 50 - 60 °C overnight, followed by dissolution and dilution in sample buffer (50 mM $NaHCO_3$, pH = 8.4). Subsequently, 200 µL of the diluted samples were mixed with 300 µL of 4 mM dabsyl chloride, vortexed for 30 seconds, and heated at 70 °C for 20 minutes. A diluent solution comprising a mixture of 50 mM sodium phosphate buffer (pH = 7.0) and HPLC-grade ethanol (500 µL) was then added. The resulting solutions were filtered through a 0.45 µm Nylon filter for HPLC analysis, conducted using a Zorbax Eclipse Plus C18

column under the following condition: injection volume of 10 µL, flow rate of 1 mL/min, and column temperature of 40 °C. The UV-Vis detector wavelength was set at 436 nm. Mobile phase A comprised sodium acetate buffer (25 mM, pH = 6.5) containing 4 % dimethylformamide, while mobile phase B consisted of acetonitrile. A gradient elution program was applied, with time (min)/percentage B values as follows: 0/15, 20/40, 32/70, 34/70, 35/15, 45/15. For the standard curve, an amino acid (AA) standard mixture (Sigma, AA-S-18) containing 17 AA standards was utilized. The standards were prepared at concentrations of 1.56, 3.13, 6.25, 12.50, and 25.00 nanomoles of all amino acid standards in tubes using the sample buffer. Protein content determination was computed by summing the weights of all amino acids.

Determination of total polysaccharide.

For the determination of total polysaccharide content, the phenol-sulfuric acid method outlined by Nielsen (2017) was followed with slight modifications. In brief, a 1 mL sample (1 mg/mL) was mixed with 25 µL of 80 % phenol solution and 2.5 mL of concentrated sulfuric acid. After cooling to room temperature, the absorbance was measured at 490 nm, with glucose serving as the standard for quantification.

SDS-PAGE for characterization of albumin extract and their fractions.

Samples were dissolved in 1xPBS (pH = 7.4) to a final concentration of 40 mg/mL. After being vortexed for 30 minutes at room temperature, the samples were mixed with an equal volume of Laemmli buffer (Bio-Rad Laboratories, Inc., Hercules, CA, USA) containing 5% β-mercaptoethanol. This mixture was then boiled in water for 5 minutes to denature the proteins. Subsequently, 10 µL equivalent to 400 µg of each sample was

loaded into the wells of a 4-20 % SurePAGE, Bis-Tris gel (GenScript Biotech, Piscataway, NJ, USA). The proteins were separated by electrophoresis at 200 V for 35 minutes using Tris-MOPS-SDS running buffer (GenScript Biotech, Piscataway, NJ, USA) at room temperature. After separation, the gel was stained with 25 mL of Bio-Safe Coomassie R-250 blue dye for 2 hours. Following staining, the gel was washed with 50 mL of destaining solution for 2 hours, with the destaining solution being replaced every 30 minutes.

Periodic acid-schiff (PAS) stain for glycoprotein.

The preparation of samples and electrophoresis for PAS stain is the same as in section 2.8, but the staining process was different. Firstly, the gel was fixed in 100 mL of 50% methanol for 30 minutes and then washed twice in 100 mL of 3% acetic acid for 10 minutes each. Subsequently, the gel was incubated in 25 mL of oxidizing solution for 15 minutes, followed by three washes in 3% acetic acid for 5 minutes each. The glycoproteins were stained by agitating the gel in 25 mL of glycoprotein stain for 15 minutes. After staining, the gel was treated with 25 mL of reducing solution for 5 minutes and then washed with 3 % acetic acid and ultrapure water. Glycoproteins appeared as magenta bands, and the gel was stored in 3% acetic acid.

Splat assay for IRI activity determination.

The splat assay was carried out as previously reported (Knight, Hallett, & DeVries, 1988) and calculated as we previously reported (Yuan, Fomich, Dia, & Wang, 2023), with sample solutions containing varying concentrations (10 - 40 mg/mL) prepared by dissolving in 1xPBS. Samples were prepared in duplicate, and each sample was analyzed

twice in independent slides. The slide was annealed at -8 °C for 30 min, and three pictures were captured from each slide, from which the Feret's maximum diameter was averaged by ImageJ software (Saad, Fomich, Día, & Wang, 2023). The relative IRI activity was calculated by dividing the average ice crystal size (ICS%) of the treated sample by that of the control sample, which contained polyethylene glycol at the same concentration in the same dispersing media.

Protein identification by LC/MS methods.

Protein bands of SDS-PAGE were digested using chymotrypsin (Promega V1061) in a Tris buffer (100mM Tris-HCl, pH 8.0, 10mM $CaCl_2$). Desalted peptides, concentrated using C18 tips (Pierce Cat# 87774), were analyzed by LC/MS on a Bruker tims TOF-PRO system. Portein analysis was conducted using a Bruker timsTOF-PRO system coupled with a nanoElute system for liquid chromatography. A Pepsep25 analytical column (Bruker 25 cm × 75 μm, 1.9 μm ReproSil-AQ C18) was used for protein separation. A 1 μL sample was injected onto the column, and the proteins were eluted using a gradient of acetonitrile (Solvent B: 99.9 % acetonitrile, 0.1 % formic acid) at a flow rate of 300 nL/min. The elution gradient was as follows: starting with 3% B, ramping to 17 % B over 10 minutes, followed by an increase to 25 % B over 5 minutes, 35 % B over 10 minutes, and a final ramp to 90 % B over 5 minutes. The system was returned to 3 % B and held for 5 minutes to re-equilibrate the column. The total run time for the gradient was 30 minutes. The timsTOF-PRO mass spectrometer was operated in positive-ion mode with a data-dependent acquisition method. Full MS scans were acquired in the m/z range of 100-1700 with a resolution of 60000. For MS/MS, the ten

most intense precursor ions were selected for fragmentation using higher-energy collisional dissociation at a normalized collision energy of 30 %. Dynamic exclusion was enabled to prevent repeated selection of the same precursor ions, with an exclusion duration of 60 s. Proteins were identified using Bruker's proprietary software, with mass spectra calibrated using internal standards.

Molecular dynamic simulation analysis.

All MD simulations were conducted using the GROMACS simulation suite (version 2021.5) (Chen, Wu, Cai, & Wang, 2021), and made use of the CHARMM36m force-field (Huang et al., 2017). The LC-MS raw data were transferred to the PEAKS-11 server (Bioinformatics Solutions Inc) and analyzed against the Uniprot-Bovine database to identify related amino acid sequences. Protein structures were predicted using AlphaFold2 (https://github.com/google-deepmind/alphafold) (Jumper et al., 2021). It should be noted that for the protein models examined, post-translational cleavage was not considered, and the full sequences were modeled. For simulation preparation, the CHARMM-GUI was used to set up the protein within a water box (Jo, Kim, Iyer, & Im, 2008), and the salt concentration is 150 mM NaCl. As the aim of the simulations was to examine the protein under ice-forming conditions, all solvent molecules initially placed by CHARMM-GUI were removed and the box was then re-solvated using GROMACS utilities with the TIP5P water model. The use of the TIP5P water model had previously been shown to better reflect the water melting point (274 K) in closer agreement with the known experimental value (273 K) (Mahoney & Jorgensen, 2000). After solvation with TIP5P, a model of an Ice I_h surface with the same XY box dimensions of the protein-

containing water-box was subsequently generated using the GenIce2 (https://pypi.org/project/GenIce2/) utility (Matsumoto, Yagasaki, & Tanaka, 2018). The ice model was then translated “below” the protein-containing water box and merged using the TopoTools (Kohlmeyer, Vermaas, & Braun, 2022) package within the VMD modeling tool (Humphrey, Dalke, & Schulten, 1996). The addition of the Ice I_h surface to the water-box was used as an ice seed to facilitate ice growth during the simulations. The system underwent an initial energy minimization using 5000 steps of the steepest descent algorithm, followed by a 125 ps simulation in the canonical (NVT) ensemble, employing the Nose-Hoover thermostat to maintain a stable temperature of 265.15 K. This was succeeded by a 125 ps simulation in the isobaric-isothermal (NPT) ensemble, with the Parrinello-Rahman barostat to keep the pressure isotropic at 1 bar. The simulation culminated in either a 100 or 150 ns MD simulation in an NPT ensemble, also at 265.15 K and 1 bar pressure, with each sample repeated three times to ensure reproducibility. The blank control was prepared using identical steps, excluding the incorporation of the protein structure. In addition, a trypsin inhibitor from soybean [soybean Kunitz-type trypsin inhibitor (KTI), accession number P25273|KTI2_SOYBN, molecular weight 22,800 Da], which did not exhibit IRI activity (demonstrating an ICS of 89.3% at a concentration of 40 mg/mL in 1xPBS) and shares similar biochemical function, was used as a negative control in the simulations. The number of water molecules existing in the ice vs water phase was determined using the water and ice molecules were identified by CHILL + algorithm (Nguyen & Molinero, 2015) included in the OVITO (Stukowski, 2009) modeling package. Simulation analysis was performed using the GROMACS

utilities, unless otherwise noted, and results were visualized with Pymol ("The PyMOL Molecular Graphics System, Version 1.2r3pre, Schrödinger, LLC.,") software. Radial distribution functions, root-mean-squared deviations of the proteins from their initial configurations, mean-squared displacement profiles (MSD), hydrogen-bonding counts and hydrogen-bond autocorrelation functions were calculated using the built-in GROMACS utilities. Water tetrahedrality calculations were performed using an in-house tcl-script using the VMD software package. All simulations and analysis were performed in triplicate using different random seeds for velocities. Analysis examining the behavior of the solvation shell waters was performed by extending each simulation from their final snapshots by an additional 2ns and increasing the frame saving rate from once every 100ps to once every 0.5ps.

Statistical analysis.

Statistical analysis was conducted using data from two independent fractionation experiments. All analytical assays were done three replicates. Results were expressed as mean ± standard deviation and analyzed using Excel 2016 and SPSS 22.0. Graphs were generated with Origin 2021 Pro and Matplotlib. The significance of the findings was assessed using analysis of variance (ANOVA), followed by Duncan's test, with a significance threshold set at $P < 0.05$.

Results and Discussion

Identification of compound with IRI activity from crude wheat albumin extract.

Table 5.1. shows that crude wheat albumin extracted from flour using Osborne fractionation demonstrated the ability to reduce ice crystal size by 38.7 % at a

concentration of 40 mg/mL in 1xPBS. This extract was a complex mixture of proteins and polysaccharides. Prior research has demonstrated that both individual wheat gluten hydrolysates (Zhang et al., 2022) and polysaccharides from wheat bran possess IRI activities (Zhao, Shi, Yang, Gu, Jiang, & Wang, 2022). It is therefore crucial to identify whether the IRI activity stems from polysaccharides or proteins component of the crude extract. To investigate this, enzymatic treatments (Alcalase and cellulase) followed by dialysis were utilized to selectively remove proteins by Alcalase hydrolysis and to remove polysaccharides by cellulase treatment from the mixture, with the compositional outcomes of these processes detailed in **Table 5.1**. Although prolonged hydrolysis did not completely remove all proteins or polysaccharides, it was observed that the samples exhibited higher activity following cellulase treatment and dialysis compared to Alcalase hydrolysis. Furthermore, an increase in Alcalase hydrolysis time correlated with a decrease in IRI activity, suggesting that proteins play a more significant role than polysaccharides in inhibiting ice crystal growth (**Table 5.1.**).

Isolation of IRI active wheat albumin fraction by gel filtration chromatography.

To continue isolating antifreeze proteins with high IRI activities, gel filtration chromatography was employed to obtain fraction 1-7 (F1-F7). This method separated proteins based on their size, as depicted in **Figure 5.1**. and detailed in **Table 5.2**. Notably, proteins detected in F7 were not used for further analysis due to insufficient sample mass for splat assay evaluation. Similarly, F6, which consisted of only 16 % protein and polysaccharides, indicating a predominance of small molecules or salts in the remaining 84 %, was also excluded from subsequent analysis.

Among the fractions analyzed, F1 stood out with the highest protein content and the most potent IRI activity, reducing ice crystal growth by 40.8 % at a concentration of 40 mg/mL and by 31.9 % at 20 mg/mL. This underscores the critical role of proteins in antifreeze functionality. Despite an increase in protein content from 21.5 % to 56.6 %, F1 also contained polysaccharides, as evidenced by PAS staining (**Figure 5.2**) which revealed two distinct bands: glycoproteins at the bottom and soluble polysaccharides at the top. It is in line with previous research, which indicated that some wheat albumins are glycoprotein (Kasar et al., 2017). However, the results obtained now cannot exclude the potential enhancing effect of these polysaccharides on IRI activity. Monalisa, Shibata, and Hagiwara (2023) found that wheat flour has a synergistic effect with antifreeze protein III on IRI behavior.

Further analysis showed that despite higher protein levels in F2 and F3 (43.0 % and 37.4 %, respectively) compared to the crude albumin at 21.5 %, the ICS at 40 mg/mL decreased to 73.5 % and 78.2 %, respectively. These 3 fractions (F2, F3 and crude albumin) as seen in **Figure 5.1**, consist of different protein mixtures with average molecular weights of 9.0 kDa, 4.6 kDa, and 12.7 kDa, respectively. These differences in molecular weight and protein composition have likely contributed to the observed variations in IRI activity.

Additionally, fractions F4 and F5, where polysaccharide content significantly exceeds protein content (with protein levels less than 10 %), exhibited weak IRI activity, reducing ice crystal size by only 20 %. This finding corroborates the observations that while polysaccharides from wheat may exhibit some IRI activity, proteins themselves play an

important role in antifreeze functionality. This also aligns with the results in Section 3.1, highlighting the importance of protein content in inhibiting ice crystal growth and suggesting that other factors, including protein composition and molecular weight, significantly influence the overall IRI activity of the samples.

In addition, as shown in **Table 5.1.** and **Table 5.2**., the dialyzed albumin exhibits comparable ICS% to that of the F1 fraction under different concentration. The straightforward and sample preparation of dialyzed albumin further highlights its potential for practical applications in the food industry.

LC/MS analysis of the potent species in wheat albumin fractions.

Building on the observed differences in IRI activity among various proteins, the fractions exhibiting the highest antifreeze activity, F1 and F2, were chosen for further analysis using LC/MS. A total of 26 proteins of varying molecular weights were identified. The top three proteins based on the relative abundance, along with their corresponding UniProt accession numbers, are presented in **Table 5.3**. Among these, the top two proteins are dimeric alpha-amylase inhibitors with similar molecular weight; therefore, only the first dimeric alpha-amylase inhibitor (AAI) and Alpha-amylase inhibitor WDAI-3 (WDAI-3) were selected for molecular simulation studies. The structures of these two proteins and a control sample from soybean (soybean KTI) were predicted using AlphaFold and are illustrated in **Figure 5.3.**

MD simulation analysis of alpha-amylase inhibitor protein-water-ice interactions under freezing-like conditions.

To compare how different alpha-amylase inhibitor proteins affect water dynamics and ice formation under freezing conditions, **Figures 5.4**. and **5.5**. illustrate the percentage of ice formation and representative snapshots across all systems, respectively, during a 100 or 150 ns simulation at 265.15 K. The ice formation rates for two wheat-derived proteins stabilized after approximately 60 ns, whereas for the soybean KTI, stabilization only occurs after 100 ns, so an extended simulation period of 150 ns for this sample was used. The results show an increasing trend in ice formation over time for all tested samples. Notably, WDAI-3 exhibited the lowest ice formation rates, suggesting it possesses superior IRI activity compared to the other two samples. In contrast, AAI exhibited weak activity. Although the percentage of ice formation in the soybean KTI ultimately exceeds that of AAI at equilibrium, AAI shows a slightly higher percentage of ice formation than the soybean KTI at the 100 ns, illustrating variations in IRI activity even among proteins from similar origin. This variation highlights the impact of molecular weight and structure on IRI activity, aligning with findings from previous studies on peptides (Chen et al., 2021).

Beyond the visualization of freezing and quantification of ice formation, a characterization of the structure and dynamics of each protein's hydration shell water (**Figure 5.6.**) was also performed after the simulation boxes reached a steady state (i.e. post-freezing). While the increase in mobility as shown in proximal radical distribution (pRDF), and associated decrease in water-water hydrogen-bond autocorrelation, is not

entirely unexpected for WDAI-3, given the observation that the simulations maintain the largest amount of non-frozen water, the observation that the water within the WDAI-3 solvation shell adopts the largest tetrahedrality order parameter, where 1 would correspond to a perfectly frozen crystalline state, and features a distinct second peak in its protein-water proximal (protein surface-area normalized) radial distribution function, is surprising. This observation suggests that WDAI-3 may have a stronger interaction with liquid water than the other proteins.

Turning to an examination of the proteins' own conformational motion and self-interactions (**Figure 5.7.**) indicates that throughout the simulations the radius of gyration (R_g) for WDAI-3 consistently decreased, stabilizing after 60 ns, whereas the R_g for AAI and soybean KTI remained relatively stable over 100 ns. This indicates that WDAI-3 became more compact during the simulation. Furthermore, **Figure 7B** illustrates normalized hydrogen bonding within the proteins, an indicator of structural rigidity and protein stability (Hubbard & Kamran Haider, 2010; Pace et al., 2014). The normalization was calculated by dividing the number of hydrogen bonds formed per timeframe between the protein and protein by the total number of possible hydrogen bonds.

Despite its relatively rigid structure, WDAI-3 exhibited larger fluctuations in root mean square deviation (RMSD), as shown in **Figure 5.7C**, suggesting a degree of enhanced conformational flexibility. The pronounced fluctuation observed in WDAI-3 can be primarily attributed to its smaller molecular weight (4797 Da), especially when compared to AAI and soybean KTI, which have molecular weights of 14982 Da and 22800 Da, respectively. It has been reported that for smaller proteins, minor structural adjustments

can result in significant conformational changes (Sargsyan, Grauffel, & Lim, 2017), thereby leading to elevated RMSD values. This behavior may also correlate with the rapid decrease in the R_g during the simulation, as shown in **Figure 4.7A**, where WDAI-3 undergoes significant compaction over time. However, an examination of the residue-averaged root-mean-squared fluctuations each of the proteins during the last 50ns of each trajectory (from 50ns to 100ns for WDAI-3 and AAI, and 100ns to 150ns for soybean KTI), indicates that even accounting for the decrease in R_g, WDAI-3 retains more internal mobility compared to the other two proteins, with WDAI-3 exhibiting an of 0.273nm ± 0.195 (std. dev) while AAI and soybean KTI exhibited ~0.119nm ± 0.797 (std. dev.) and 0.123nm ± 0.0856 (std. dev), respectively.

In this study, the mean square displacement (MSD) of the proteins were also computed (**Figure 5.7D**), using the last 50 ns of each simulation. An examination of the MSD lags from 0 to 5ns reveals that WDAI-3 remains highly dynamic, compared to the other 2 larger proteins (AAI and soybean KTI). Prior work by Sun et al. (2024) and Yang, Liao, Shi, and Sun (2023), showed that polysaccharides with high MSD are more effective in disrupting interfacial water, thereby hindering ice formation along the primary prism plane. Given the combination of evidence of a potentially strong coupling between the hydration-shell water of WDAI-3 and the conformational and translational freedom of WDAI-3, compared to the other two proteins, it is possible that as hydration waters localize, and order near WDAI-3 surface, they are ‘dragged’ along with the protein and in-turn are unable to adopt the appropriate water-water hydrogen-bonding necessary to

join the growing ice surface, which may account for the experimentally and computationally observed IRI activity of the protein.

Overall, from both protein structural and water–protein interaction perspectives, WDAI-3 exhibits a more compact, yet simultaneously more conformationally and translationally dynamic, structure compared to AAI and soybean KTI. This is evidenced by its marked decrease in R_g over time, coupled with higher RMSF and MSD. Furthermore, the extended second hydration-shell peak in WDAI-3's protein-water pRDF suggests a longer-range and potentially stronger interaction with water molecules than is observed for AAI and soybean KTI. Such enhanced protein–water interactions, as shown in **Figure 5.8.**, likely interfere with water–water hydrogen bonding and may thus contribute to the disruption of ice formation.

While these findings provide valuable insights into behavior of the proteins under the freezing environment examination of interactions and provide a potential mechanism for antifreeze activity, we caution that this analysis still represents a preliminary exploration. The IRI activity of WDAI-3 and AAI proteins cannot be directly correlated with experimental data due to the use of unpurified protein samples with IRI experiments. Furthermore, the F1, F2, and F3 fractions contain not only protein but also polysaccharides, so the role of polysaccharides and proteins synergy cannot be addressed in this study. The complex mechanisms underlying these interactions and their precise relationship to antifreeze properties necessitate further investigation. Furthermore, our simulations differ from those typically conducted for true AFPs or AFGPs, which focus on direct protein–ice binding. We did not observe any distinct protein–ice interactions,

implying that different proteins may inhibit ice crystal growth by different mechanisms. This view is supported by the comparatively high effective concentration required for F1 (approximately 20 mg/mL at ICS % below 70 %), whereas AFPs can be effective at below 1 mg/mL (Biggs, Stubbs, Graham, Fayter, Hasan, & Gibson, 2019). However, the presence of multiple proteins and polysaccharides in the F1 fraction likely obscures the high IRI activity of WDAI-3 alone.

Conclusion

In summary, this study characterized the IRI activity of the water-soluble portion of wheat flour and demonstrates that this activity originates from proteins rather than polysaccharides. Further, purification, characterization, and simulations studies of two proteins identified during the purification that may be of interest (a dimeric α-amylase inhibitor, AAI, and an α-amylase inhibitor, WDAI-3) were performed. Using a soybean Kunitz-type trypsin inhibitor as a control, MD simulations of these two novel antifreeze proteins under freezing-like conditions, clearly show that WDAI-3 exhibits the highest amount of IRI activity and rapidly stunts the growth of large ice structures within the simulations while AAI has a comparable IRI to the soybean KTI (control). Further analysis explains the high IRI activity of WDAI-3 from two perspectives: protein structure and water-protein interactions. This study provides valuable insights into the potential application of the water-soluble portion of wheat flour, particularly its dialyzed part, as a natural antifreeze agent for enhancing food preservation during cold storage.

REFERENCES

Akhlaghi, Y., Ghaffari, S., Attar, H., & Alamir Hoor, A. (2015). A rapid hydrolysis method and DABS-Cl derivatization for complete amino acid analysis of octreotide acetate by reversed phase HPLC. *Amino Acids, 47*(11), 2255-2263. https://doi.org/10.1007/s00726-015-1999-9.

Biggs, C., Stubbs, C., Graham, B., Fayter, A. E. R., Hasan, M., & Gibson, M. I. (2019). Mimicking the ice recrystallization activity of biological antifreezes. when is a new polymer "active"? *Macromol Biosci, 19*(7), e1900082. https://doi.org/10.1002/mabi.201900082.

Chen, X., Li, L., Yang, F., Wu, J., & Wang, S. (2020). Effects of gelatin-based antifreeze peptides on cell viability and oxidant stress of Streptococcus thermophilus during cold stage. *Food and Chemical Toxicology, 136*, 111056. https://doi.org/https://doi.org/10.1016/j.fct.2019.111056.

Chen, X., Wu, J., Cai, X., & Wang, S. (2021). Production, structure-function relationships, mechanisms, and applications of antifreeze peptides. *Compr Rev Food Sci Food Saf, 20*(1), 542-562. https://doi.org/10.1111/1541-4337.12655.

Damodaran, S., & Wang, S. (2017). Ice crystal growth inhibition by peptides from fish gelatin hydrolysate. *Food Hydrocolloids, 70*, 46-56. https://doi.org/10.1016/j.foodhyd.2017.03.029.

Fomich, M., Día, V. P., Premadasa, U. I., Doughty, B., Krishnan, H. B., & Wang, T. (2023). Ice recrystallization inhibition activity of soy protein hydrolysates. *Journal of Agricultural and Food Chemistry, 71*(30), 11587-11598.

Fu, W., Wang, P., Chen, Y., Lin, J., Zheng, B., Zeng, H., & Zhang, Y. (2019). Preparation, primary structure and antifreeze activity of antifreeze peptides from Scomberomorus niphonius skin. *LWT, 101*, 670-677. https://doi.org/https://doi.org/10.1016/j.lwt.2018.11.067.

Geisslitz, S., Weegels, P., Shewry, P., Zevallos, V., Masci, S., Sorrells, M., . . . Brouns, F. (2022). Wheat amylase/trypsin inhibitors (ATIs): occurrence, function and health aspects. *Eur J Nutr, 61*(6), 2873-2880. https://doi.org/10.1007/s00394-022-02841-y.

Ghalamara, S., Silva, S., Brazinha, C., & Pintado, M. (2022). Structural diversity of marine anti-freezing proteins, properties and potential applications: a review. *Bioresources and Bioprocessing, 9*(1). https://doi.org/10.1186/s40643-022-00494-7.

Huang, J., Rauscher, S., Nawrocki, G., Ran, T., Feig, M., de Groot, B. L., . . . MacKerell, A. D., Jr. (2017). CHARMM36m: an improved force field for folded and intrinsically disordered proteins. *Nat Methods, 14*(1), 71-73. https://doi.org/10.1038/nmeth.4067.

Hubbard, R. E., & Kamran Haider, M. (2010). Hydrogen Bonds in Proteins: Role and Strength. In *Encyclopedia of life sciences*.

Humphrey, W., Dalke, A., & Schulten, K. (1996). VMD: Visual molecular dynamics. *Journal of Molecular Graphics, 14*(1), 33-38. https://doi.org/https://doi.org/10.1016/0263-7855(96)00018-5.

Jo, S., Kim, T., Iyer, V. G., & Im, W. (2008). CHARMM-GUI: a web-based graphical user interface for CHARMM. *Journal of computational chemistry, 29*(11), 1859-1865.

Jumper, J., Evans, R., Pritzel, A., Green, T., Figurnov, M., Ronneberger, O., . . . Hassabis, D. (2021). Highly accurate protein structure prediction with AlphaFold. *Nature, 596*(7873), 583-589. https://doi.org/10.1038/s41586-021-03819-2.

Kasar, S. S., Marathe, K. R., Bhide, A. J., Herwade, A. P., Giri, A. P., Maheshwari, V. L., & Pawar, P. K. (2017). A glycoprotein alpha-amylase inhibitor from Withania somnifera differentially inhibits various alpha-amylases and affects the growth and development of Tribolium castaneum. *Pest Manag Sci, 73*(7), 1382-1390. https://doi.org/10.1002/ps.4467.

Knight, C. A., Hallett, J., & DeVries, A. (1988). Solute effects on ice recrystallization: an assessment technique. *Cryobiology, 25*(1), 55-60.

Kohlmeyer, A., Vermaas, J., & Braun, E. (2022). akohlmey/topotools: Release 1.9 (v1.9). https://doi.org/https://doi.org/10.5281/zenodo.7071898.

Lookhart, G. E. O. R., and Scott Bean. (1995). Separation and characterization of wheat protein fractions by high-performance capillary electrophoresis. *Cereal Chemistry, 72*(6), 527-532.

Mahoney, M. W., & Jorgensen, W. L. (2000). A five-site model for liquid water and the reproduction of the density anomaly by rigid, nonpolarizable potential functions. *The Journal of chemical physics, 112*(20), 8910-8922.

Matsumoto, M., Yagasaki, T., & Tanaka, H. (2018). GenIce: hydrogen-disordered ice generator. Wiley Online Library.

Midya, U. S., & Bandyopadhyay, S. (2014). Hydration behavior at the ice-binding surface of the Tenebrio molitor antifreeze protein. *J Phys Chem B, 118*(18), 4743-4752. https://doi.org/10.1021/jp412528b.

Mochizuki, K., & Molinero, V. (2018). Antifreeze glycoproteins bind reversibly to ice via hydrophobic groups. *J Am Chem Soc, 140*(14), 4803-4811. https://doi.org/10.1021/jacs.7b13630.

Monalisa, K., Shibata, M., & Hagiwara, T. (2023). Ice recrystallization inhibition behavior by wheat flour and its synergy effect with antifreeze protein III. *Food Hydrocolloids, 143*. https://doi.org/10.1016/j.foodhyd.2023.108882.

Naullage, P. M., & Molinero, V. (2020). Slow Propagation of Ice Binding Limits the Ice-Recrystallization Inhibition Efficiency of PVA and Other Flexible Polymers. *J Am Chem Soc, 142*(9), 4356-4366. https://doi.org/10.1021/jacs.9b12943.

Nguyen, A. H., & Molinero, V. (2015). Identification of Clathrate Hydrates, Hexagonal Ice, Cubic Ice, and Liquid Water in Simulations: the CHILL+ Algorithm. *J Phys Chem B, 119*(29), 9369-9376. https://doi.org/10.1021/jp510289t.

Nielsen, S. S. (2017). *Food analysis laboratory manual*: Springer.

Pace, C. N., Fu, H., Lee Fryar, K., Landua, J., Trevino, S. R., Schell, D., . . . Grimsley, G. R. (2014). Contribution of hydrogen bonds to protein stability. *Protein Sci, 23*(5), 652-661. https://doi.org/10.1002/pro.2449.

Piergiovanni, A. R. (2007). Extraction and separation of water-soluble proteins from different wheat species by acidic capillary electrophoresis. *Journal of Agricultural and Food Chemistry, 55*(10), 3850-3856.

The PyMOL Molecular Graphics System, Version 1.2r3pre, Schrödinger, LLC.

Saad, J., Fomich, M., Día, V. P., & Wang, T. (2023). A novel automated protocol for ice crystal segmentation analysis using Cellpose and Fiji. *Cryobiology, 111*, 1-8. https://doi.org/https://doi.org/10.1016/j.cryobiol.2023.02.002.

Sargsyan, K., Grauffel, C., & Lim, C. (2017). How Molecular Size Impacts RMSD Applications in Molecular Dynamics Simulations. *J Chem Theory Comput, 13*(4), 1518-1524. https://doi.org/10.1021/acs.jctc.7b00028.

Silano, V., Pocchiari, F., & Kasarda, D. D. (1973). Physical characterization of α-amylase inhibitors from wheat. *Biochimica et Biophysica Acta (BBA)-Protein Structure, 317*(1), 139-148.

Stukowski, A. (2009). Visualization and analysis of atomistic simulation data with OVITO–the Open Visualization Tool. *Modelling and simulation in materials science and engineering, 18*(1), 015012.

Sun, X., Guo, R., Zhan, T., Kou, Y., Ma, X., Song, H., . . . Wu, Y. (2024). Retarding ice recrystallization by tamarind seed polysaccharide: Investigation in ice cream mixes and insights from molecular dynamics simulation. *Food Hydrocolloids, 149*. https://doi.org/10.1016/j.foodhyd.2023.109579.

Wang, S., Agyare, K., & Damodaran, S. (2009). Optimisation of hydrolysis conditions and fractionation of peptide cryoprotectants from gelatin hydrolysate. *Food Chemistry, 115*(2), 620-630. https://doi.org/10.1016/j.foodchem.2008.12.079.

Yang, W., Liao, Y., Shi, Q., & Sun, Z. (2023). The Atomistic Understanding of the Ice Recrystallization Inhibition Activity of Antifreeze Glycoproteins. *Crystals, 13*(3). https://doi.org/10.3390/cryst13030405.

Yuan, Y., Dia, V. P., & Wang, T. (2024). The ice recrystallization inhibition activity of wheat glutenin hydrolysates and effect of salt on their activity. *Food Hydrocolloids, 154*. https://doi.org/10.1016/j.foodhyd.2024.110153.

Yuan, Y., Fomich, M., Dia, V. P., & Wang, T. (2023). Succinylation of zein and gelatin hydrolysates improved their ice recrystallization inhibition activity. *Food Chem, 424*, 136431. https://doi.org/10.1016/j.foodchem.2023.136431.

Zhang, Y., Wang, W., Liu, Y., Liu, X., Wang, H., & Zhang, H. (2022). Cryoprotective effect of wheat gluten enzymatic hydrolysate on fermentation properties of frozen dough. *Journal of Cereal Science, 104*. https://doi.org/10.1016/j.jcs.2022.103423.

Zhao, A., Shi, P., Yang, R., Gu, Z., Jiang, D., & Wang, P. (2022). Isolation of novel wheat bran antifreeze polysaccharides and the cryoprotective effect on frozen dough quality. *Food Hydrocolloids, 125*. https://doi.org/10.1016/j.foodhyd.2021.107446.

Zhou, W., Wang, F., Yu, J., Li, X., & Liu, Y. (2019). Cryoprotective Effects of Protein Hydrolysates Prepared from By-Products of Silver Carp (Hypophthalmichthys

Molitrix) on Freeze-Thawed Surimi. *Applied Sciences, 9*(3). https://doi.org/10.3390/app9030563.

APPENDIX

Table 4.1. Impact of enzymatic hydrolysis on protein and polysaccharides content and IRI activity of crude wheat albumin isolated from wheat flour.

Sample		Protein content (%)	Polysaccharides content (%)	ICS (%)* in 1xPBS		
Enzyme	**Hydrolysis time (h)**			**40mg/mL**	**20mg/mL**	**10mg/mL**
Crude albumin		21.5±4.2^{c}	63.9±2.4^{a}	61.3±1.0^{d}	71.8±4.3^{c}	104.5±4.4^{ab}
Albumin after dialysis		47.7±0.6^{b}	42.1±1.7^{bc}	56.2±1.8^{d}	67.1±0.3b^{c}	84.9±2.9^{b}
Alcalase	0.5	28.3±2.6^{c}	55.5±2.7^{ab}	91.5±1.9^{b}	103.3±4.0^{a}	112.8±5.3^{a}
	1	21.6±1.3^{c}	61.7±3.8^{a}	96.3±1.8^{ab}	99.1±6.6^{a}	110.3±0.8^{a}
	24	15.8±2.2^{c}	62.7±2.7^{a}	102.6±5.6^{a}	105.9±7.9^{a}	100.7±6.2^{ab}
Cellulase	12	41.4±6.1^{b}	54.0±6.2^{ab}	89.5±2.3^{b}	101.1±5.3^{a}	107.8±12.6^{a}
	24	68.1±7.2^{c}	32.3±2.1^{cd}	79.5±0.4^{c}	96.4±6.6^{a}	102.4±5.8^{ab}
	48	64.1±4.6^{c}	26.2±0.1^{d}	79.2±1.2^{c}	87.6±4.1^{ab}	94.6±6.0^{ab}

Different lowercase letters in the same column indicates significant differences among means ($P < 0.05$)

*The IRI activity was expressed as the average ice crystal size (ICS) relative to a PEG negative control at the same concentration (40 mg/mL) in 1x PBS. Lower ICS values indicate greater activity

Table 4.2. The average molecular weight, protein and polysaccharides composition, and IRI activity of crude wheat albumin extract and their corresponding fractions separated by gel filtration chromatography.

Sample	Average MW (KDa)	Protein content (%)	Polysaccharide content (%)	ICS (%) in 1xPBS		
				40mg/mL	20mg/mL	10mg/mL
Crude Albumin	12.7±0.3^{ab}	21.5±4.2^{de}	63.9±2.4^{b}	61.3±1.0^{d}	71.8±4.3^{bc}	104.5±4.4^{abc}
After filter	12.6±0.3^{ab}	28.4±0.7^{cd}	67.7±1.8^{b}	67.9±0.2^{cd}	76.1±5.9^{bc}	93.2±0.6^{bcd}
F1	15.4±4.4^{a}	54.4±2.1^{a}	38.6±0.4^{c}	59.2±2.2^{d}	68.1±2.6^{c}	80.9±4.2^{d}
F2	9.0±0.9^{bc}	43.0±5.6^{b}	45.5±1.8^{c}	73.5±1.8^{bc}	80.1±1.1^{bc}	102.3±6.6^{abc}
F3	4.6±0.5^{cd}	37.4±7.9^{bc}	70.3±0.7^{b}	78.2±4.1^{b}	86.4±2.6^{b}	95.8±3.5^{bcd}
F4	1.9±0.0^{d}	12.9±2.1^{ef}	95.6±4.6^{a}	76.5±4.1^{bc}	84.6±7.8^{b}	110.9±9.0^{ab}
F5	0.2±0.0^{d}	2.9±1.0^{f}	75.7±2.0^{b}	81.2±3.5^{b}	79.4±3.8^{bc}	90.9±3.8^{cd}
F6	0.2±0.0^{d}	1.3±0.3^{f}	14.7±2.3^{d}	132.3±0.5^{a}	123.3±2.5^{a}	117.8±6.9^{a}

Different lowercase letter in the same column indicates significant differences among means ($P < 0.05$)

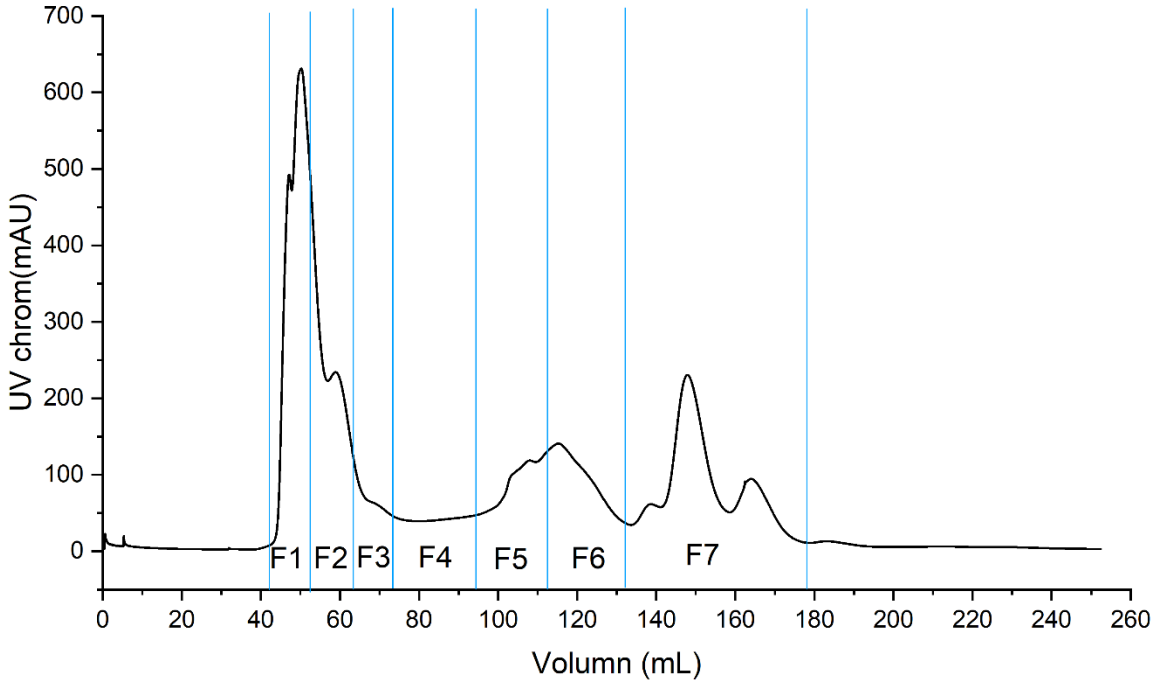

Figure 4.1. Fractionation of filtered crude wheat albumin extract by gel filtration chromatography

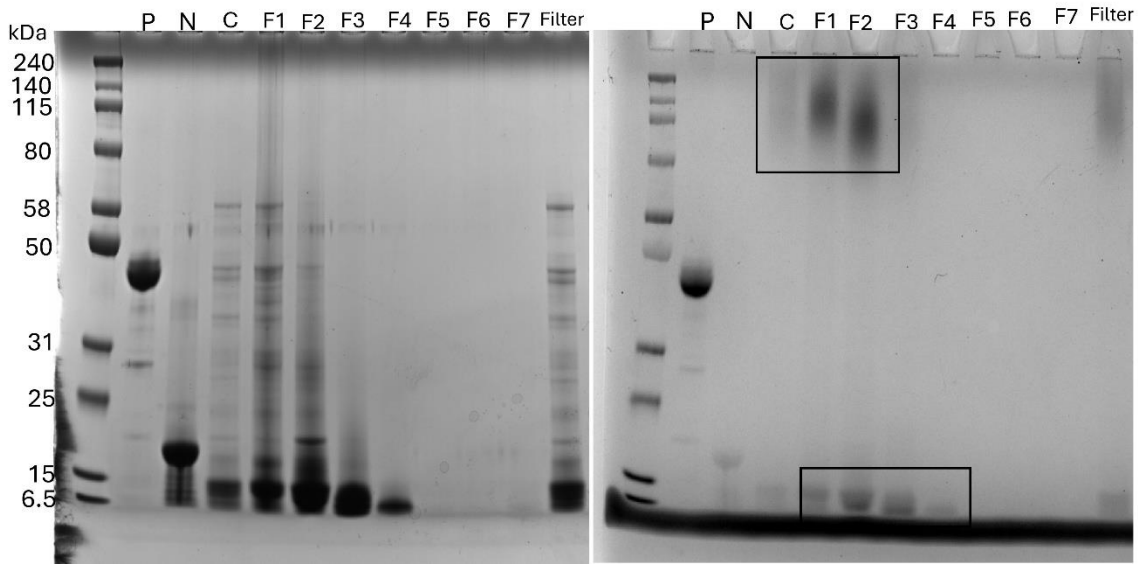

Figure 4.2. SDS-PAGE (left figure) and PAS glycoprotein analysis (right figure) of albumin and different fractions with controls. P: positive control for glycoprotein detection, N: negative control for glycoprotein detection, C: crude albumin extract from wheat, F followed by a number refers to a gel filtration chromatography fraction, filter: albumin after 0.22 µm filtration using PVDF membrane.

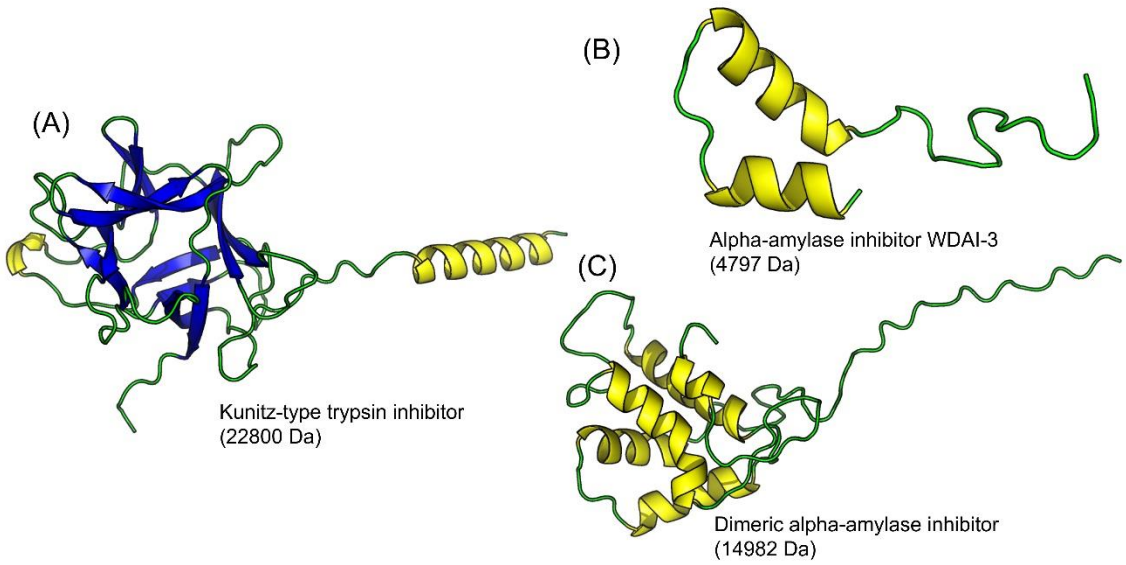

Figure 4.3. The structural models of trypsin inhibitors from soybean (A) and wheat alpha-amylase inhibitors proteins (B-C). Yellow: α-helix, Blue: β-sheet, Green: loops and undefined structures

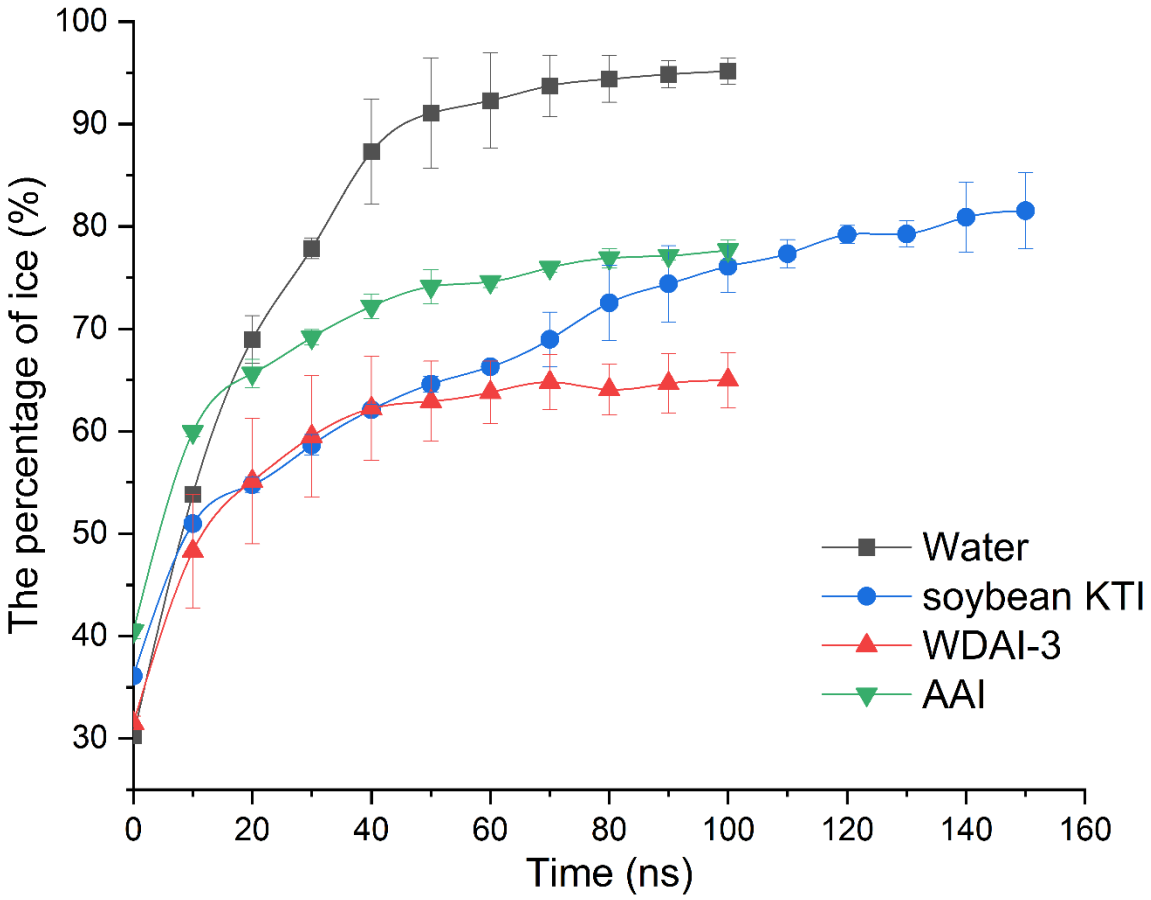

Figure 4.4. Time evolution of the percentage of ice molecules during the simulation. The error bars represent the standard deviation calculated from 3 independent simulation runs.

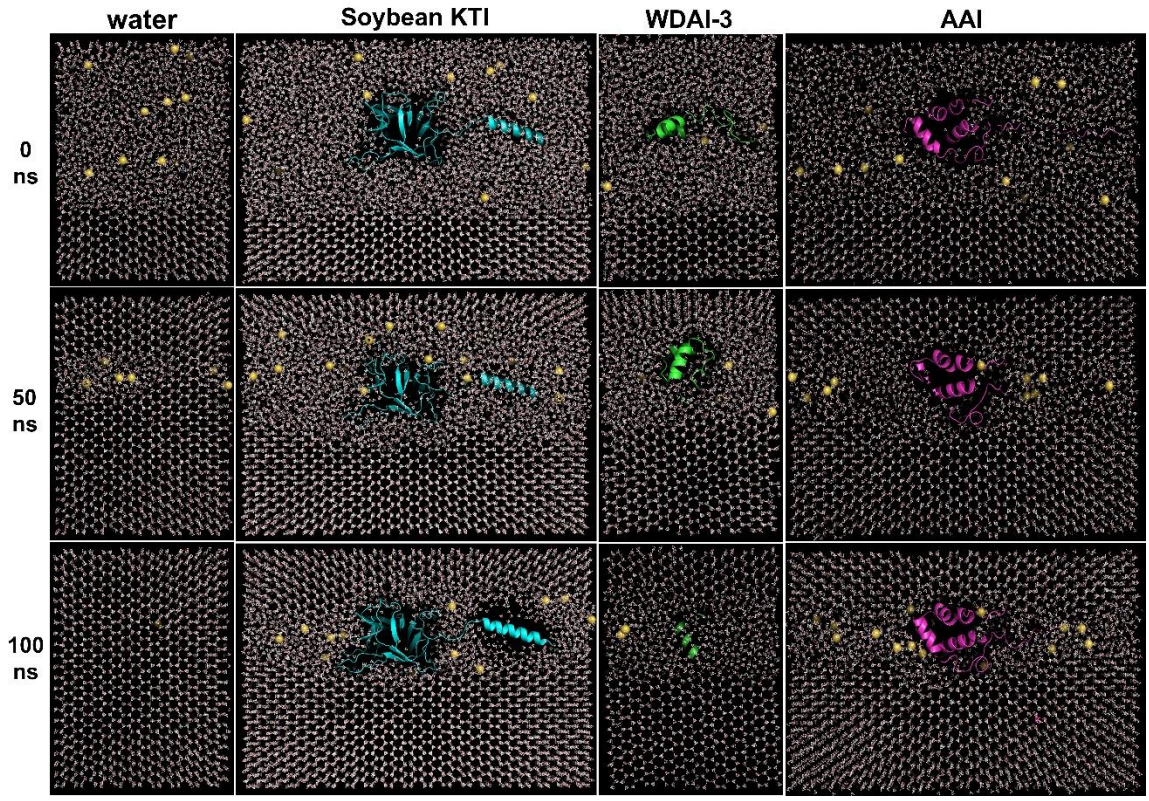

Figure 4.5. Corresponding representative snapshots of simulation systems during 100 ns at 265.15 K. Yellow: ions of sodium chloride.

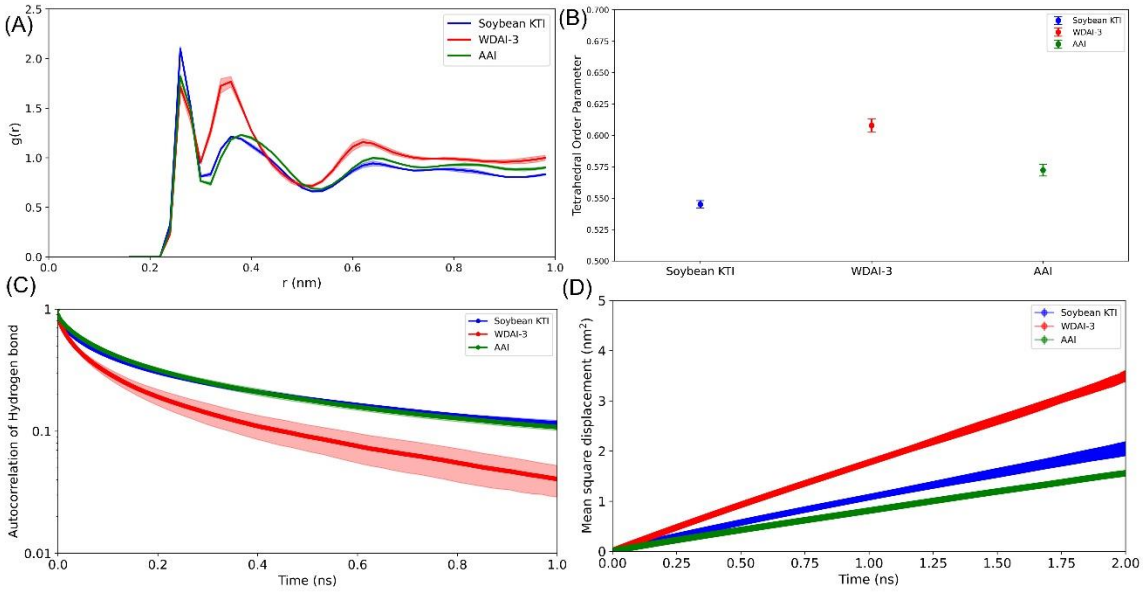

Figure 4.6. Time evolution of water and water interactions among three proteins during simulation. (A) the proximal radial distribution function between the water oxygen atoms and the protein non hydrogen atoms of the three different proteins, (B) tetrahedral order parameters of oxygen atom of water molecules, (C) autocorrelation of hydrogen bond between water and water, (D) mean squared displacement of oxygen atom of water molecules. The shaded areas around each curve represent the standard deviation (SD) values

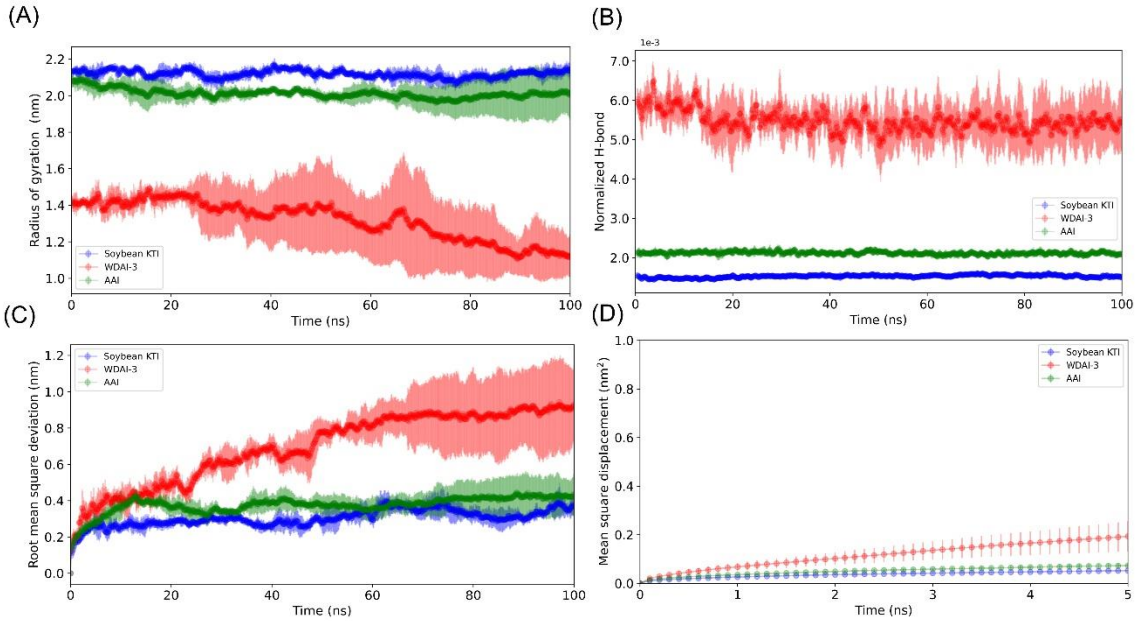

Figure 4.7. Time evolution of conformational changes among three proteins during simulation. (A) radius of gyration, (B) normalized hydrogen bond between protein and protein based on total possible hydrogen bond, (C) root mean square deviation of protein, (D) mean squared displacement of protein. The shaded areas around each curve represent the standard deviation (SD) values. Note that MSD calculations were performed over the timeframe 50ns to 100ns.

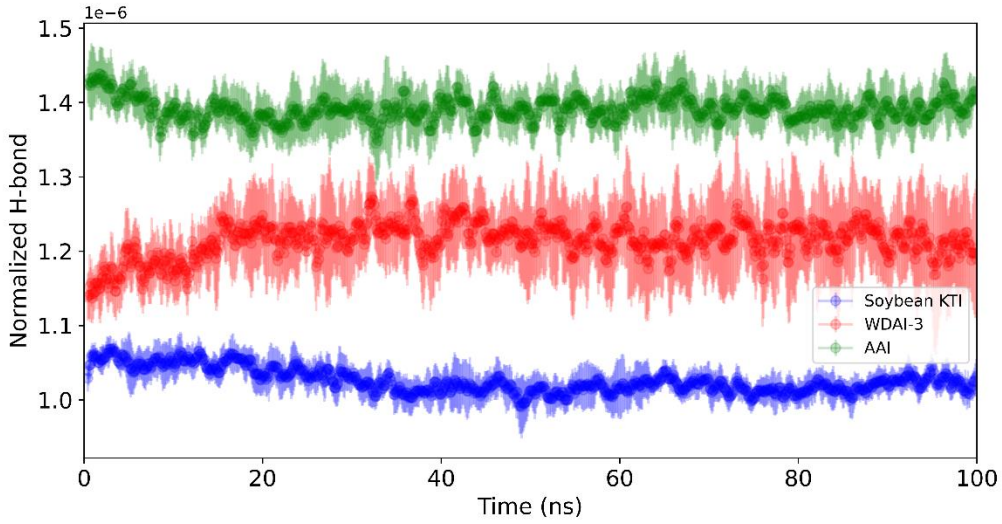

Figure 4.8. Time evolution of normalized hydrogen bond between water and protein during simulation.

CHAPTER FIVE

ICE RECRYSTALLIZATION ACTIVITY OF GELATIN HYDROLYSATES IS AFFECTED BY THE PRESENCE OF XANTHAN GUM

Abstract

This study investigates the influence of xanthan gum (XG) on the ice recrystallization inhibition (IRI) activity of gelatin hydrolysates prepared by enzymatic hydrolysis using trypsin and Alcalase at different times. The results demonstrated that XG significantly enhanced the IRI activity of gelatin hydrolysates even at very low concentrations (0.1 % and equals to the 5 % of the total solute), and this enhancement plateaued at higher XG concentrations. Furthermore, the molecular weight (MW) of the gelatin hydrolysates influenced their IRI effectiveness of mixture, with higher MW hydrolysates (3 kDa) exhibiting greater IRI activity than lower MW hydrolysates (0.5 kDa). Mechanical mixing further influenced the complex structures and their IRI activity. Specifically, a short stirring time (5 min) facilitated the formation of more rigid and ordered secondary structures (α-helix and β-sheet), corresponding to greater IRI activity. These findings provide valuable insights into how polysaccharides content, MW, and mechanical processing affect antifreeze activity of protein hydrolysates.

Introduction

While antifreeze proteins (AFPs) are commonly extracted and purified from natural sources, enzymatic hydrolysis of food proteins is more frequently used to prepare antifreeze peptides because of the low cost and wide applications. Among these, gelatin and collagen hydrolysates prepared under different hydrolysis conditions have been extensively studied (Cao et al., 2016; Damodaran, 2007; Damodaran & Wang, 2017; Wang et al., 2015). However, real food systems contain multiple components beyond proteins or peptides, such as polysaccharides, which may influence their ice recrystallization inhibition (IRI) activity. In our previous study, we found that the water-soluble fractions from wheat and black soldier fly larvae (comprising approximately 50 % polysaccharides and 50% proteins) exhibited the highest IRI activity (Fomich et al., 2025). However, no research has explored how these polysaccharides influence the IRI activity of proteins hydrolysates.

Some polysaccharides themselves are used to prevent frozen damage of foods, such as κ-carrageenan (Leiter et al., 2018). Additionally, polysaccharides have been shown to influence the activity of AFPs. For example, the presence of corn starch (Monalisa, et al., 2021) and wheat flour (Monalisa et al., 2023) can reduce ice crystal size in systems containing AFP III. This synergistic effect may be attributed to the hydration properties of starch, which may weaken water-AFP III interactions while simultaneously enhancing protein binding to ice crystal surfaces (Monalisa et al., 2023). Moreover, gum-based polysaccharides, including κ-carrageenan, also show cryoprotective synergy when combined with AFP I and antifreeze glycoproteins (AFGPs) (Gaukel, Leiter, & Spieß,

2014). However, other studies have showed antagonistic effects: In a system with whey protein isolate (WPI) and carrageenan, adding 5 % WPI resulted in larger ice crystals than using carrageenan alone (Chun, Kim, & Min, 2012). This contrasting behavior highlights the complexity of protein-polysaccharide interactions and the resulting IRI activity.

Building on these observations, the present study focuses on gelatin hydrolysate, which are the most extensively studied antifreeze hydrolysates and its interactions with xanthan gum (XG). In this study, gelatin hydrolysates were prepared using two different enzymes under varying hydrolysis durations to determine how the presence of polysaccharides and the hydrolysates' molecular characteristics (molecular weight) affect IRI activity. XG was chosen as a representative food-grade polysaccharide due to its high-water solubility, stability over wide pH ranges, and frequent usage in commercial products such as sauces and beverages.

Soluble peptides and polysaccharides will naturally form complexes because of electrostatic interactions (Schmitt et al., 2009), which can further aggregate to form a three-dimensional network due to charge neutralization. During cold storage, gelatin has a triple helix structure (Liu et al, 2021), while XG solution has a helical conformation (Bercea & Morariu, 2020). The uniqueness of gelatin and XG mixture is their conformational changes and interactions as temperature decreases. Specifically, XG molecules transition from disordered coils to ordered helices, and gelatin molecules form triple helical structures below their transition temperature (Wang et al., 2016). These gelatin helices may connect and stabilize the XG complexes through hydrogen bonding,

ultimately forming a network of biopolymer-rich domains (Wang et al., 2018). Our previous study demonstrated a significant relationship between α-helix content or conformational rigidity and antifreeze activity (Yuan et al., 2024), suggesting that structural shifts in XG-gelatin complexes could be crucial to their IRI performance.

In addition, mechanical treatment can also impact the microstructure and coacervation behavior of mixtures (Ould et al., 2006). Depending on the intensity, shear can either induce aggregate formation or promote aggregate break-up. For instance, moderate shear of β-lactoglobulin/acacia gum mixtures increased complex size due to partial protein denaturation and subsequent aggregation (Sanchez et al., 2001). Conversely, for lactoglobulin/carrageenan gels, shear produced a more compact but less homogeneous network, which could be disrupted under excessive conditions (Ould et al., 2006). Hence, shearing may also modulate the conformational stability and network structure of the XG and gelatin hydrolysate system, ultimately impacting its antifreeze capacity.

The hypothesis of this work is that the IRI activity of gelatin hydrolysates can be enhanced in the presence of XG due to interactions resulting in unique conformational changes. Moreover, mechanical shear may further alter the structural conformation and IRI activity of these complexes. Therefore, the objectives of this study are to study the IRI activity of gelatin hydrolysates in the presence of different concentrations of XG, and to investigate the influence of additional mechanical shear on their structural properties and IRI activity changes.

Methods and materials

Preparation of protein hydrolysates

Knox gelatin (type A) was purchased from a local supermarket and then dissolved in deionized water at 2 % (w/v), after which the pH was adjusted to 8.0 using 1 M NaOH to facilitate hydrolysis by trypsin and Alcalase. The optimal hydrolysis temperatures were 37 °C for trypsin used at 280 Au/g protein, and 55 °C for Alcalase used at 0.176 Au/g protein. Trypsin hydrolysis was carried out for 1, 3, or 6 hours, whereas Alcalase hydrolysis was conducted for 5, 10, or 30 min. Following hydrolysis, the samples were boiled for 10 minutes to inactivate the enzymes and then freeze-dried for further use.

Measurement of the molecular weight of gelatin hydrolysates by HPLC

The molecular weight of gelatin hydrolysates was analyzed with a BioSep-SEC-s2000 column (Phenomenex, Torrance, CA, USA). The mobile phase comprised 45:55 (v/v) acetonitrile and HPLC-grade water, supplemented with 0.05% trifluoroacetic acid, and detected at 214 nm. Molecular size distribution was evaluated by comparing retention profiles to protein standards (albumin, aprotinin, bradykinin acetate, bradykinin fragment 1-5, glutathione, and glycine). A linear calibration curve was obtained by plotting retention times against the logarithms of the standards' molecular weight (M_w), which was used to calculate the M_w of each chromatographic peak. The overall average molecular weight of hydrolysates was determined by the proportional contribution of each peak, based on its integrated area.

Preparation of XG-protein hydrolysates mixture or complex

Different concentrations of XG (0.1, 0.2, 0.3 and 0.4 %) were prepared in 1xPBS, and stored at 4 °C overnight (24 hours) to ensure complete solubility. Subsequently, each XG concentration was combined with corresponding gelatin hydrolysates concentration (1.9, 1.8, 1.7, and 1.6 %) to maintain the total solute mass concentration of 2 % (20 mg/mL). Therefore, the final percentages of XG in the mixtures are 5, 10, 15 and 20 %. There are 3 mixing treatments in this study: 1) no mixing of mixture, 2) mixing by vortex for 5 min (2000 rpm) at room temperature, and 3) extended mixing for 60 min at the same speed. All samples were stored at 4 °C overnight (18 hours) prior to IRI activity analysis.

Measurement of IRI activity by splat assay

The assay procedure and data analysis were conducted in accordance with our previously methods (Saad et al., 2023; Yuan et al., 2023). The complex prepared by last section was used to compare the ice crystal size after annealed at -8 °C for 30 min. Each sample was prepared in duplicate, and every replicate was examined twice using separate slides. Three images per slide were captured, and the Feret's maximum diameter for each ice crystal was determined using ImageJ software. To calculate the relative IRI activity, the average ice crystal size in the sample was divided by the average of a control solution containing polyethylene glycol at the same concentration (2 % w/w), and expressed as ICS %.

Measurement of the surface amphiphilicity by the pendant drop method

The complex preparation followed the procedure described in previous section. Briefly, the complexes were initially dissolved in 1× PBS to obtain final concentrations of either

0.3 % XG with 1.7 % gelatin hydrolysates or 0.4 % XG with 1.6 % gelatin hydrolysates, resulting in a total solute concentration of 2 %. The prepared solutions were subsequently diluted with 1× PBS to achieve final concentrations of 1.75, 1.5, 1.0, 0.5, 0.25, 0.125, and 0.0625 %. Surface tension (SFT) was measured using a DSA100 drop shape analyzer (KRÜSS, Hamburg, Germany) with the pendant drop method. Each sample was measured in triplicate. For each measurement, approximately 18 μL of the sample was suspended from a metal needle with a diameter of 1.822 mm. The droplet was allowed to equilibrate for 60 seconds to ensure surface saturation before data collection. SFT was recorded for 120 seconds at a frequency of 2 frames per second, yielding a total of 240 data points. All measurements and data analyses were conducted using the ADVANCE software (KRÜSS).

Measurement of microstructure of complex by confocal laser scanning microscopy (CLSM)

A 0.1 mL aliquot of the complex was stained with 50 μL of 0.05 mg/mL fluorescein 5-isothiocyanate (FITC; Sigma-Aldrich) to label proteins (green fluorescence) and 50 μL of 0.05 mg/ mL Rhodamine B (Sigma-Aldrich) to label carbohydrates (red fluorescence). Due to the limited water solubility of FITC, a stock solution (1 mg/mL) was initially prepared in dimethyl sulfoxide (DMSO) and subsequently diluted in 1× PBS buffer to obtain the desired working concentration (0.05 mg/mL). After staining, the samples were stored at 4 °C overnight to allow complete dye incorporation. The excitation/emission wavelengths for FITC and Rhodamine B were 488 nm/518 nm and 543 nm/567 nm, respectively. Microstructural analysis was performed using an inverted confocal laser

scanning microscope (CLSM; Leica Microsystems, Baden-Württemberg, Germany). Three images were taken from each sample randomly.

Measurement of secondary structure of complex by circular dichroism (CD)

The secondary structure of the complexes was analyzed using a J-1500 CD spectrophotometer (JASCO, Tokyo, Japan) at 25 °C with a 0.2 mm quartz cell. Samples were prepared as described in previous section and diluted with DI water to a final concentration of 0.4 mg/mL. A background spectrum was recorded using 20 µL of 1× PBS diluted in 980 µL DI water. Spectra were collected from 176 to 400 nm with a 1 nm bandwidth and a 0.5 nm step resolution. CD signals were recorded in millidegrees (mdeg, θ). The secondary structure content was determined using DichroWeb (http://dichroweb.cryst.bbk.ac.uk/html/home.shtml) with the CONTIN algorithm. During the calculation, the mean residue weight was set at 110 Da, and the protein reference data set was according to Sreerama and Woody (2000).

Statistical analysis

"Statistical analyses were performed using data obtained from two independent experiments, each conducted in triplicate. Results were expressed as mean ± standard deviation and analyzed using Excel 2020. Graphs and regression models' analysis were generated with Origin 2021 Pro.

Results and discussion

The impact of XG on the IRI activity of gelatin hydrolysates

In this study, six gelatin hydrolysates made by two proteases (Alcalase and trypsin) with 3 different times were analyzed for their IRI activities. Furthermore, the impact of XG

addition on the IRI activity of these six hydrolysates was investigated. **Figure 5.1** illustrates that all gelatin hydrolysates exhibited negligible IRI activity, as the ICS remains above 100 % at a concentration of 20 mg/mL. However, the addition of XG significantly reduced ice crystal size, indicating enhanced IRI activity of gelatin hydrolysates, even at relatively low concentrations (as low as 5% of the total solute concentration). Pure XG alone exhibited no intrinsic IRI activity, with ICS values of 113.8%, 112.4%, 114.0%, and 92.97% at concentrations ranging from 0.1% to 0.4%. This observation shows that XG and gelatin hydrolysates could have synthetic effect on inhibiting ice recrystallization.

Furthermore, ice crystals size shows a clear decreasing trend of decreasing with increasing XG concentration added in the gelatin hydrolysates. This relationship aligns well with a second-order polynomial fit, as indicated by the fitted equation $y=130.59612+(-6.05517)\ x+(0.13314)\ x^2$, where y represents ICS %, and x represents XG concentration. This shows a quadratic relationship where ICS decreases rapidly at the lower XG concentrations (0.1 and 0.2 %) but also shows a potential leveling off or slight rebound at higher XG concentration (0.4 %). This indicates that the enhancement of IRI activity becomes less significant as XG concentration increases. This trend was consistent across all hydrolysates produced by both proteases, indicating that the influence of XG on IRI activity is independent of the enzyme used for hydrolysis. The model's adjusted R^2 value of 0.66071 suggests a moderate correlation, explaining approximately 66.1 % of the variance in ICS based on XG concentration. The confidence intervals, as shown by

the shaded red region in the figure, indicate increasing uncertainty at higher XG concentrations.

The impact of the molecular weight (MW) of hydrolysates on IRI activity of complex

The MW of hydrolysates is commonly regarded as a key determinant of their IRI activity (Chen, Wu, Cai, & Wang, 2021). Therefore, the MW profiles of the six hydrolysates, as well as their ICS in the presence of varying XG concentrations (0, 0.1, 0.2, 0.3, and 0.4 %), are presented in **Table 5.1** and **Figure 5.2** to show whether the observed enhancement in IRI activity with XG addition is linked to MW of hydrolysates. Linear regression analysis was performed to explore the relationship between ICS and hydrolysate MW at different XG concentrations.

Notably, at 0.1 % XG (5% of the total solute concentration), a strong negative correlation ($R^2 = 0.92$) was observed between ICS and MW, suggesting that higher MW peptides reduced ice crystal size more effectively. This trend still can be observed at the higher XG concentrations (0.3 and 0.4%), but the R^2 is reduced associated with the effect of gelatin hydrolysates made by trypsin for 1 hour resulting poor correlation. This suggests that while hydrolysate MW plays a crucial role in determining IRI activity, additional factors, such as structural characteristics or specific interactions with XG, may also influence the overall effect.

The impact of stirring time on the IRI activity of complex

Figure 5. 3 shows the effect of 3 mechanical stirring times on the IRI activity of hydrolysate-XG complexes. In general, samples mixed for 5 min exhibited the smallest ice crystal size, whereas extended mixing for 60 min tended to increase crystal size.

However, this trend was not consistent across all samples. This discrepancy may be attributed to prolonged stirring altering the microstructure and secondary structure of the complex, which in turn could influence their IRI activity.

Confocal laser scanning microscopy (CLSM) observation of the complex

To investigate the structural changes induced by mechanical mixing, CLSM was used to visualize the spatial distribution and interactions between gelatin hydrolysates and XG (**Figure 5.4**). In the no mixing sample, proteins and polysaccharides were relatively homogeneously distributed, indicating that the two components were well separated in the dispersion without interaction.

However, after 5 minutes of mixing, small aggregates were observed, suggesting the interactions between XG and hydrolysates. This interaction might be related with their higher IRI activity, as larger size of self-assembly polymer is often linked to enhanced IRI effects likely due to improved steric hindrance, cooperative surface interactions, and increased interfacial area (Fu et al., 2023; Georgiou et al., 2021; Li, Li, Zhong, & Wu, 2020). However, when the mixing time was extended to 60 minutes, larger clusters were formed, corresponding to reduced IRI activity. The CLSM images showed that these large clusters were predominantly red-stained polysaccharide aggregates, with hydrolysates only loosely associated around the polysaccharide network. This suggests that prolonged mixing induced excessive aggregation of XG, forming a dense gel-like network. This structural change could trap or spatially exclude molecules, preventing them from freely diffusing to ice water interfacial, thereby reducing their ability to participate in effective IRI action (Monalisa et al., 2023). Similar behavior has been

reported for κ-carrageenan, where salt-induced gelation limited the number of mobile and surface-active molecules, resulting in lower IRI activity (Leiter et al., 2018). In the current system, the formation of large XG aggregates similarly reduces the population of free, surface-active complexes that can engage in effective antifreeze action.

Surface amphiphilicity of the complex

The critical micelle concentration (CMC) represents the key threshold at which micelles or other assembled structures begin to form (Sara et al., 2020). The native XG does not have CMC in aqueous solution (Krstonošić, Milanović, & Dokić, 2019), but the complex containing 85 % of gelatin hydrolysates may allow them to self-assemble into micelle-like aggregates in aqueous environments, due to presence of hydrophobic peptide segment and hydrophilic segments.

As shown in **Figure 5A-C**, both the "no mixing" and "5 min vortex" samples with 0.3 % XG exhibited distinct CMC-like behavior, while the "60 min vortex" sample did not. These findings suggest that prolonged stirring alters the self-assembly behavior of the system, requiring a higher concentration for micelle formation. CLSM analysis (**Figure 5.4**) confirms that extended mixing promotes the formation of large XG-rich aggregates, with hydrolysates adhering to the surface or being trapped within these clusters. This extensive aggregation alters the balance between free and aggregated species, removing a large fraction of the hydrolysates from the dynamic equilibrium responsible for micelle formation. As a result, the system no longer exhibits a clear CMC because the molecular species responsible for micelle formation are sequestered into large aggregates, leaving fewer free hydrolysate molecules available to participate in cooperative self-assembly.

Further supporting this interpretation, additional experiments (**Figure 5.5D-F**) with altered composition (1.6 % gelatin hydrolysates + 0.4 % XG) showed that both 5 min and 60 min mixing samples lost their CMC, while the "no mixing" sample still exhibited a clear CMC transition. This slightly higher XG proportion may enhance XG-XG interactions, further promoting aggregation at the expense of hydrolysate-XG complexes. This observation also aligns with the data shown in **Figure 5.1**, where ICS decreased rapidly as XG concentration is low (0.1 to 0.2 %) but appeared to plateau at high XG concentrations (0.3 to 0.4 %).

Figure 5.5 also demonstrates that extended stirring leads to an increase in surface tension at the total solute concentration is of 2 %, regardless of whether the XG concentration was 0.3 or 0.4 %. This phenomenon could be attributed to the exposure or shielding of specific hydrophilic or hydrophobic groups during stirring (Wang, Xiang, Li, Zhang, & Bai, 2021). These changes can further induce molecular conformational transitions, such as from a random coil structure to more ordered structures like helices or even aggregated networks. These conformational changes impact the interactions at the water-air interface, leading to variations in surface tension. In aqueous solutions containing XG, random coil conformations are more effective at reducing surface tension than helical structures (Young & Torres, 1989). This is because random coils exhibit greater flexibility, allowing them to spread more efficiently at the interface and make more extensive contact. Thus, the observed increase in surface tension with stirring time may reflect a decrease in the proportion of random coil conformations and an increase in more

rigid helical or ordered structures. This suggests potential structural alterations that could influence their IRI activity.

Conformational changes of complex by mixing

To further investigate the structure differences induced by mixing time, and their potential relationship with the IRI activity, CD spectroscopy was used to analyze the corresponding secondary structures. When the XG concentration was 0.3 %, the "5 min vortex" samples always exhibited a higher proportion of β-sheet and α-helix content, and a lower percentage of β-turn and unordered structures compared to the other treatments (as shown in **Table 5.3**). This suggests that shorter mixing times promoted a more ordered conformation, which aligns with earlier surface tension measurements (**Figure 5.5**). This also provide a possible reason for their high IRI activity, because a more rigid and ordered structure has been associated with higher IRI activity (Patel & Graether, 2010; Yuan Yuan et al., 2024). Such structural ordering may arise from the formation of small, well-organized aggregates (**Figure 5.4**), which could enhance molecular interactions. In contrast, prolonged mixing (60 min) resulted in a loss of β-sheet and α-helix content, suggesting that the formation of an extensive gel-like network by XG may have disrupted ordered molecular interactions. This structural transition likely contributed to the decrease in IRI activity observed in long-mixing samples.

Conclusion

In summary, the IRI activity of gelatin hydrolysates may be enhanced in the presence of XG, with a significant effect observed even at low XG concentrations (as low as 0.1 %). However, this enhancement plateaued at higher XG concentrations, reaching a maximum

of around 0.3 %. The extent of this enhancement was further influenced by the molecular weight (MW) of the hydrolysates and the mixing conditions. Specifically, higher-MW hydrolysates (~3 kDa) and short mixing durations (5 min) exhibited greater IRI activity. The conformational structure of the XG-gelatin hydrolysate complexes also played a key role in modulating IRI activity. Samples subjected to short mixing (5 min) showed the highest IRI activity, likely due to the formation of small, ordered aggregates enriched in β-sheet and α-helix structures-both of which have been associated with improved antifreeze properties. Surface tension measurements further supported this, revealing increased surface amphiphilicity in the 5 min mixed samples. Overall, this study demonstrates the synergistic effect of XG on the antifreeze activity of gelatin hydrolysates and underscores the importance of molecular conformation in governing IRI performance. Further investigations using precisely controlled mixing intensities and peptides with narrow molecular weight distributions may provide deeper mechanistic insights and help quantify structure-function relationships in IRI activity.

REFERENCES

Bercea, M., & Morariu, S. (2020). Real-time monitoring the order-disorder conformational transition of xanthan gum. *Journal of Molecular Liquids, 309*, 113168. https://doi.org/https://doi.org/10.1016/j.molliq.2020.113168.

Cao, H., Zhao, Y., Zhu, Y., Xu, F., Yu, J., & Yuan, M. (2016). Antifreeze and cryoprotective activities of ice-binding collagen peptides from pig skin. *Food Chemistry, 194*, 1245-1253. https://doi.org/https://doi.org/10.1016/j.foodchem.2015.08.102.

Chen, X., Wu, J., Cai, X., & Wang, S. (2021). Production, structure-function relationships, mechanisms, and applications of antifreeze peptides. *Compr Rev Food Sci Food Saf, 20*(1), 542-562. https://doi.org/10.1111/1541-4337.12655.

Chun, J.-Y., Kim, J.-M., & Min, S.-G. (2012). Effect of whey protein isolate on ice recrystallization characteristics in whey protein isolate/κ-carrageenan matrix. *Food Science of Animal Resources, 32*(5), 627-634.

Damodaran, S. (2007). Inhibition of ice crystal growth in Ice cream mix by gelatin hydrolysate. *J. Agric. Food Chem.*(55), 10918–10923.

Damodaran, S., & Wang, S. (2017). Ice crystal growth inhibition by peptides from fish gelatin hydrolysate. *Food Hydrocolloids, 70*, 46-56. https://doi.org/10.1016/j.foodhyd.2017.03.029.

Fomich, M., Yuan, Y., Krishnan, H., Dia, V., & Wang, T. (2025). Isolation and characterization of ice recrystallization inhibitory molecules from black soldier fly larvae. *Journal of Insects as Food and Feed, 1*(aop), 1-21.

Fu, Y., Li, Y., Weng, S., Qi, W., Su, H., & Li, T. (2023). Amyloid protein fibrils show enhanced ice recrystallization inhibition activity when serve as pickering emulsion stabilizer. *Food Hydrocolloids, 139*. https://doi.org/10.1016/j.foodhyd.2023.108581.

Gaukel, V., Leiter, A., & Spieß, W. E. L. (2014). Synergism of different fish antifreeze proteins and hydrocolloids on recrystallization inhibition of ice in sucrose solutions. *Journal of Food Engineering, 141*, 44-50. https://doi.org/10.1016/j.jfoodeng.2014.05.016.

Georgiou, P. G., Marton, H. L., Baker, A. N., Congdon, T. R., Whale, T. F., & Gibson, M. I. (2021). Polymer Self-Assembly Induced Enhancement of Ice Recrystallization Inhibition. *J Am Chem Soc, 143*(19), 7449-7461. https://doi.org/10.1021/jacs.1c01963.

Krstonošić, V., Milanović, M., & Dokić, L. (2019). Application of different techniques in the determination of xanthan gum-SDS and xanthan gum-Tween 80 interaction. *Food Hydrocolloids, 87*, 108-118. https://doi.org/https://doi.org/10.1016/j.foodhyd.2018.07.040.

Leiter, A., Emmer, P., & Gaukel, V. (2018). Influence of gelation on ice recrystallization inhibition activity of κ-carrageenan in sucrose solution. *Food Hydrocolloids, 76*, 194-203. https://doi.org/10.1016/j.foodhyd.2016.11.028.

Li, T., Li, M., Zhong, Q., & Wu, T. (2020). Effect of Fibril Length on the Ice Recrystallization Inhibition Activity of Nanocelluloses. *Carbohydrate Polymers, 240*, 116275. https://doi.org/https://doi.org/10.1016/j.carbpol.2020.116275.

Liu, K., Chen, Y. Y., Zha, X. Q., Li, Q. M., Pan, L. H., & Luo, J. P. (2021). Research progress on polysaccharide/protein hydrogels: Preparation method, functional property and application as delivery systems for bioactive ingredients. *Food Res Int, 147*, 110542. https://doi.org/10.1016/j.foodres.2021.110542.

Monalisa, K., Shibata, M., & Hagiwara, T. (2021). Ice Recrystallization Behavior of Corn Starch/Sucrose Solutions: Effects of Addition of Corn Starch and Antifreeze Protein III. *Food Biophysics, 16*(2), 229-236. https://doi.org/10.1007/s11483-020-09664-6.

Monalisa, K., Shibata, M., & Hagiwara, T. (2023). Ice recrystallization inhibition behavior by wheat flour and its synergy effect with antifreeze protein III. *Food Hydrocolloids, 143*. https://doi.org/10.1016/j.foodhyd.2023.108882.

Ould Eleya, M. M., Leng, X. J., & Turgeon, S. L. (2006). Shear effects on the rheology of β-lactoglobulin/β-carrageenan mixed gels. *Food Hydrocolloids, 20*(6), 946-951. https://doi.org/10.1016/j.foodhyd.2005.08.003.

Patel, S. N., & Graether, S. P. (2010). Increased flexibility decreases antifreeze protein activity. *Protein Sci, 19*(12), 2356-2365. https://doi.org/10.1002/pro.516.

Saad, J., Fomich, M., Día, V. P., & Wang, T. (2023). A novel automated protocol for ice crystal segmentation analysis using Cellpose and Fiji. *Cryobiology, 111*, 1-8. https://doi.org/https://doi.org/10.1016/j.cryobiol.2023.02.002.

Sanchez, C., Despond, S., Schmitt, C., & Hardy, J. (2001). Effect of heat and shear on β-lactolobulin-acacia gum complex coacervation. In E. Dickinson, R. Miller, E.

Dickinson & R. Miller (Eds.), *Food Colloids Fundamentals of Formulation* (p. 0): The Royal Society of Chemistry.

Sara, H., Yahoum, M. M., Lefnaoui, S., Abdelkader, H., & Moulai-Mostefa, N. (2020). New alkylated xanthan gum as amphiphilic derivatives: Synthesis, physicochemical and rheological studies. *Journal of Molecular Structure, 1207*. https://doi.org/10.1016/j.molstruc.2020.127768.

Schmitt, C., Aberkane, L., & Sanchez, C. (2009). Protein–polysaccharide complexes and coacervates. In *Handbook of Hydrocolloids* (pp. 420-476).

Sreerama, N., & Woody, R. W. (2000). Estimation of protein secondary structure from circular dichroism spectra: comparison of CONTIN, SELCON, and CDSSTR methods with an expanded reference set. *Anal Biochem, 287*(2), 252-260. https://doi.org/10.1006/abio.2000.4880.

Wang, C., Natale, G., Virgilio, N., & Heuzey, M. C. (2016). Synergistic gelation of gelatin B with xanthan gum. *Food Hydrocolloids, 60*, 374-383. https://doi.org/10.1016/j.foodhyd.2016.03.043.

Wang, C., Virgilio, N., Wood Adams, P. M., & Heuzey, M. C. (2018). A gelation mechanism for gelatin/polysaccharide aqueous mixtures. *Food Hydrocolloids, 79*, 462-472. https://doi.org/10.1016/j.foodhyd.2018.01.016.

Wang, L., Xiang, D., Li, C., Zhang, W., & Bai, X. (2021). Effects of lyophilization and low-temperature treatment on the properties and conformation of xanthan gum. *Food Hydrocolloids, 112*. https://doi.org/10.1016/j.foodhyd.2020.106352.

Wang, W., Chen, M., Wu, J., & Wang, S. (2015). Hypothermia protection effect of antifreeze peptides from pigskin collagen on freeze-dried Streptococcus thermophiles and its possible action mechanism. *LWT - Food Science and Technology*, *63*(2), 878-885. https://doi.org/https://doi.org/10.1016/j.lwt.2015.04.007.

Young, S.-L., & Torres, J. A. (1989). Xanthan: effect of molecular conformation on surface tension properties. *Food Hydrocolloids*, *3*(5), 365-377. https://doi.org/https://doi.org/10.1016/S0268-005X(89)80011-6.

Yuan, Y., Dia, V. P., & Wang, T. (2024). The ice recrystallization inhibition activity of wheat glutenin hydrolysates and effect of salt on their activity. *Food Hydrocolloids*, *154*. https://doi.org/10.1016/j.foodhyd.2024.110153.

Yuan, Y., Fomich, M., Dia, V. P., & Wang, T. (2023). Succinylation of zein and gelatin hydrolysates improved their ice recrystallization inhibition activity. *Food Chem*, *424*, 136431. https://doi.org/10.1016/j.foodchem.2023.136431.

APPENDIX

Table 5.1. The molecular weight profiles of gelatin hydrolysates.

Sample	Molecular weight distribution (kDa), %				Average
	≥10	5-9.9	1-4.9	≤1	MW (kDa)
Try 1h	1.4±1.2	17.4±0.5	62.3±1.4	20.1±1.5	2.9±0.1
Try 3h	0.0±0.0	12.2±0.1	62.9±0.3	24.9±0.4	2.3±0.0
Try 6h	0.0±0.0	11.4±0.5	66.2±2.7	22.4±2.2	2.6±0.1
Alc 5m	5.1±0.8	14.1±0.9	53.9±5.0	26.9±3.2	3.0±0.2
Alc 10m	0.2±0.1	5.9±1.6	53.1±1.2	40.8±0.3	1.9±0.0
Alc 30m	0.0±0.0	0.0±0.0	4.3±1.1	95.7±1.1	0.5±0.0

Table 5.2. Statistical analysis results of linear regression models at different xanthan gum concentrations

	Concentration of xanthan gum				
	0%	0.1%	0.2%	0.3%	0.4%
Residual Sum of Squares	2.12826	0.12272	10.33297	133.92339	60.25328
Pearson's R	0.66628	-0.95918	0.06614	-0.58826	-0.00905
R-Square (COD)	0.44392	0.92002	0.00438	0.34605	8.19833E-5
Adj. R-Square	0.30491	0.90002	-0.24453	0.18256	-0.2499

Table 5.3. The secondary structure profile of XG-gelatin hydrolysates complex

XG content (%)	Gelatin hydrolysates type	Mixing time (min)	Content (%)			
			α-helix	β-sheet	β-turn	unordered
15 %	Trypsin 1h	0	19.1	30.3	19.3	31.3
		5	19.8	32.5	17.7	30.0
		60	17.5	31.7	21.0	29.8
	Trypsin 3h	0	19.2	32.8	18.4	29.7
		5	19.8	36.5	16.4	27.2
		60	20.8	31.8	18.1	29.3
	Trypsin 6h	0	19.9	32.1	18.6	29.4
		5	20.1	37.9	14.5	27.5
		60	18.0	32.2	19.7	30.2
20 %	Trypsin 1h	0	12.1	23.4	28.5	36.0
		5	15.6	24.6	23.5	36.3
		60	16.1	21.3	26.2	36.3
	Trypsin 3h	0	18.0	31.6	20.2	30.0
		5	13.7	24.3	26.5	35.5
		60	14.0	24.0	25.7	36.4
	Trypsin 6h	0	19.3	33.6	17.7	29.4
		5	12.9	24.6	26.7	35.7
		60	12.7	26.1	26.3	35.0

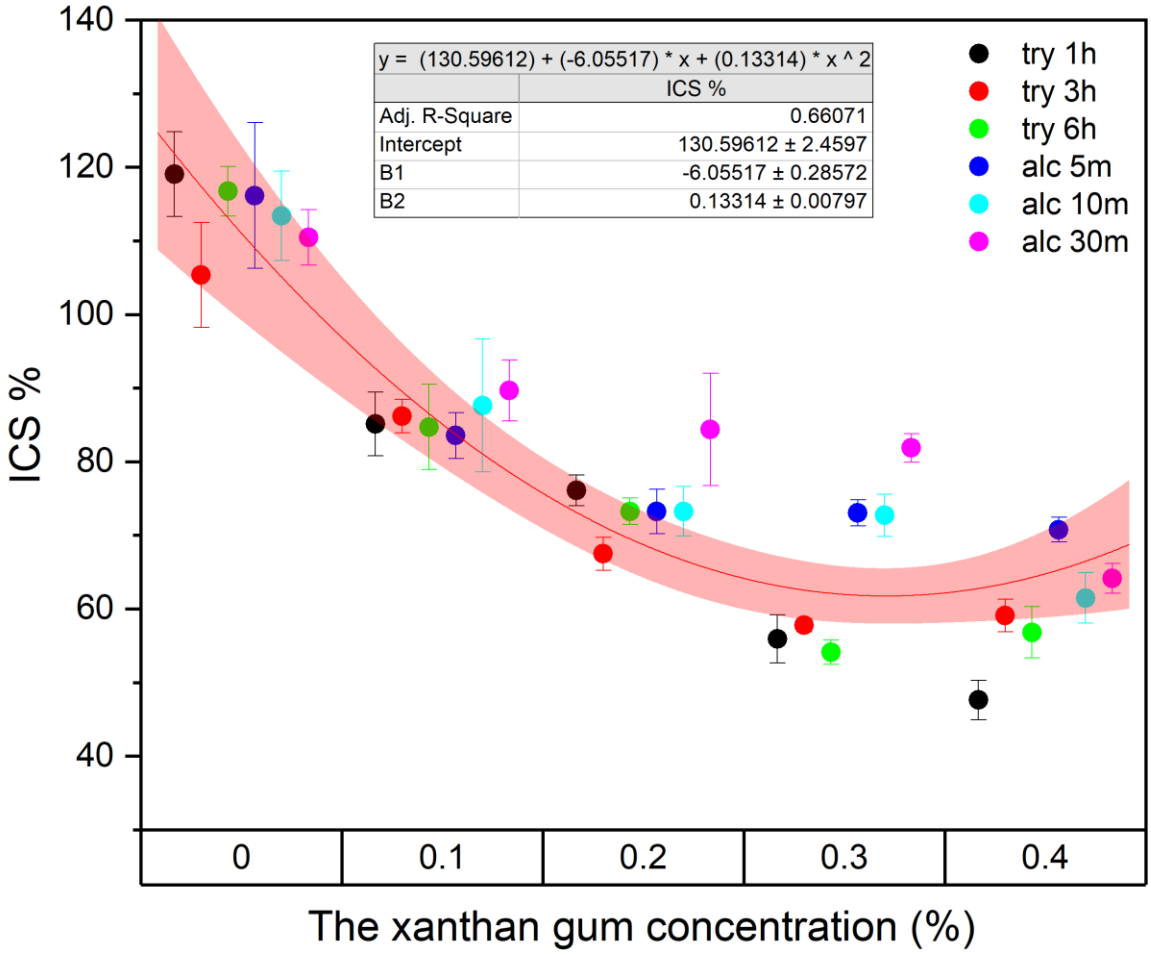

Figure 5.1. The average ice crystal size (ICS) relative to the same concentration of negative control sample (PEG) under the different percentages of xanthan gum. The red curve represents the quadratic fitting model, while the shaded area indicates the 95% confidence interval of ICS predictions.

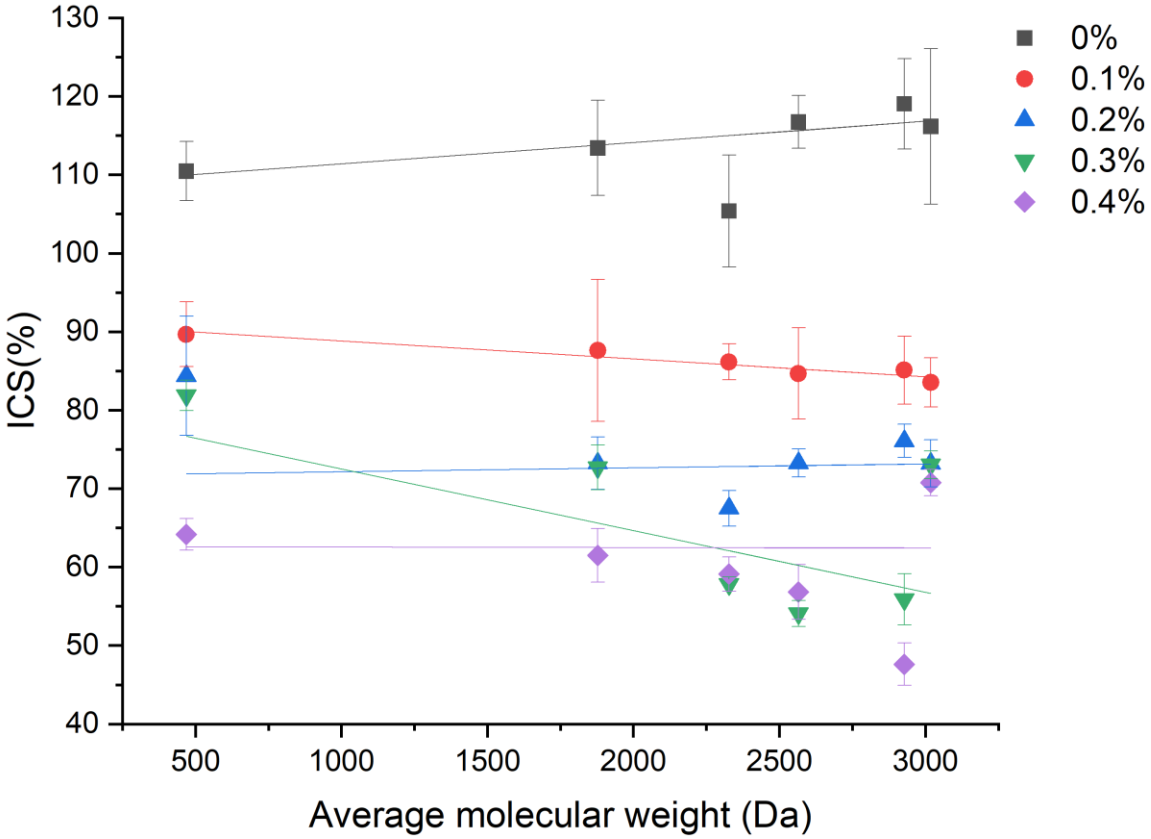

Figure 5.2. The relationship between the molecular weight and ICS of gelatin hydrolysates at different xanthan gum concentrations.

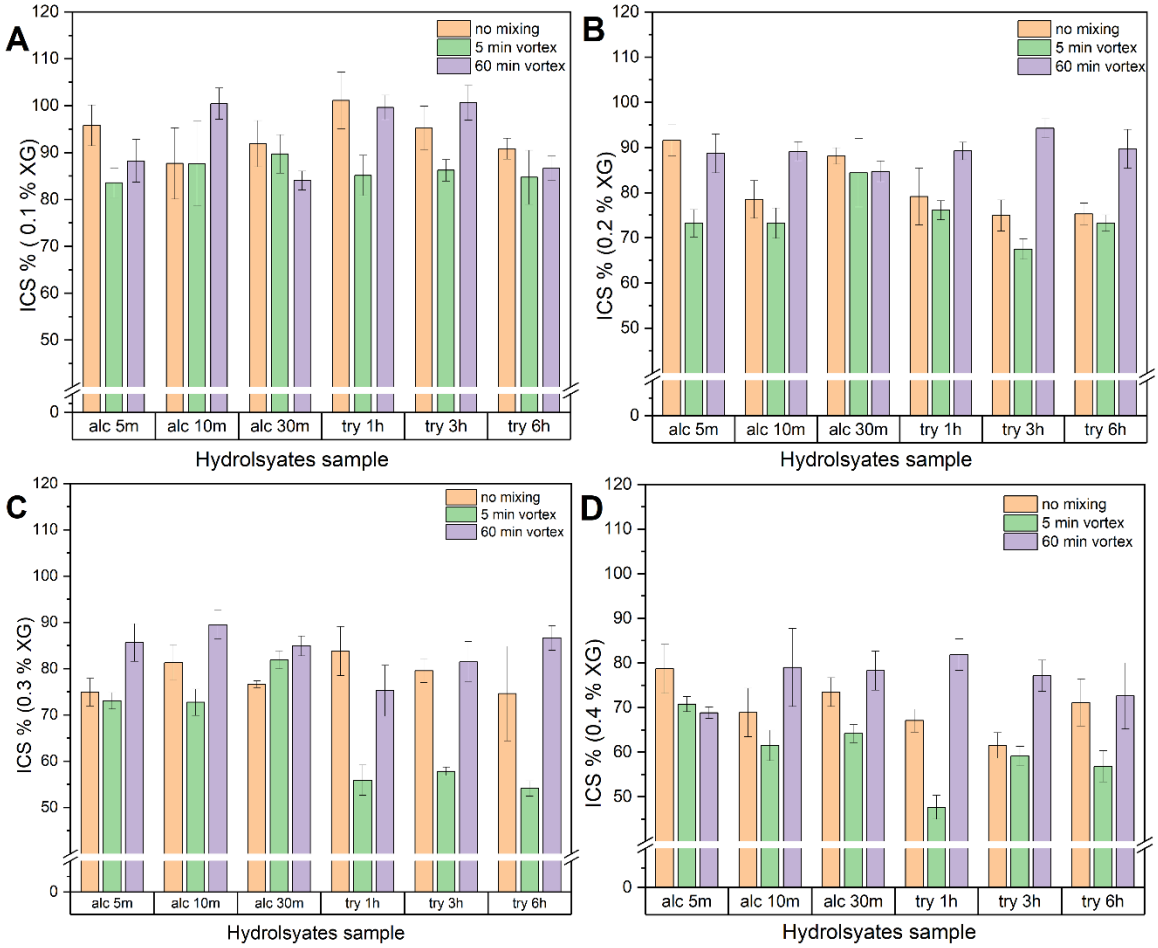

Figure 5.3. Effect of physical mixing on the IRI activity of XG-hydrolysate mixtures at different XG concentrations: (A) 0.1 %, (B) 0.2 %, (C) 0.3 %, and (D) 0.4 %.

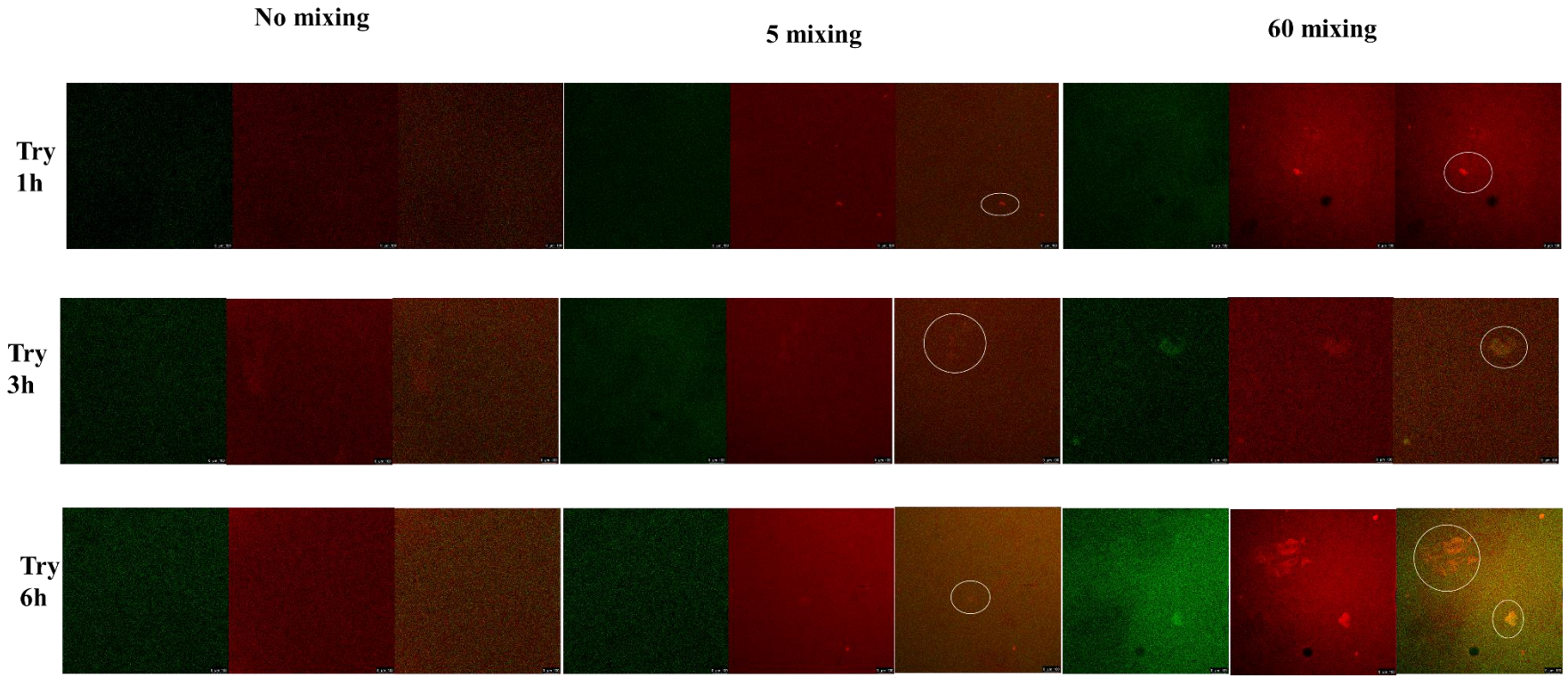

Figure 5.4. Confocal laser scanning microscopy images of the polysaccharides stained with rhodamine B (red) and, proteins stained with fluorescein 5-isothiocyanate (green) for gelatin hydrolysates-xanthan gum mixtures. The white circle means the formation of small aggregations.

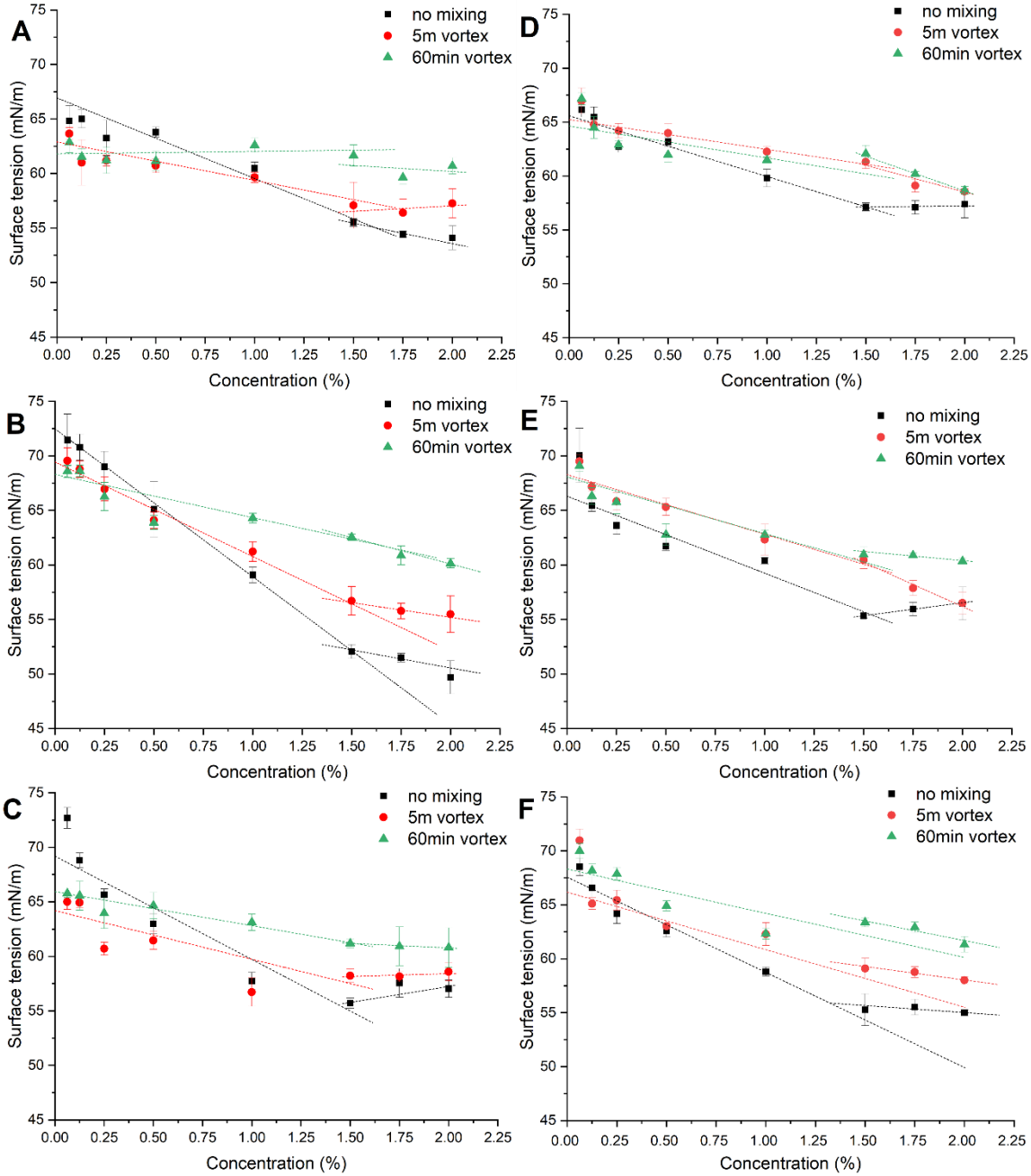

Figure 5.5. Critical micelle concentration of complexes formed with gelatin hydrolysates produced by trypsin at different hydrolysis durations (1h, 3h, and 6h) and two XG concentrations (0.3 and 0.4%). A-C corresponds to 0.3 % XG: (A) 1 hour hydrolysis, (B) 3 hours hydrolysis, (C) 6 hours hydrolysis. D-F corresponds to 0.4 % XG: (D) 1 hour hydrolysis, (E) 3 hours hydrolysis, (F) 6 hours hydrolysis.

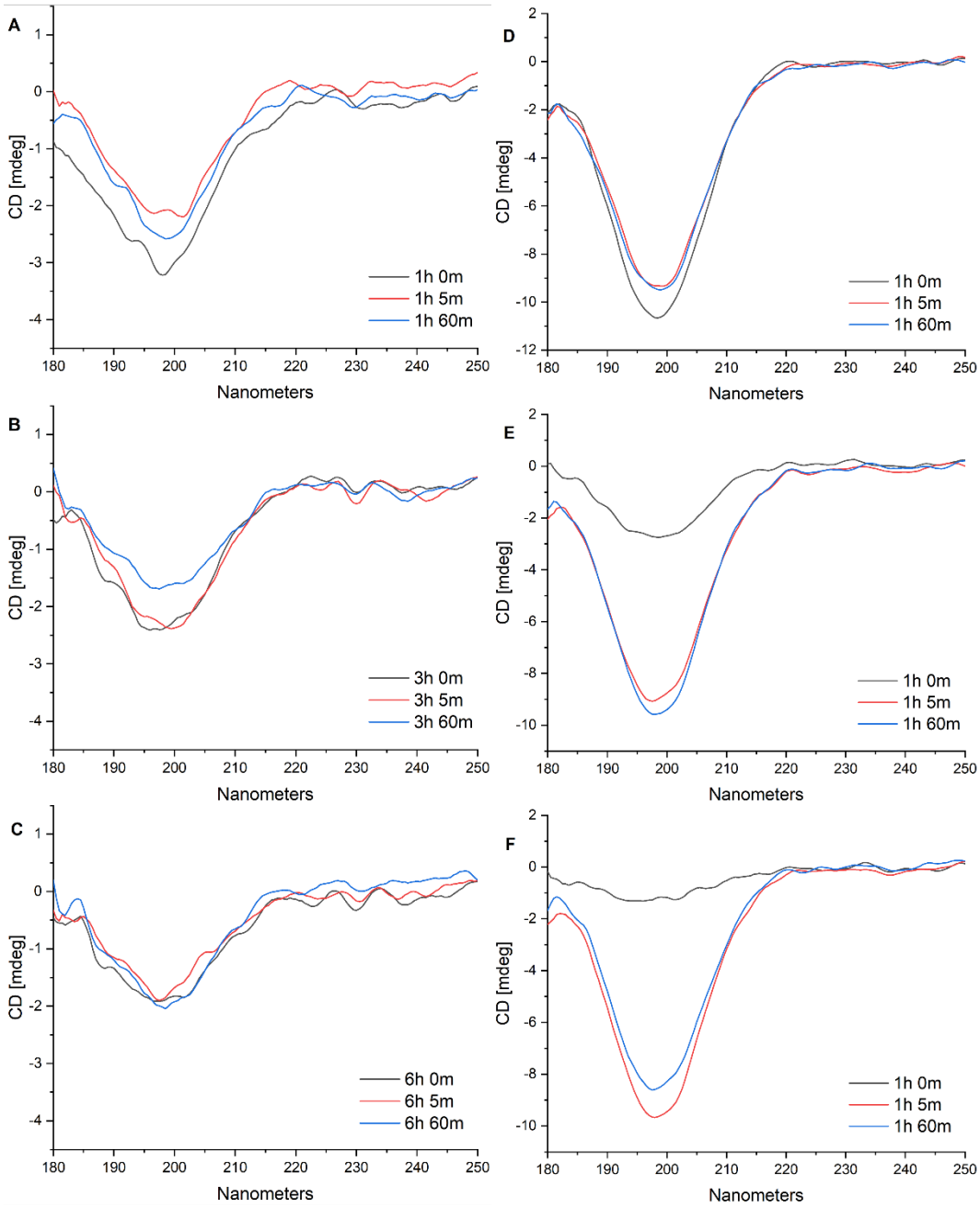

Figure 5.6. Circular dichroism spectra of complexes with different hydrolysis times (1h, 3h, and 6h) and two XG concentrations (0.3 and 0.4%). (A–C) Correspond to 0.3 % XG: (A) 1 hour hydrolysis, (B) 3-hour hydrolysis, (C) 6-hour hydrolysis. (D–F) Correspond to 0.4 % XG: (D) 1 hour hydrolysis, (E) 3-hour hydrolysis, (F) 6-hour hydrolysis.

CHAPTER SIX

EXPLORING THE ROLE OF SECONDARY STRUCTURE ON THE ANTIFREEZE ACTIVITY OF PLANT FOOD DERIVED PEPTIDES: A MOLECULAR DYNAMICS STUDY

Abstract

This study investigates the relationship between secondary structure and chain length of plant-derived peptides and their antifreeze activity through molecular dynamics simulations. Three peptide groups with different chain lengths—namely short, intermediate, and long (20-25, 35-40, and 55-60 amino acids respectively)—with distinct secondary structural motifs (α-helix, β-sheet, and random coil), were used to determine the relationship between antifreeze activity and peptide structural properties. The results indicate that peptides with stable and rigid secondary structures, especially the α-helix, exhibit higher antifreeze activity across the 3 chain length groups. Additionally, peptides demonstrating extensive interactions with water molecules display enhanced antifreeze properties, even those with relatively flexible conformations. This suggests that peptide-water interaction is important in enhancing antifreeze activity. These findings improve the understanding of structure-function relationships in antifreeze peptides and provide practical insights for designing novel and potentially cost-effective peptides for applications in food preservation and biological cryopreservation.

Introduction

Protein hydrolysates from various sources have demonstrated significant ice recrystallization inhibition (IRI) activity (Damodaran & Wang, 2017; Fomich et al., 2023; Yuan et al., 2023; Zhou et al., 2019), and recent studies suggest that their secondary structures are crucial determinants of this activity (Madison Fomich, Dia, & Wang, 2024). Some evidence indicates that peptides with more rigid conformations, such as α-helix and β-sheet, exhibit enhanced IRI activities. For example, wheat glutenin hydrolysates exhibit higher IRI activity when adopting α-helical conformations (Yuan, Dia, & Wang, 2024). Similarly, Yang et al. (2022) highlighted the importance of α-helical conformation and amino acid hydrogen bonding sites for the antifreeze activity of Takifugu obscurus skin hydrolysates, emphasizing that structural stability maintained by α-helices is critical for function. Consistent with these findings, certain natural antifreeze proteins (AFPs) such as Marinomonas primoryensis AFP (MpAFP, bacterial) and Lolium perenne AFP (LpAFP, plant) also have stable and rigid structures (Garnham et al., 2008; Middleton et al., 2009). In contrast, however, other studies have reported that antifreeze polysaccharides (Sun et al., 2024), proteins (Fomich et al., 2025), and glycoproteins (Fomich et al., 2025) may benefit from greater structural flexibility under freezing conditions, enabling stronger interactions with interfacial water and thus improved antifreeze activity.

These differences may be particularly due to the size of the molecules and their ability to interact with water or ice. Previous studies reported conflicting observations on optimal molecular size for IRI activity. Wang et al., (2009) have found that gelatin peptides with

average molecular mass in the range of 700-1400 Da have the highest IRI activity, while (Nguyen et al., 2018) observed that collagen peptide with molecular weight below 3 kDa exhibit high antifreeze activity. On the other hand, Fomich et al. (2023) suggest that the primary antifreeze activity of soy protein isolate hydrolysates originates from peptides with molecular weights of 5-15 kDa. This variability was reported in other studies on synthetic antifreeze agents, such as poly(vinyl alcohol) (PVA), where an adequate chain length (at least eight repeating units) is essential for effective ice-binding (Bachtiger et al., 2021), with increased chain length generally correlating to enhanced antifreeze activity.

To address the current knowledge gaps, molecular dynamics (MD) simulation can be used as a powerful tool to investigate antifreeze mechanisms at the molecular scale, allowing detailed characterization of how specific peptide structures and key amino acid residues influence their binding to ice. Previous studies suggest that AFPs not only passively bind to ice surfaces but also actively prearrange their hydration water into an ice-like structure, lowering the energetic barrier for binding (Nutt & Smith, 2008). Furthermore, the disruption of water structure around the non-ice-binding regions helps prevent AFPs from being fully overgrown by ice (Midya & Bandyopadhyay, 2024). Despite these significant advances, the structure-function relationships of plant protein-derived antifreeze peptides remain largely unexplored at the molecular level. Few studies have systematically investigated how peptide chain length and secondary structure collectively influence antifreeze activity, particularly in plant-derived peptides. To address this gap, we hypothesize that peptides rigid secondary structures such as alpha-

helix and beta-sheet are critical for antifreeze activity. In this study, peptides derived from plant protein (soybean, wheat, rice, and potato), prepared by trypsin protease to generate consistent C-terminus and three different chain lengths, were evaluated. MD simulations technology was used to probe how peptide length and secondary structure may influence antifreeze ability, with the aim to provide mechanistic insights which may be useful in guiding the design of novel antifreeze peptides in the future.

Methods

Experimental design

In this study, the computational flow chart as shown in **Figure 6.1** was used. Peptides were generated by enzymatic hydrolysis using trypsin. Then, these peptides were categorized into three groups based on their amino acid (AA) chain length: short (20-25 AAs), intermediate (35-40 AAs), and long (55-60 AAs). Within each group, three distinct peptides were selected, each characterized by a specific secondary structure type (α-helix, β-sheet, or random coil). By comparing the antifreeze activity of these 9 peptides, this study aimed to assess the impact of secondary structure on antifreeze activity and how molecular size influences this relationship.

Protein selection

The amino acid sequences of plant proteins were obtained from the UniProt database (https://www.uniprot.org/). Proteins from four sources (wheat, soybean, rice, and potato) were selected to generate peptides with diverse secondary structures, including α-helices, β-sheets, and random coils, and three different chain length groups (20-25AAs, 35-40AAs, and 55-60AAs).

Peptides preparation and modeling

Peptides were generated by enzymatically cleaving the selected proteins at lysine (K) and arginine (R) residues using an automated script, to mimic trypsin hydrolysis. The 3D structures of long peptides ($\geqslant$ 30AAs) were generated using the ColabFold webserver (Mirdita et al., 2022), while structures of short ($\leqslant$ 30AAs) were generated using PyPept (Ochoa et al., 2023) with secondary structure constraints provided by SSPred (Yan et al., 2013). The secondary structure composition of these peptides was calculated by secondary structure algorithm in PyMOL ("The PyMOL Molecular Graphics System, Version 1.2r3pre, Schrödinger, LLC.,").

MD simulation

An automated script making use of GenIce2 (Matsumoto et al., 2018, 2024) was utilized to place the 3D peptide structure at an ice-water (Ih prism) interface. GROMACS topology files were generated, and the system for MD simulations under freezing conditions was prepared. The TIP5P water model with an initial ice fraction of 50 % and a salt concentration of 0.1 M NaCl was used. The minimum distance between the solute and the simulation box boundary was set to 1.5 nm. Energy minimization was performed using 5000 steps of the steepest descent algorithm. Equilibration was conducted in two stages: a 125 ps simulation in the canonical (NVT) ensemble at 265.15 K, controlled by the Nose-Hoover thermostat, followed by a 125 ps simulation in the isobaric-isothermal (NPT) ensemble at 1 bar, using the Parrinello-Rahman barostat. Production MD simulations were performed in the NPT ensemble at 265.15 K and 1 bar. Each system

was simulated for either 100 or 150 ns, with three independent replicates to ensure reproducibility.

Trajectory analysis was performed using a combination of OVITO (Stukowski, 2009) and GROMACS (Chen et al., 2021) built-in utilities. These include tracking the number of water molecules existing in the ice vs water phase as identified by CHILL + algorithm (Nguyen. & Molinero, 2015) included in the OVITO (Stukowski, 2009) modeling package. Structural and dynamics parameters of radius of gyration (Rg), root mean square deviation (RMSD), root mean square fluctuation (RMSF), mean squared displacement (MSD), and hydrogen bond counts, were calculated using GROMACS built-in utilities. Specifically, RMSF values were averaged over the last 50 ns of each simulation, and MSD values were calculated over the last stable 10 ns of each simulation, while other parameters were averaged across the entire simulation trajectory. The trajectory frames were saved every 100 ps.

Statistical analysis

In this study, all simulations were repeated three times, and standard deviation and variance analysis were calculated using SPSS 22.0 software. Figures were generated using the Matplotlib library.

Results and Discussion

Peptides and their secondary structure

Table 6.1 and **Figure 6.2** present the source, amino acid sequences, and secondary structure compositions for all nine peptides analyzed in this study, categorized by chain length (short, intermediate, and long). Among peptides with similar chain lengths,

secondary structures percentages for helix, sheet, and random coil structures were varied with one peptide lacking beta-sheet, another peptide lacking helical structures, and the third peptide lacking both helical and beta-sheet structures.

Ice percentage changes of these peptides during freezing conditions

Figure 6.3 shows the changes in the average percentage of ice content during the 100 ns simulation. The ice fraction at 0 ns was slightly below the initial setting of 50 % (**Figure 3**), as the systems underwent a preliminary equilibration phase consisting of 5000 steps of energy minimization, followed by 125 ps of NVT and 125 ps of NPT equilibrations. For intermediate and long chain peptides (**Figure 3B** and **3C**), unordered structure (coil) always shows a higher ice percentage than rigid structure (β-sheet and α-helix). Even in the short chain length, the peptide with a helical structure (22helix) initially had a delay in ice formation but ultimately reached a slightly higher final ice content than peptides with sheet (21sheet) or coil (23coil) structures. This seems to indicate that the small and mid-MW peptides with helix structure will have higher antifreeze activity. This is consistent with previous studies on AFPs and glycoproteins (AFGP), whose inhibition of ice recrystallization has been associated with their helical-ice-binding structures which prevent further ice growth (Olijve et al., 2016). For example, Type I AFP from winter flounder predominantly consists of α-helices, enabling specific and stable binding to ice crystal pyramidal planes (Houston et al., 1998). AFGPs, which consist of repeating glycopeptide units with polyproline type II helical structure, exhibit spatial segregation of hydrophilic and hydrophobic moieties, facilitating their adsorption onto ice surfaces and inhibiting further ice growth (Mochizuki & Molinero, 2018).

Notably, the 37helix peptides from soybeans can be regarded as potent antifreeze peptides, because the ice percentage is much lower than the other 8 peptides. Potent IRI means that ice crystal size is 30 % below that of control (Delesky & Srubar, 2022). Soy protein hydrolysates made by trypsin have been found to have IRI activity in our previous study (Fomich et al., 2023). To further visualize how peptide secondary structure correlates with antifreeze activity, additional 3D plots were constructed (**Figure 6.4**). **Figure 6.4A** illustrates the relationship between the average ice content and the corresponding percentages of helical and coil structures. Similarly, **Figure 6.4B** depicts the relationship between ice content and the percentages of β-sheet and coil structures. These plots clearly demonstrate a structural dependence of peptides with higher helical content generally exhibiting lower ice percentages, confirming the trend observed in **Figure 6.3**.

In addition, the chain length itself influences antifreeze activity of peptides. All intermediate-chain peptides (molecular weight ~4 kDa, **Figure 6.3B**) show the slowest ice formation rates, reaching equilibrium after approximately 40 ns. In contrast, the peptides in the short (below 3 kDa) and long chain groups (above 7 kDa) reach the stable ice percentages at 20 and 30 ns, respectively. In addition, the ice percentage of three peptides in short chain groups is less than that of long chain groups. This aligns well with previous findings suggesting that peptides with high molecular weights tend to lose their ice recrystallization inhibition activity (Luo et al., 2023; Nguyen et al., 2018; Zhu et al., 2022).

The relationship between conformation flexibility and antifreeze activity of peptides

Figure 6.5 shows the time evolution of the Rg and the number of peptide-peptide hydrogen bonds for each peptide during the simulation. The number of peptide-peptide H-bond is crucial for folding and structure, and can be regarded as an indicator of peptide conformational rigidity (Hubbard & Haider, 2010), with higher values typically implying greater structural rigidity. The helix-structured peptides exhibit a consistently higher number of peptide-peptide H-bonds in all three groups, which may correlate with higher antifreeze activity. Additionally, the Rg value remain stable indicating that both the short and intermediate peptides do not undergo a substantial collapse or expansion throughout the simulation (Sneha et al., 2016). These suggest that they maintain relatively stable under freezing conditions. In contrast, the coil peptide of the long chain showed a marked decrease in Rg, indicating substantial structural compaction and instability during the simulation when its chain length is long.

Figure 6.6 shows helical and sheet structure's greater conformational rigidity that generally corresponds to lower RMSD, reflecting minimal overall structural deviation from a reference configuration. Also, lower RMSF alone AA chain indicates reduced local flexibility of individual AA residues (Sneha et al., 2016). However, the intermediate peptide group exhibits a different trend. Considering their relatively higher antifreeze activity, this aligns with previous studies reporting that antifreeze glycoproteins (Fomich et al., 2025) from cheese whey and protein from Tenebrio molitor (Midya & Bandyopadhyay, 2014) have a higher RMSD values. This may imply that other factors or

environmental interactions significantly affect the RMSD values of the 37helix and 37sheet peptides, beyond the inherent structural rigidity.

The relationship between protein-water interaction and their antifreeze activity

To further determine the influence of other factors, water-peptide interactions were analyzed. As shown in **Figure 6.7A**, although only the 90-95 ns segment is displayed, the mean peptide MSD values were calculated over the final 10 ns (90-100 ns) of simulation. Notably, the MSD is higher for the 37helix and 37sheet peptides, indicating greater molecular mobility. A plausible explanation is that these peptides form extensive interactions with surrounding water molecules. While some water molecules bind directly to the peptide surface, others enhance peptide diffusion in solutions, contributing to elevated MSD values. Specifically, the 37helix frequently interacts with water molecules, effectively disrupting the orderly formation or recrystallization of ice crystals. Consequently, the higher RMSD and RMSF values observed for the helix peptide primarily result from active peptide-water interactions rather than intrinsic structural instability. To further verify this interpretation, a correlation analysis between peptide-water hydrogen bonding and peptide RMSD was conducted (**Figure 6.8**). A significant negative correlation ($R^2 = 0.502$, $p = 0.0326$) confirmed that increased peptide-water interactions are indeed associated with enhanced conformational fluctuations, supporting the idea that water interactions rather than structural instability drive the observed RMSD and RMSF trends.

This strong interaction with water was also supported by the higher number of H-bonds between the peptide and water (shown in **Figure 6.7E**). To further quantify these

interactions, a GROMACS energy group analysis was performed (**Table 6.2**). Interestingly, peptides like 56coil had much lower total interaction energy (–6709.2 ± 192.7 kJ/mol), despite showing poorer antifreeze performance. This suggests that overall interaction strength alone does not fully determine antifreeze activity. Rather, the spatial and structural specificity of water binding, such as those captured by hydrogen bonding patterns, plays a more decisive role. The observed MSD and peptide-water hydrogen bonding values also explain why the ice percentage for the 22helix peptide continues to increase in the later stages of simulation. Although 22helix has a helical structure, its limited interactions with water molecules prevent it from effectively inhibiting ice formation.

Differences in peptide-water and peptide-ice interactions may stem from distinct amino acid compositions, significantly influencing peptide surface amphiphilicity. Amino acid composition and specific residues are known to critically determine peptide surface amphiphilicity and surface charge, both widely recognized as essential for antifreeze activity. It is generally accepted that effective antifreeze peptides require a balanced amphiphilic property, with greater amphiphilicity correlating with enhanced antifreeze performance (Biggs et al., 2019). Additionally, even among peptides derived from the same source, incorporating alkaline or negatively charged amino acid residues can further improve antifreeze activity by facilitating hydrogen bond formation with water and ice molecules (Luo et al., 2023; Yuan et al., 2024).

Taken together, these results suggest a complex interplay between peptide rigidity, secondary structure, and interaction with water via hydrogen bond. While peptides with

greater intrinsic rigidity typically exhibit stronger antifreeze activities, the extent of peptide-water interactions also emerges as a critical determinant. Increased peptide-water interactions correlate with elevated RMSD and RMSF values; however, this does not necessarily imply structural instability. The 37helix peptide, characterized by a rigid backbone coupled with extensive water interactions, exemplifies how pronounced peptide-water interactions significantly enhance antifreeze activity, despite higher observed RMSD and RMSF values.

Conclusion

In summary, this study shows an example of how to use MD simulation to show the influence of secondary structure and peptide chain length on the antifreeze activity of plant-based peptides. We found that stable secondary structures, particularly α-helices and β-sheets improved antifreeze activity across all different chain length groups with molecular weights of 2-7 kDa. Peptides with stable secondary structures, particularly those with higher structural rigidity such as α-helices or β-sheets, generally exhibited stronger antifreeze properties for short and mid-size-peptides chains.. However, for the higher-molecular-weight peptides (5-7 kDa) we tested, enhanced activity also arose from extensive peptide-water interactions despite greater conformational flexibility, indicating that water-mediated effects can offset reduced structural rigidity in enhancing antifreeze activity. These observations underscore the ability of peptides to actively engage and interact with water or ice molecules, and its critical role for high antifreeze activity. Building on these findings, we propose two preliminary design heuristics for future peptide discovery and engineering: (1) short peptides (≤ 4 kDa) should contain one or

more continuous α helix or β sheet stretches that span at least ~ 40 % of the sequence, thereby supplying a rigid ice binding scaffold; (2) medium sized peptides (5-7 kDa) can tolerate greater backbone flexibility, provided their residues form persistent peptide water hydrogen bond networks capable of disrupting ice growth. Furthermore, the MD workflow presented in this study (comprising secondary-structure analysis, ice-binding assessment, and water-interaction profiling) should be viewed as a modular protocol rather than a single end-point study. The nine peptides analyzed serve only as a proof-of-concept dataset; the same protocol can be scaled to high-throughput in silico screening campaigns to rank hundreds of candidate sequences before experimental validation. By clarifying this broader applicability, we emphasize that the present work illustrates just one concrete example of how MD simulations can accelerate the discovery of next-generation antifreeze peptides.

REFERENCES

Bachtiger, F., Congdon, T. R., Stubbs, C., Gibson, M. I., & Sosso, G. C. (2021). The atomistic details of the ice recrystallisation inhibition activity of PVA. Nat Commun, 12(1), 1323. https://doi.org/10.1038/s41467-021-21717-z.

Biggs, C., Stubbs, C., Graham, B., Fayter, A. E. R., Hasan, M., & Gibson, M. I. (2019). Mimicking the ice recrystallization activity of biological antifreezes. when is a new polymer "active"? Macromol Biosci, 19(7), e1900082. https://doi.org/10.1002/mabi.201900082.

Chen, X., Wu, J., Cai, X., & Wang, S. (2021). Production, structure-function relationships, mechanisms, and applications of antifreeze peptides. Compr Rev Food Sci Food Saf, 20(1), 542-562. https://doi.org/10.1111/1541-4337.12655.

Damodaran, S., & Wang, S. (2017). Ice crystal growth inhibition by peptides from fish gelatin hydrolysate. Food Hydrocolloids, 70, 46-56. https://doi.org/10.1016/j.foodhyd.2017.03.029.

Delesky, E. A., & Srubar, W. V., 3rd. (2022). Ice-binding proteins and bioinspired synthetic mimics in non-physiological environments. iScience, 25(5), 104286. https://doi.org/10.1016/j.isci.2022.104286.

Fomich, M., Dia, V., & Wang, T. (2024). Soy protein processing impacts the ice recrystallization inhibition activity of protein hydrolysates. Sustainable Food Proteins, 2(4), 223-235.

Fomich, M., Día, V. P., Premadasa, U. I., Doughty, B., Krishnan, H. B., & Wang, T. (2023). Ice recrystallization inhibition activity of soy protein hydrolysates. Journal of Agricultural and Food Chemistry, 71(30), 11587-11598.

Fomich, M., Yuan, Y., Krishnan, H. B., Dia, V. P., & Wang, T. (2025). Isolation and characterization of ice recrystallization inhibitory molecules from black soldier fly larvae. Journal of Insects as Food and Feed, 1(aop), 1-21.

Fomich, M., Yuan, Y., Smith, M. D., Krishnan, H. B., Dia, V., & Wang, T. (2025). Glycosylated peptides isolated from cheese whey have antifreezing activity. Food Chemistry, 469, 142530. https://doi.org/https://doi.org/10.1016/j.foodchem.2024.142530.

Garnham, C. P., Gilbert, J. A., Hartman, C. P., Campbell, R. L., Laybourn-Parry, J., & Davies, P. L. (2008). A Ca2+-dependent bacterial antifreeze protein domain has a novel beta-helical ice-binding fold. Biochem J, 411(1), 171-180. https://doi.org/10.1042/bj20071372.

Houston, M. E., Chao, H., Hodges, R. S., Sykes, B. D., Kay, C. M., Sönnichsen, F. D., . . . Davies, P. L. (1998). Binding of an Oligopeptide to a Specific Plane of Ice*. Journal of Biological Chemistry, 273(19), 11714-11718. https://doi.org/https://doi.org/10.1074/jbc.273.19.11714.

Hubbard, R. E., & Haider, M. K. (2010). Hydrogen bonds in proteins: role and strength. Encyclopedia of life sciences, 1, 1-6.

Luo, W., Yuan, C., Wu, J., Liu, Y., Wang, F., Li, X., & Wang, S. (2023). Inhibition mechanism of membrane-separated silver carp hydrolysates on ice crystal growth

obtained through experiments and molecular dynamics simulation. Food Chem, 414, 135695. https://doi.org/10.1016/j.foodchem.2023.135695.

Matsumoto, M., Yagasaki, T., & Tanaka, H. (2018). GenIce: hydrogen-disordered ice generator. Wiley Online Library.

Matsumoto, M., Yagasaki, T., & Tanaka, H. (2024). GenIce-core: Efficient algorithm for generation of hydrogen-disordered ice structures. The Journal of chemical physics, 160(9).

Middleton, A. J., Brown, A. M., Davies, P. L., & Walker, V. K. (2009). Identification of the ice-binding face of a plant antifreeze protein. FEBS Lett, 583(4), 815-819. https://doi.org/10.1016/j.febslet.2009.01.035.

Midya, U. S., & Bandyopadhyay, S. (2014). Hydration behavior at the ice-binding surface of the Tenebrio molitor antifreeze protein. J Phys Chem B, 118(18), 4743-4752. https://doi.org/10.1021/jp412528b.

Midya, U. S., & Bandyopadhyay, S. (2024). Ice Recrystallization Unveils the Binding Mechanism Operating at a Diffused Interface. J Phys Chem B, 128(5), 1170-1178. https://doi.org/10.1021/acs.jpcb.3c05934.

Mirdita, M., Schütze, K., Moriwaki, Y., Heo, L., Ovchinnikov, S., & Steinegger, M. (2022). ColabFold: making protein folding accessible to all. Nature Methods, 19(6), 679-682. https://doi.org/10.1038/s41592-022-01488-1.

Mochizuki, K., & Molinero, V. (2018). Antifreeze glycoproteins bind reversibly to ice via hydrophobic groups. J Am Chem Soc, 140(14), 4803-4811. https://doi.org/10.1021/jacs.7b13630.

Nguyen, C. T., Yuan, M., Yu, J. S., Ye, T., Cao, H., & Xu, F. (2018). Isolation of ice structuring collagen peptide by ice affinity adsorption, its ice-binding mechanism and breadmaking performance in frozen dough. Journal of Food Biochemistry, 42(3). https://doi.org/10.1111/jfbc.12506.

Nguyen., & Molinero, V. (2015). Identification of Clathrate Hydrates, Hexagonal Ice, Cubic Ice, and Liquid Water in Simulations: the CHILL+ Algorithm. J Phys Chem B, 119(29), 9369-9376. https://doi.org/10.1021/jp510289t.

Nutt, D. R., & Smith, J. C. (2008). Dual function of the hydration layer around an antifreeze protein revealed by atomistic molecular dynamics simulations. Journal of the American Chemical Society, 130(39), 13066-13073.

Ochoa, R., Brown, J. B., & Fox, T. (2023). pyPept: a python library to generate atomistic 2D and 3D representations of peptides. Journal of Cheminformatics, 15(1), 79. https://doi.org/10.1186/s13321-023-00748-2.

Olijve, L. L., Meister, K., DeVries, A. L., Duman, J. G., Guo, S., Bakker, H. J., & Voets, I. K. (2016). Blocking rapid ice crystal growth through nonbasal plane adsorption of antifreeze proteins. Proc Natl Acad Sci U S A, 113(14), 3740-3745. https://doi.org/10.1073/pnas.1524109113.

The PyMOL Molecular Graphics System, Version 1.2r3pre, Schrödinger, LLC.

Sneha, P., & George Priya Doss, C. (2016). Chapter Seven - Molecular Dynamics: New Frontier in Personalized Medicine. In R. Donev (Ed.), Advances in Protein Chemistry and Structural Biology (pp. 181-224): Academic Press.

Stukowski, A. (2009). Visualization and analysis of atomistic simulation data with OVITO–the Open Visualization Tool. Modelling and simulation in materials science and engineering, 18(1), 015012.

Sun, X., Guo, R., Zhan, T., Kou, Y., Ma, X., Song, H., . . . Wu, Y. (2024). Retarding ice recrystallization by tamarind seed polysaccharide: Investigation in ice cream mixes and insights from molecular dynamics simulation. Food Hydrocolloids, 149. https://doi.org/10.1016/j.foodhyd.2023.109579.

Wang, S., Agyare, K., & Damodaran, S. (2009). Optimisation of hydrolysis conditions and fractionation of peptide cryoprotectants from gelatin hydrolysate. Food Chemistry, 115(2), 620-630. https://doi.org/10.1016/j.foodchem.2008.12.079.

Yan, R., Xu, D., Yang, J., Walker, S., & Zhang, Y. (2013). A comparative assessment and analysis of 20 representative sequence alignment methods for protein structure prediction. Scientific Reports, 3(1), 2619. https://doi.org/10.1038/srep02619.

Yang, F., Jiang, W., Chen, X., Chen, X., Wu, J., Huang, J., . . . Wang, S. (2022). Identification of novel antifreeze peptides from takifugu obscurus skin and molecular mechanism in inhibiting ice crystal growth. J Agric Food Chem, 70(44), 14148-14156. https://doi.org/10.1021/acs.jafc.2c04393.

Yuan, Y., Dia, V. P., & Wang, T. (2024). The ice recrystallization inhibition activity of wheat glutenin hydrolysates and effect of salt on their activity. Food Hydrocolloids, 154. https://doi.org/10.1016/j.foodhyd.2024.110153.

Yuan, Y., Fomich, M., Dia, V. P., & Wang, T. (2023). Succinylation of zein and gelatin hydrolysates improved their ice recrystallization inhibition activity. Food Chem, 424, 136431. https://doi.org/10.1016/j.foodchem.2023.136431.

Zhou, W., Wang, F., Yu, J., Li, X., & Liu, Y. (2019). Cryoprotective Effects of Protein Hydrolysates Prepared from By-Products of Silver Carp (Hypophthalmichthys Molitrix) on Freeze-Thawed Surimi. Applied Sciences, 9(3). https://doi.org/10.3390/app9030563.

Zhu, K., Zheng, Z., & Dai, Z. (2022). Identification of antifreeze peptides in shrimp byproducts autolysate using peptidomics and bioinformatics. Food Chem, 383, 132568. https://doi.org/10.1016/j.foodchem.2022.132568.

APPENDIX

Table 6.1. Generated functioned proteins and their molecular characteristics and secondary structure compositions of peptides.

Chain length	Accession number	Source	Mw (Da)	No. AA	AA sequences	Secondary structure composition (%)		
						helix	sheet	coil
Short (20-25AA)	P18573	Wheat	2719	22	QQQQQQQQILQQILQQQLIPCR	73	0	27
	P25974	Soybean	2509	21	SSNSFQTLFENQNGRIRLLQR	0	62	38
	Q75GX9	Rice	2229	23	ATILLLLAAVLFAAAAAASGEDR	0	0	100
Intermediate (35-40AA)	P25974	Soybean	4417	37	YDDFFLSSTQAQQSYLQGFSHNILETSFHSEFEEINR	46	0	54
	Q852L2	Potato	4316	37	AFLQPSHYDADEVFYVKEGEGVIVLLREGRRESFCVR	0	38	62
	P25974	Soybean	4272	39	AELSEDDVFVIPAAYPFVVNATSNLNFLAFGINAENNQR	0	0	100
Long (55-60AA)	Q75GX9	Rice	6547	59	ILHTISVPGQIQFFFAPGGRNPESFLSSFSKGVQRAAFKISE EKLEKLLGKQDKGVIIR	36	0	64
	P25974	Soybean	6162	55	AILTLVNNDDRDSYNLHPGDAQRIPAGTTYYLVNPHDHQ NLKIIKLAIPVNKPGR	0	33	66
	P10388	Wheat	6251	56	YYPSVTCPQQVSYYPGQASPQRPGQGQQPGQGQQGYYP TSPQQPGQWQQPEQGQPR	0	0	100

Table 6.2. Peptide–water short-range interaction energies over the final 10 ns of stable simulation, including LJ-SR (short-range Lennard-Jones) and Coul-SR (short-range Coulombic energy.

Chain length	Sample	LJ-SR (kJ/mol)	Coul-SR (kJ/mol)	Total Energy (kJ/mol)
Short	22helix	-196.9±38.1	-2787.6±91.9	-2984.5±72.9
(20-25AA)	21sheet	-214.0±22.3	-1956.3±211.0	-2170.2±225.0
	23coil	-277.0±49.1	-2555.0±70.9	-2832.0±118.9
Intermediate	37helix	-301.5±54.3	-4712.4±276.5	-5013.9±248.2
(35-40AA)	37sheet	-233.6±72.1	-5240.6±170.4	-5474.3±198.1
	39coil	-372.3±68.5	-3980.0±137.6	-4352.3±160.7
Long	59helix	-362.9±89.6	-6491.9±113.9	-6854.9±122.4
(55-60AA)	55sheet	-707.9±72.9	-5459.0±78.7	-6166.9±140.6
	56coil	-465.0±135.4	-6244.3±211.0	-6709.2±192.7

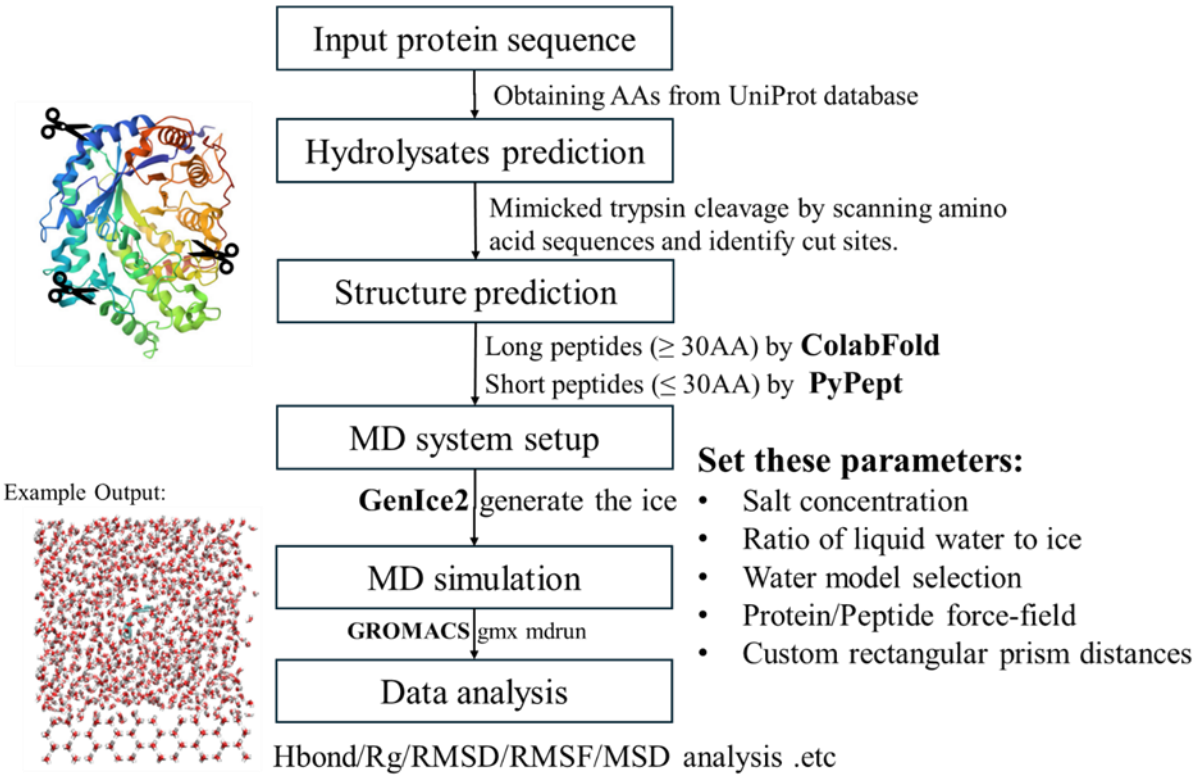

Figure 6.1. Molecular dynamics workflow for antifreeze peptide discovery.

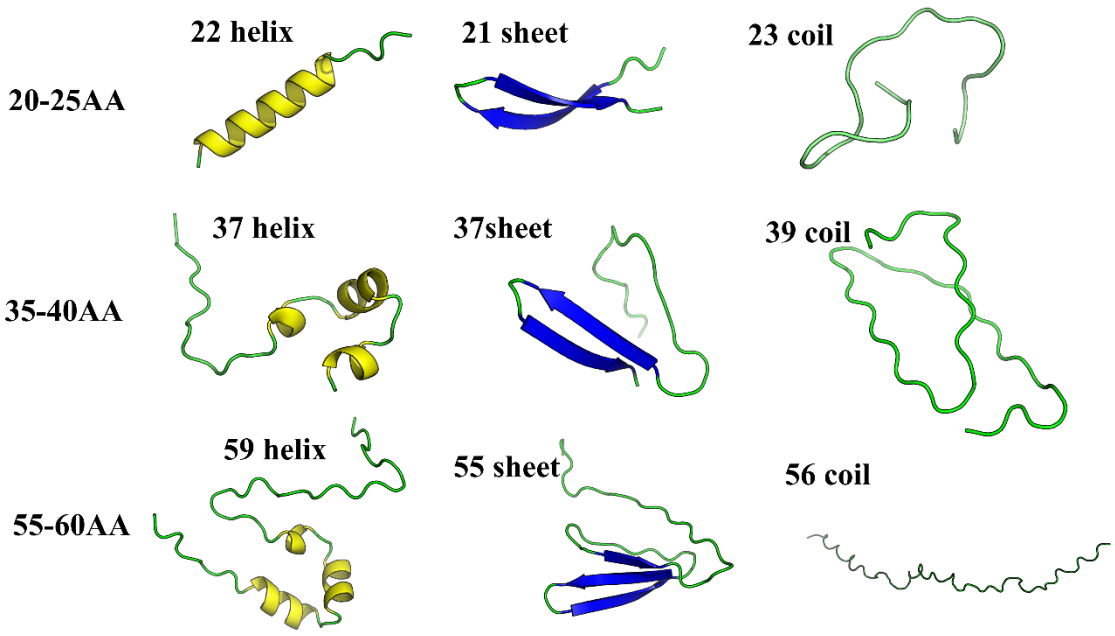

Figure 6.2. The structural models of peptides with different secondary structures and chain lengths. The number before each structure type indicates the peptide length in amino acid residues.

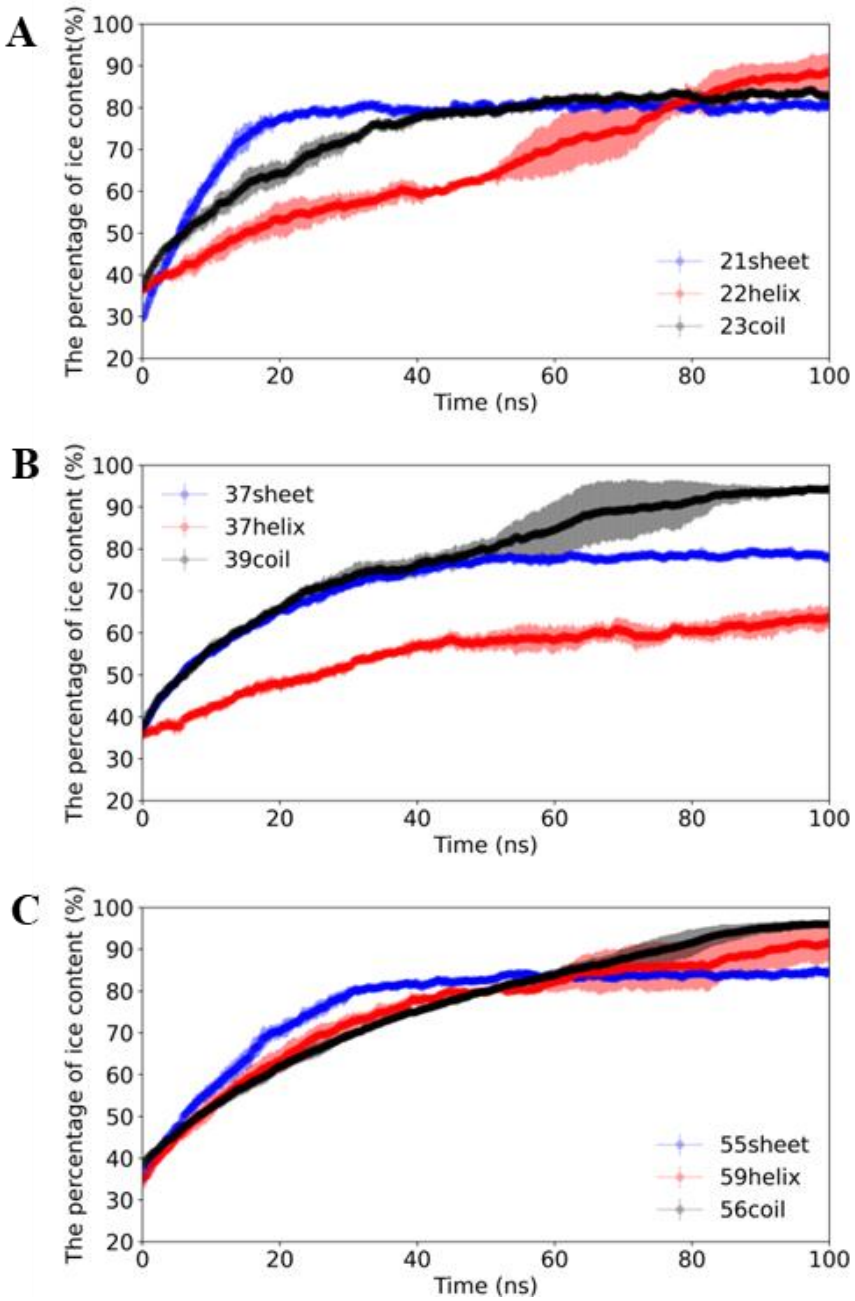

Figure 6.3. Time evolution of the percentage of ice molecules during the simulation. A: short chain length group, B: intermediate chain length group, C: long chain length group. Shaded areas represent the standard deviation based on three independent simulation replicates.

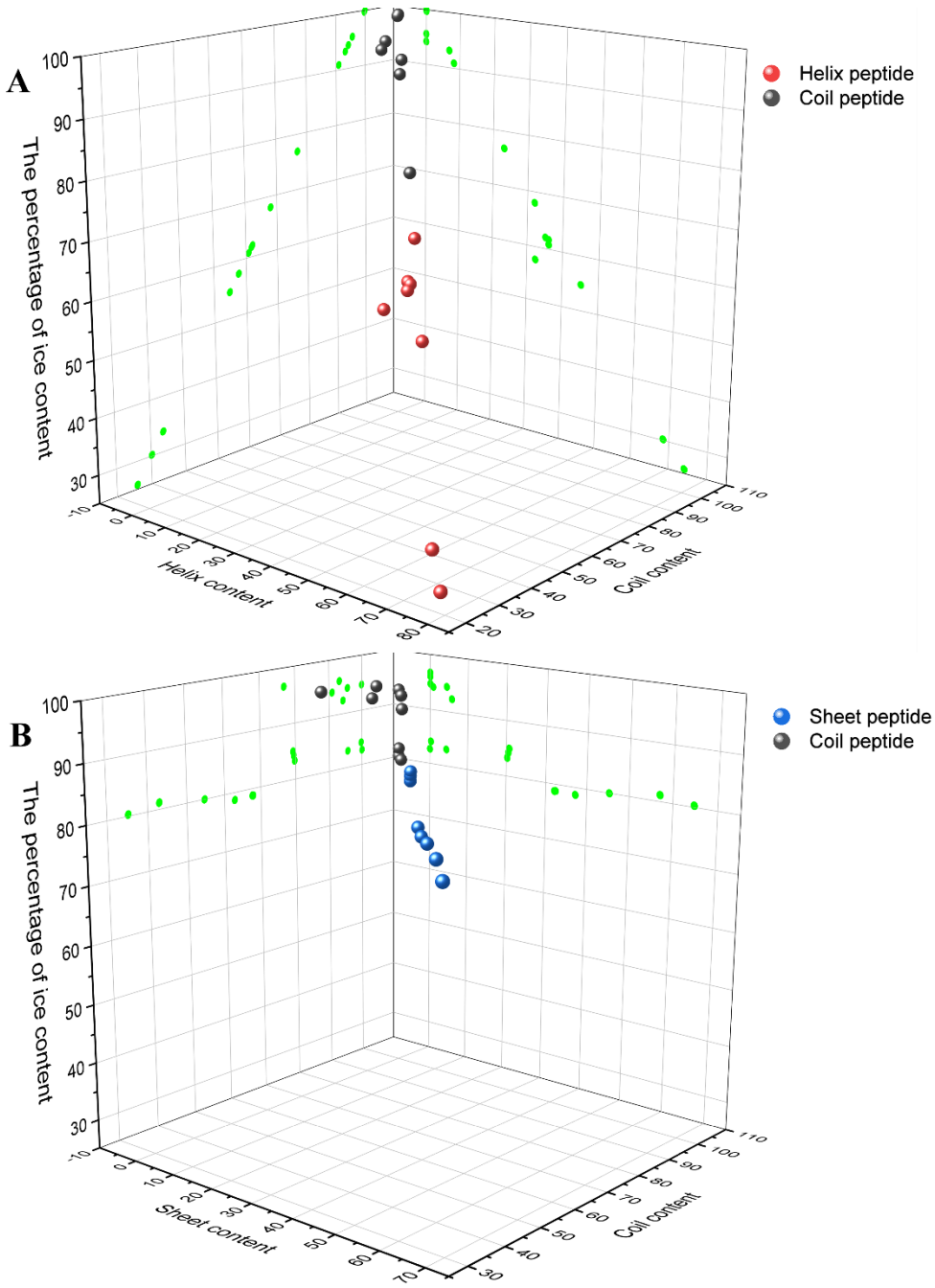

Figure 6.4. The relationship between peptide secondary structure and average ice content. A) Ice content as a function of helical and coil structure, B) Ice content as a function of sheet and coil structure.

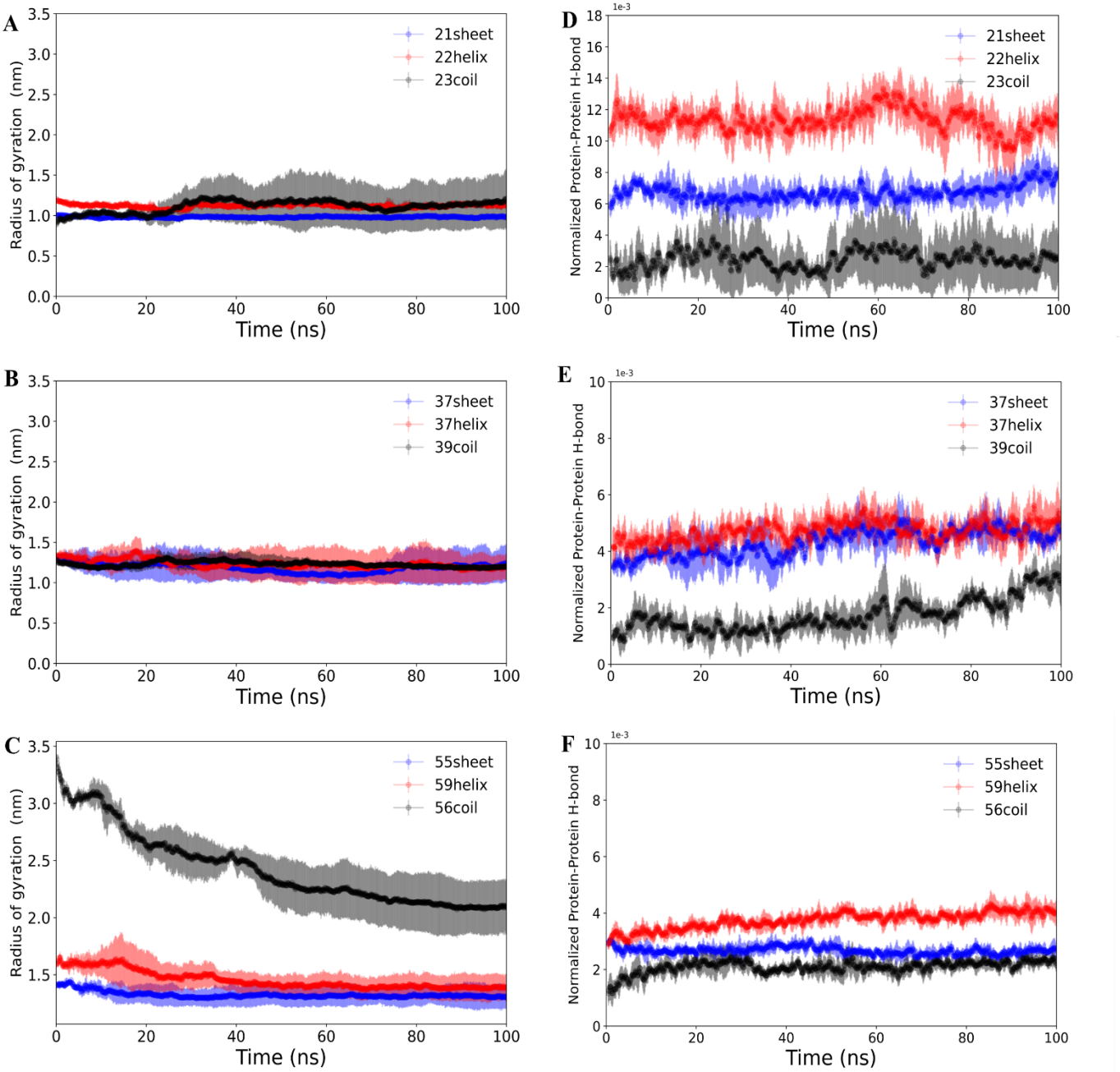

Figure 6.5. Time evolution of radius of gyration (A-C) and normalized hydrogen bond between peptide and peptide (D-F) during 100 ns simulations, categorized by peptide chain length (A and D for short, B and E for intermediate, and C and F for long).

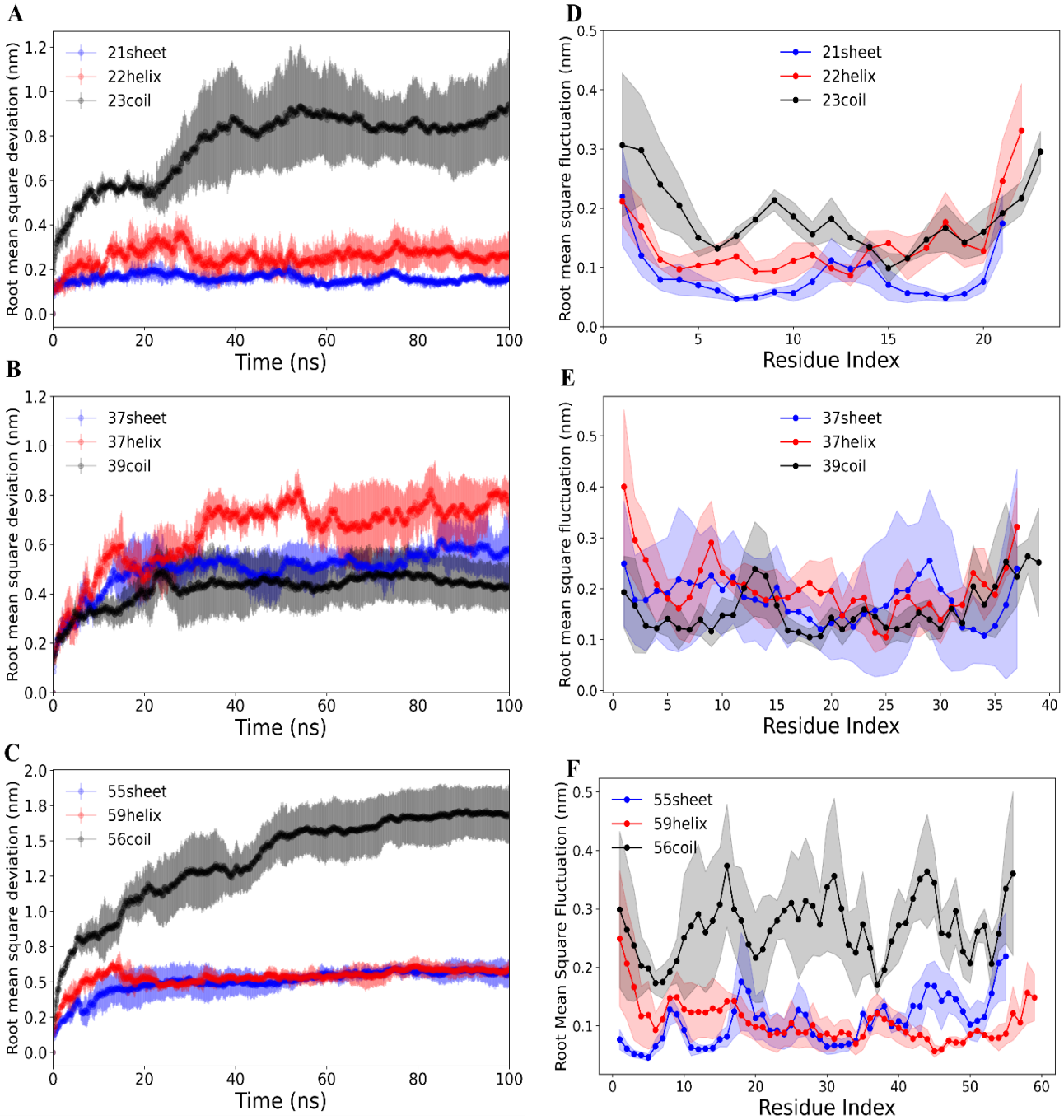

Figure 6.6. Time evolution of root mean square deviation (A-C) and root mean square fluctuation (D-F) of peptides during 100 ns simulations, categorized by peptide chain length (A and D for short, B and E for intermediate, and C and F for long).

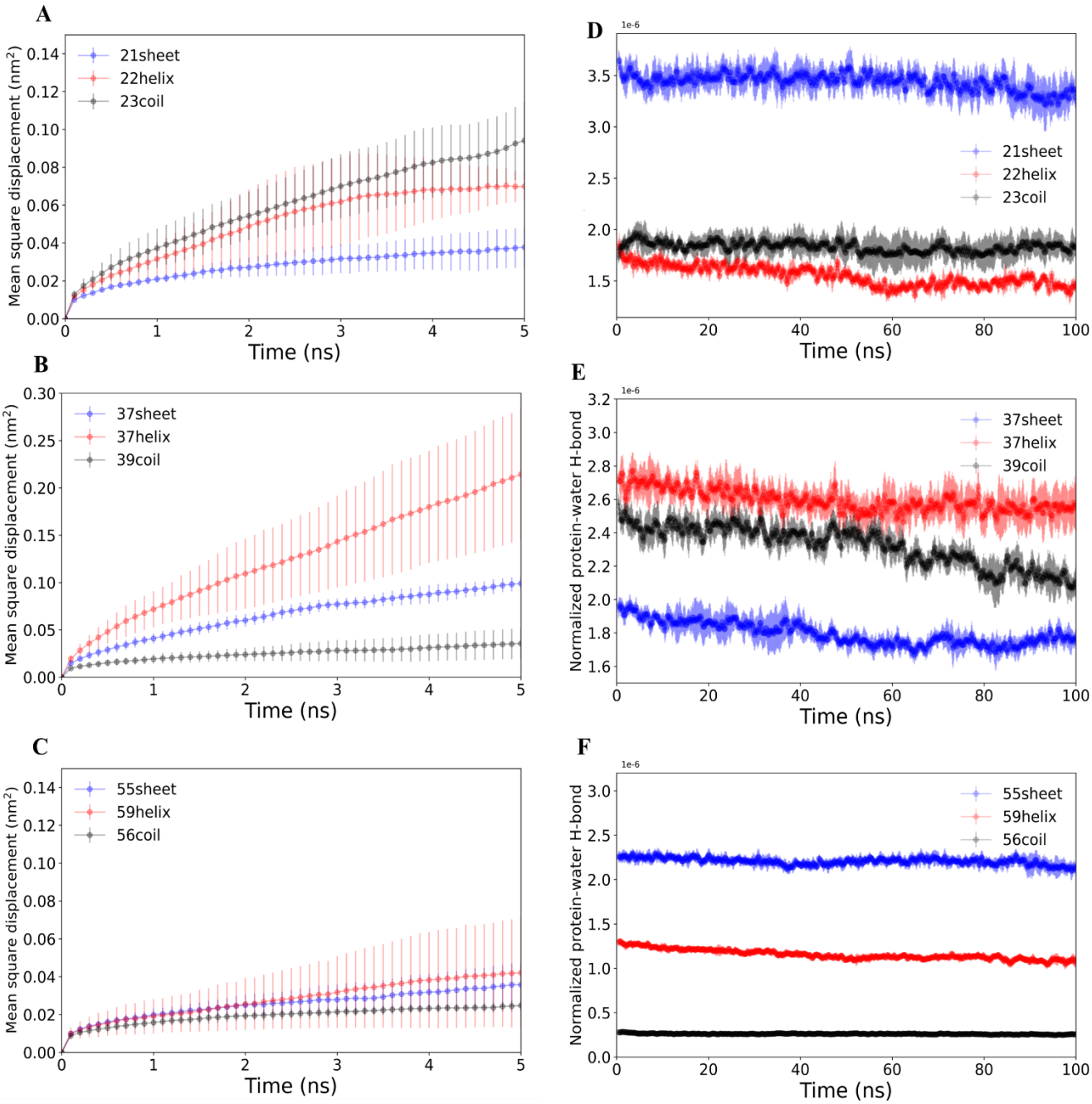

Figure 6.7. Time evolution of mean square displacement (A-C) and normalized peptide-water hydrogen bonds (D-F) for peptides during 100 ns simulations, categorized by chain length (A and D for short, B and E for intermediate, and C and F for long).

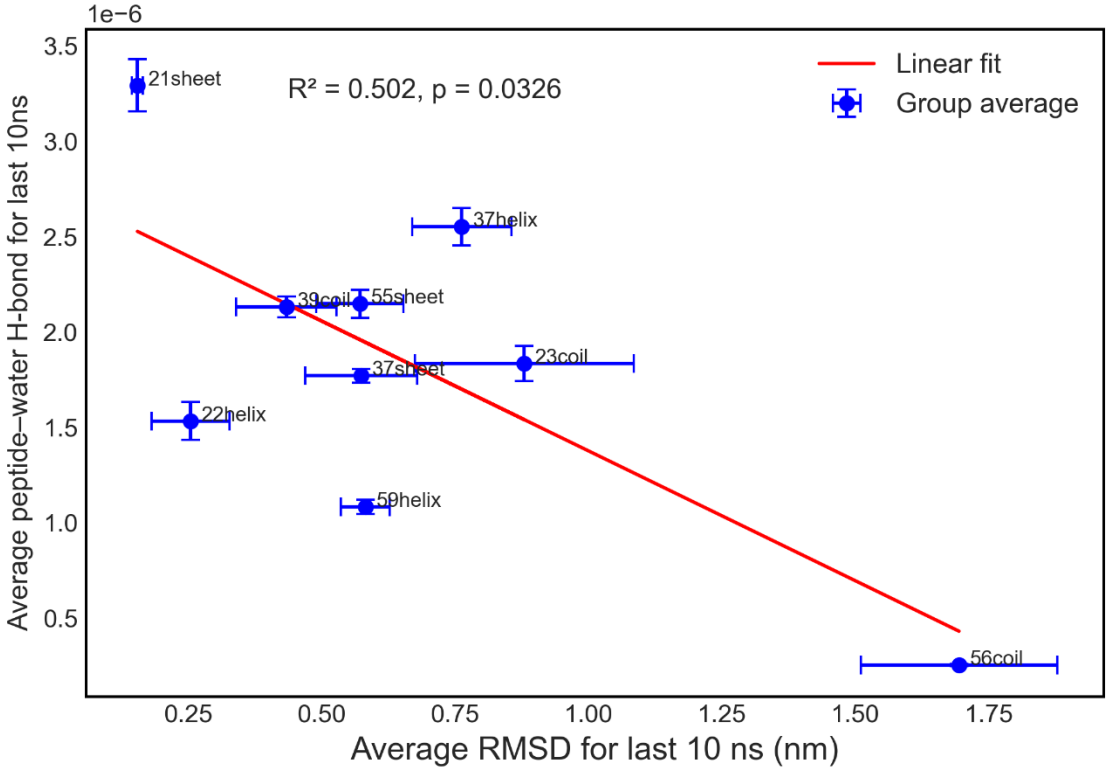

Figure 6.8. Correlation between average peptide structural flexibility (RMSD) and hydration bonds between peptides and water molecules during the final 10 ns of simulation.

CHAPTER SEVEN

CONCLUSION AND FUTURE WORK

Summary and key findings

This dissertation demonstrated that the IRI activity of peptides derived from various food proteins could be significantly enhanced through enzymatic hydrolysis, chemical modification, and controlled interaction with salts and polysaccharides. The work focused on understanding structure-function relationships to develop novel ice crystal inhibitors for food preservation.

The first part of the study explored succinylation as a method to improve the antifreeze activity of zein and gelatin hydrolysates. Succinylation effectively modified peptide amphiphilicity, significantly enhancing IRI activity at low concentrations. Furthermore, solution pH influenced peptide charge, directly impacting antifreeze effectiveness. The second chapter investigated wheat glutenin hydrolysates prepared with Alcalase and trypsin, revealing IRI activity was influenced by amino acid composition and secondary structure. Trypsin-derived hydrolysates consistently showed higher antifreeze potential. Salt concentration and type affected IRI activity, correlating with structural rigidity characterized by increased α-helix content. The third part characterized water-soluble wheat flour proteins responsible for IRI activity. Purification identified two promising proteins: a dimeric α-amylase inhibitor and an α-amylase inhibitor. Molecular dynamics simulations indicated the superior antifreeze activity of latter one is related to their structural rigidity and strong protein-water interactions. The fourth chapter demonstrated xanthan gum enhanced gelatin hydrolysate antifreeze activity significantly at low

concentrations (0.1 %). Molecular weight and mixing duration further influenced the antifreeze activity. Surface tension measurements and CD confirmed increased amphiphilicity and rigid conformation correlated with improved IRI. The final chapter used molecular dynamics simulations to elucidate the relationship between secondary structure and IRI activity across peptides of varying lengths generated by trypsin hydrolysis of food-derived proteins, providing deeper insights into structural determinants of antifreeze activity.

Overall, this dissertation provides foundational insights for designing novel, efficient antifreeze peptides for food preservation applications.

Future work

The results in this study have developed some novel antifreeze hydrolysates with high IRI activity and highlight the importance of their surface amphiphilicity and secondary structure on the IRI activity. Future work should further explore several important areas to build upon these findings:

(1) Evaluate the application of the developed antifreeze peptides in actual food systems, such as frozen seafood, dough, dairy products, and ice cream, to ensure compatibility with existing industrial food production processes.

(2) Investigate the effects of antifreeze peptides on nutritional stability within food matrices, such as vitamin stability, lipid oxidation, and other essential nutritional components during processing and frozen storage.

(3) Expand potential applications of these peptides into biomedical fields, such as cellular preservation, tissue cryopreservation, or medical cryoprotection. Preliminary cell-based

studies could explore the feasibility and efficacy of antifreeze peptides in medical and pharmaceutical contexts.

(4) Develop scalable and economically viable production processes for antifreeze peptides, focusing on eco-friendly hydrolysis and chemical modification methods. Ensuring compatibility with existing food industry practices will be crucial for successful commercialization.

VITA

Yuan Yuan was born on July 14th, 1995, in China. After finishing her studies in elementary, middle and high school, she entered Jilin Agriculture University to pursue a bachelor's degree in food science and engineering. After finishing the master program in Nanjing Agricultural university, she was accepted into the PhD program in Food Science at the University of Tennessee, Knoxville, TN, USA in 2021.